CONTRACT SERIAL NO. 99275-01-SQ
CONTRACT REQUISITION NO. 9-9275
CONTRACTOR: NOVA HUSKY RESEARCH CORP.

CRITICAL PARAMETERS INFLUENCING MICROBIAL CORROSION

(50/50 Cost Shared)

Final Report

by:

F. Grant Ferris

Reviewed by:

M. McD. Francis

NOVA HUSKY Research Corporation
2928 16th Street N.E.
Calgary, Albert.
T2E 7K7

Work on this project was conducted under the auspices of the Canada Centre for Mineral and Energy Technology, Energy, Mines and Resources Canada.

DSS File No.: 014SQ.23440-9-9275
DSS Contract Serial No.: 23440-9-9275/01-SQ
CANMET Scientific Authority: R.G.L. McCready
Date: March 31, 1991

MICROMEDIA

87 pp

© 1991 NOVA HUSKY RESEARCH CORPORATION

DISTRIBUTION LIST

	Copies
CANMET - Energy, Mines, and Resources Canada:	
Dr. R.G.L. McCready	10
Husky Oil Ltd., Calgary:	
Leon Olson	1
Husky Oil Ltd., Lloydminster:	
Ed Rogoz	2
NOVA HUSKY Research Corporation:	
T. Jack	1
G. Ferris	1
M. Francis	1
B. Bramhill	1
NHRC Library	1
NOVA Library	1
Husky Library	1
Files	1
TOTAL NUMBER OF COPIES	**21**

© 1991 NOVA HUSKY RESEARCH CORPORATION

TABLE OF CONTENTS

Page #

LIST OF TABLES iv

LIST OF FIGURES v

EXECUTIVE SUMMARY ..... viii-ix

SOMMAIRE EXECUTIF x

1.0 OBJECTIVES 1

2.0 INTRODUCTION 1

3.0 METHODS 2

- 3.1 Field Test Facility 2
- 3.2 Sample Collection and Processing 2
- 3.3 Analytical Methodology 3
- 3.4 Corrosion Rate Measurements 3
- 3.5 Electron Microscopy 4

4.0 RESULTS 4

- 4.1 Bacterial Surface Colonization 4
- 4.2 Corrosion Rates 5
- 4.3 Injection Water Chemistry and Bacterial Populations 6
- 4.5 Transition of Bacterial Field Populations 8
- 4.6 Corrosion Deposit Structure and Composition 8

5.0 DISCUSSION 9

6.0 CONCLUSIONS 15

7.0 REFERENCES 16

8.0 TABLES 19

9.0 FIGURES 23

© 1991 NOVA HUSKY RESEARCH CORPORATION

LIST OF TABLES

1. Treatment protocols for first and second experimental runs.

2. Corrosion rates measured at week 4 (prior to chemical treatment) in first and second experimental runs.

3. Injection water chemistry at week 2 of the first and second experimental runs.

© 1991 NOVA HUSKY RESEARCH CORPORATION

LIST OF FIGURES

FIGURE 1. Mean values of viable counts for sulfate-reducing and acid producing bacteria after four weeks of colonization at the field test facility.

FIGURE 2. Sulfate-reducing bacterial counts during the first experimental run.

FIGURE 3. Acid-producing bacterial counts during the first experimental run.

FIGURE 4. Sulfate-reduction activity during the first experimental run.

FIGURE 5. Sulfate-reducing bacterial counts during the second experimental run.

FIGURE 6. Acid-producing bacterial counts during the second experimental run.

FIGURE 7. Sulfate-reduction activity during the second experimental run.

FIGURE 8. Enhancement of general corrosion rates after chemical treatment in the first experiment.

FIGURE 9. Enhancement of pitting tendency rates after chemical treatment in the first experiment.

FIGURE 10. Enhancement of general corrosion rates after chemical treatment in the second experiment.

FIGURE 11. Enhancement of pitting tendency rates after chemical treatment in the second experiment.

FIGURE 12. Fluctuations in sodium, potassium, calcium, magnesium, iron, and manganese concentrations over the first experimental run.

FIGURE 13. Fluctuations in chloride, phosphate, and sulfide concentrations over the first experimental run.

FIGURE 14. Fluctuations in sulfate and nitrate levels over the first experimental run.

FIGURE 15. Fluctuations in alkalinity, total suspended solids, and total organic carbon over the first experimental run.

FIGURE 16. Fluctuations in sodium, potassium, calcium, magnesium, iron, and manganese concentrations over the second experimental run.

FIGURE 17. Fluctuations in chloride, sulfate, nitrate, phosphate,and sulfide concentrations over the second experimental run.

FIGURE 18. Fluctuations in alkalinity, total suspended solids, and total organic carbon over the second experimental run.

FIGURE 19. Scatter plot of sulfate-reducing bacterial counts and iron concentrations in the first experiment.

FIGURE 20. Scatter plot of acid-producing bacterial counts and iron concentrations in the first experiment.

FIGURE 21. Scatter plot of sulfate-reducing bacterial counts and iron concentrations in the second experiment.

© 1991 NOVA HUSKY RESEARCH CORPORATION

FIGURE 22. Scatter plot of acid-producing bacterial counts and iron concentrations in the second experiment.

FIGURE 23. Scatter plot of sulfate-reducing bacterial counts and magnesium concentrations in the first experiment.

FIGURE 24. Scatter plot of acid-producing bacterial counts and magnesium concentrations in the first experiment.

FIGURE 25. Scatter plot of sulfate-reducing bacterial counts and sulfate concentrations in the first experiment.

FIGURE 26. Scatter plot of acid-producing bacterial counts and sulfate concentrations in the first experiment.

FIGURE 27. Scatter plot of sulfate-reducing bacterial counts and phosphate concentrations in the first experiment.

FIGURE 28. Scatter plot of acid-producing bacterial counts and phosphate concentrations in the first experiment.

FIGURE 29. Scatter plot of sulfate-reducing bacterial counts and nitrate concentrations in the first experiment.

FIGURE 30. Scatter plot of acid-producing bacterial counts and nitrate concentrations in the first experiment.

FIGURE 31. Scatter plot of sulfate-reducing bacterial counts and sulfide concentrations in the first experiment.

FIGURE 32. Scatter plot of acid-producing bacterial counts and sulfide concentrations in the first experiment.

FIGURE 33. Scatter plot of sulfate-reducing bacterial counts and sulfide concentrations in the second experiment.

FIGURE 34. Scatter plot of acid-producing bacterial counts and sulfide concentrations in the second experiment.

FIGURE 35. Scatter plot of sulfate-reducing bacterial counts and total suspended solids in the first experiment.

FIGURE 36. Scatter plot of acid-producing bacterial counts and total suspended solids in the first experiment.

FIGURE 37. Scatter plot of sulfate-reducing bacterial counts and total suspended solids in the second experiment.

FIGURE 38. Scatter plot of acid-producing bacterial counts and total suspended solids in the second experiment.

FIGURE 39. Scatter plot of sulfate-reducing bacterial counts and total organic carbon in the first experiment.

© 1991 NOVA HUSKY RESEARCH CORPORATION

FIGURE 40. Scatter plot of acid-producing bacterial counts and total organic carbon in the first experiment.

FIGURE 41. Scatter plot of sulfate-reducing bacterial counts and total organic carbon in the second experiment.

FIGURE 42. Scatter plot of acid-producing bacterial counts and total organic carbon in the second experiment.

FIGURE 43. Bacterial counts on bull plugs from Unit # 1 before and after exposure at the field test facility.

FIGURE 44. Bacterial counts on bull plugs from Unit # 28 before and after exposure at the field test facility.

FIGURE 45. Bacterial counts on bull plugs from Unit # 6 and Wildmere Washtank before and after exposure at the field test facility.

FIGURE 46. Bacterial counts on bull plugs from Unit # 5 before and after exposure at the field test facility.

FIGURE 47. Bacterial counts on bull plugs from Unit # 14 before and after exposure at the field test facility.

FIGURE 48. Back-scattered electron image of surface on a sample coupon from the field test facility showing a mixture of corrosion deposits.

FIGURE 49. Energy dispersive X-ray spectrum arising from the surface of a sample coupon from the field test facility.

FIGURE 50. Scanning electron micrography showing bacterial cells (arrows) near the surface of the iron sulfide corrosion deposit matrix.

FIGURE 51. Thin-section transmission electron micrograph showing bacterial cells (arrows) embedded within the iron sulfide corrosion deposit matrix.

FIGURE 52. Thin-section transmission electron micrograph showing a heavily mineralized cellular ghost.

FIGURE 53. Energy dispersive X-ray spectrum from amorphous iron sulfide matrix in thin-sections of corrosion deposits from field test facility sample coupons.

FIGURE 54. Atom percent of iron, sulfur, and chlorine in the amorphous matrix and crystalloids of corrosion deposits from field test facility sample coupons.

© 1991 NOVA HUSKY RESEARCH CORPORATION

EXECUTIVE SUMMARY

The effects of injection water chemistry on the development of corrosive microbial biofilms, corrosion rates, and deposition of corrosion deposits was studied at an oil field water injection test facility near Wainwright, Alberta. Data were collected during two separate twelve week duration experimental runs. Attached bacterial populations were allowed to develop on removable steel sample coupons during the first four weeks of each experimental run. Chemical treatment started at week four, and continued uninterrupted for an additional eight weeks. Two different cocodiamine and bromonitropropane-diol based biocides were used in addition to a phosphonate scale inhibitor.

In the first four weeks of both experimental runs, all test lines were colonized to approximately 10^6 sulfate-reducing bacteria (SRB)/cm^2 and 10^3 organic acid-producing bacteria (APB)/cm^2. Once treatment started, distinct differences in the performance of the various chemicals against SRB and APB were noted. This suggests that biofilm permeability strongly influences biocide efficacy. At the same time, increases in corrosion rates were generally prevented by chemical treatment. The implication is that inactivation of sessile bacteria on steel surfaces does tend to retard the development of enhanced rates of corrosion.

Water chemistry at the field test facility was highly variable. Of the various chemical constituents present in the injection water, sulfate was notable in that it had a strong stimulative effect on SRB. Nitrate was inhibitory, whereas sulfide exhibited a positive correlation with SRB. While high concentrations of magnesium seemed to constrain SRB and APB, high bacterial counts coincided with an apparent optimal range of 15 to 20 ppm total organic carbon. When bull plugs with established biofilms were moved to the field test facility from other sites in the Wainwright oil field, SRB growth was favored over APB. These results indicate that injection water chemistry strongly influences microbial growth and population distribution in water injection systems.

Scanning electron microscopic examination of sample coupons from the field test facility revealed a variety of bacteria encrusted in successive stages of mineralization by iron sulfide corrosion deposits. No differences in corrosion deposit morphology were evident among the various chemical treatment protocols. In transmission electron microscope thin-sections, the corrosion deposits were highly porous. This observation suggests that complex pore geometries contribute to the meager permeability which constrains the penetration of biocides into biofilms.

Most of the iron sulfide corrosion deposits consisted of an amorphous sulfur-deficient chlorine-rich phase, as determined by energy dispersive X-ray spectroscopy and selected area electron diffraction. Iron sulfides are known to be highly aggressive towards steel, but tend to be easily polarized by cathodic hydrogen.

© 1991 NOVA HUSKY RESEARCH CORPORATION

Depolarization of the iron sulfide matrix by hydrogen-consuming SRB is expected to sustain high rates of corrosion, and induce the precipitation of a cationic sulfur-deficient iron sulfide phase that incorporates chloride ions to balance electrical charge.

© 1991 NOVA HUSKY RESEARCH CORPORATION

SOMMAIRE

Dans un puits-pilote d'injection aqueuse de la région pétrolière de Wainwright en Alberta, on a étudié la croissance de pellicules microbiennes corrosives, le taux de corrosion et la structure des dépôts de corrosion en fonction de la composition chimique des eaux d'injection. On a fait un bilan de travaux établis au cours de deux campagnes (distinctes) d'essais expérimentaux de 12 semaines chacune. Au cours des 4 premières semaines des essais, on a d'abord fait croître des cultures bactériologiques sur des plaquettes-échantillons amovibles d'acier, placées dans le système de circulation d'eau. Après quoi, le traitement chimique est appliqué pendant 8 semaines sans interruption. On a utilisé deux biocides différents à base de cocodiamine et de bromonitropropanediol, ainsi qu'un inhibiteur tampon à base de phosphonate.

Au bout des 4 premières semaines de chacune des 2 campagnes expérimentales, tous les échantillons témoins comportaient des colonies bactériennes réduisant le sulfate (BRS) à un taux approximatif de 10^6 bactéries/cm^2, ainsi que des colonies bactériennes produisant des acides organiques (BPA) à un taux de 10^3 bactéries/cm^2. Dès le début du traitement, on a aussitôt remarqué de nettes différences dans l'efficacité des différents produits chimiques contre les BRS et BPA. Ce fait révèle que l'efficacité des biocides est fortement fonction de la perméabilité des pellicules bactériologiques. Simultanément, le traitement chimique a empêché tout accroissement du taux de corrosion. Il en résulte que les bactéries, devenues passives mais restant toujours accrochées aux surfaces métalliques, tendent à ralentir la vitesse de corrosion.

Au cours des essais, la composition chimique des eaux d'injection au puits-pilote a été très variable. Parmi les substances présentes, les sulfates ont effectivement stimulés la croissance des BRS. Les nitrates ont eu un effet inhibiteur, tandis que les sulfures ont donné une corrélation positive avec les BRS. De fortes concentrations de magnésium semblent inhiber les BRS et BPA. On a remarqué un nombre élevé de colonies bactériennes lorsque la concentration totale en carbone organique était entre 15 et 20 ppm. Lorsqu'on a fixé des boulons-témoins comportant des pellicules microbiennes provenant d'autres puits-pilotes du site pétrolier de Wainwright, on a remarqué que la croissance des BRS était plus forte que celle des BPA. Ces résultats ont clairement démontré que la composition chimique des eaux d'injection influençait fortement la croissance et la population microbienne.

Une observation microscopique des échantillons par balayage électronique a révélé que certaines variétés de bactéries s'incrustaient dans les couches successives de sédimentation de sulfure de fer résultant de la corrosion. Aucune différence notoire n'a été remarquée dans la morphologie des dépôts de corrosion en fonction des différents traitements chimiques appliqués. Une observation microscopique par transmission lumineuse d'une couche mince des dépôts de corrosion, a révélé qu'ils étaient très poreux. Cette observation suggère qu'une géométrie poreuse et complexe contribue à amoindrir la perméabilité, facilitant ainsi la pénétration des biocides dans les pellicules microbiennes.

Une analyse spectroscopique aux rayons-X par énergie dispersée et diffraction électronique sur zone sélectionnée, a pu déterminer que les dépôts de sulfure de fer résultant de la corrosion, consistent surtout en une phase amorphe riche en chlore et déficiente en soufre. Bien qu'on sache que les sulfures de fer accélèrent la corrosion de l'acier, ceux-ci tendent facilement à être polarisés par de l'hydrogène cathodique. La dépolarisation d'une matrice de sulfure de fer par des BRS consommant de l'hydrogène entraîne une accélération de la corrosion, et provoque la précipitation d'une phase cationique de sulfure de fer déficiente en soufre et comportant des ions chlorures équilibrant les charges électriques.

© 1991 NOVA HUSKY RESEARCH CORPORATION

1.0 OBJECTIVES

Evaluate effects of injection water chemistry on microbial growth and population distributions on carbon steel coupons and bull plugs in the field under various chemical treatment protocols.

Monitor *in situ* corrosion rates, determine chemical composition of corrosion deposits, and attempt to correlate with microbiological data.

2.0 INTRODUCTION

Adherent microbial biofilms cause extensive fouling and corrosion of internal pipe surfaces in oil field water injection systems (Ruseska *et al.*, 1982). While chemical treatments for mitigation of bacterial corrosion and associated equipment failures substantially increase operating costs (Chen and Chen, 1984), little is known about the effects of various treatment protocols or injection water chemistry on attached bacterial populations and corrosion rates in the field. This basic information linking microbiological data to risk of corrosion is needed for accurate cost/benefit analyses in biocorrosion control programs.

NOVA HUSKY Research Corporation (NHRC) has an established field test facility at Unit #13 waterplant of HUSKY OIL's Wainwright oil field water injection system near Lloydminster, Alberta. This facility is unique in Canada, and permits monitoring of natural microbial biofilms on five separate flow lines. There are 40 removable coupons and individual injector systems on each line which permit *in situ* monitoring of biofilm responses to various chemicals (e.g., biocides). The field test facility is also fully instrumented to determine the extent of biofouling from the pressure drop across test lines, and can be equipped with probes to measure corrosion rates.

The impact of biocide dose on biofilm growth, microbial population density, corrosion deposits, and corrosion rates has been evaluated using the field test facility. This project was completed on 90/03/31 with funding provided on a 50/50 basis by NHRC and CANMET (DSS Contract No. 23440-9-9006/01-SQ). Results from this work suggested that biocide performance against sessile acid-producing bacteria (APB) and sulfate-reducing bacteria (SRB) is strongly influenced by injection water chemistry. This emphasized the need to assess how injection water chemistry influences the development of attached populations of corrosion enhancing bacteria and corrosion rates in oil field production operations. The present investigation was undertaken to specifically address these concerns.

© 1991 NOVA HUSKY RESEARCH CORPORATION

3.0 METHODS

3.1 Field Test Facility

For this investigation, the NHRC field test facility was equipped with 0.95 mm diameter carbon steel coupons for routine microbiological analyses over two separate experimental runs. A special test line to accommodate 1.0 inch bull plugs was designed, constructed, and installed in place of a conventional test line for the second experiment. For this special test line, adherent populations of corrosion enhancing bacteria were allowed to develop on 1.0 inch diameter bull plugs installed at various water injection facilities in the Wainwright oil field. After four weeks, two bull plugs were removed at each facility. One complete set of plugs was immediately sent to NHRC for microbiological analyses, while the other set was installed in the bull plug test line for monitoring at the field test facility.

During the first four weeks of each experimental run, untreated water from the injection system was allowed to run through the five separate test lines. This colonization period was used to monitor biofilm growth and develop attached populations of microorganisms on the removable sample coupon surfaces. Chemical treatment started at week four of each experiment, and continued uninterrupted for an additional eight weeks (see Table 1 for treatment protocols). No chemical was injected into the bull plug test line.

3.2 Sample Collection and Processing

Carbon steel sample coupons were pulled biweekly from each line in paired sets. After removal, all sample coupons were immediately placed into sterile plastic vials which were subsequently filled with untreated water from the injection system. Samples of water from up-stream of the chemical injectors were also taken for chemical analyses. Bull plugs were removed an placed in vials for microbiological analyses four weeks after being installed at the field test facility. The specimen vials and water samples were then shipped to Calgary by plane for processing at NHRC. At NHRC, all microbiological work was done in a FORMA Scientific anaerobic chamber. Water samples were sent to AGAT Laboratories in Calgary for chemical analyses.

Exposed surfaces of the sample coupons and bull plugs were scrapped using sterile scalpel blades to remove attached microorganisms. The residue recovered from the coupons and bull plugs was then placed into tubes containing 10 mL of sterile Postgate minimal salts medium supplemented with 1.0 % (w/v) NaCl (Postgate, 1984). The tubes were subsequently sonicated for 5 minutes using a Bransonic 32 sonicator to disrupt aggregates of bacterial cells. These sample suspensions were used for all microbiological analyses.

© 1991 NOVA HUSKY RESEARCH CORPORATION

3.3 Analytical Methodology

3.3.1 Enumeration of sulfate reducing bacteria

Sulfate reducing bacteria (SRB) were enumerated by the Most Probable Number (MPN) technique. Serial dilutions from 10^{-1} to 10^{-8} were prepared by adding 0.5 mL of the sample suspensions or water to tubes containing 4.5 mL of Postgate B medium supplemented with 1.0 % (w/v) NaCl (Postgate, 1984). The tubes were then incubated at 25 °C for up to 21 days. Blackening to a tube due to iron sulfide formation was a positive indication of growth by sulfate reducing bacteria. Standard probability tables were then used to express the number of positive tubes as viable SRB per cm^2 of sample coupon surface.

3.3.2 Radiolabeled sulfate reduction assay

The activity of SRB was assessed by adding 1.0 mL aliquots of sample suspensions to tubes containing 1.0 mL of Postgate C medium supplemented with 1.0 % (w/v) NaCl and 0.8 µ/mL of ^{35}S-sulfate. A cup containing a paper wick saturated with 0.5 mL of 1.5 M zinc acetate was suspended from rubber stoppers in each tube to trap evolved H_2S. The assays were terminated after 6 hours of incubation at 25 °C by adding 1.0 mL of 6 M HCl to each tube. After an additional 24 hours, the wick cup assemblies were removed and placed into 10 mL of scintillation fluid. These samples were then counted a day later using a Rack Beta Model 1211 scintillation counter, and the µmoles H_2S produced/cm2/day calculated.

3.3.3 Enumeration of acid producing bacteria

Acid producing bacteria (APB) were enumerated by serial dilution of sample suspensions and water from 10^{-1} to 10^{-7} in BTI/APB medium (Bioindustrial Technologies Inc., Grafton, New York, U.S.A.). The growth of APB was revealed by a change in culture medium colour from red to yellow; the number of APB in the original samples was then calculated from the highest dilution at which growth occurred.

3.4 Corrosion Rate Measurements

Potentiodynaic polarization measurements were done at 2 to 3 week intervals using a Petrolite model M-4100 potentiodyne analyzer. General corrosion rates were determined from current density values at the intersection point of cathodic Tafel slopes and open circuit potentials. Pitting tendency rates were estimated from current density values at the intersection of cathodic Tafel slopes and return anodic curves.

© 1991 NOVA HUSKY RESEARCH CORPORATION

3.5 Electron Microscopy

Sample coupons were taken from each test line at the conclusion of both experimental runs for electron microscopic examinations. Immediately after removal, the coupons were immersed in vials containing 5.0 % (v/v) glutaraldehyde fixative in untreated water from the injection system. In this way, the attached bacterial populations were fixed for electron microscopy under conditions similar to those experienced *in situ*.

For the scanning electron microscope (SEM), coupons were washed 3 to 5 times with 0.1 M cacodyllic buffer at pH 7.0 and dehydrated through an ethanol-freon series to 100 percent freon. The sample coupons were then allowed to air dry. For the transmission electron microscope (TEM), coupons were immediately dehydrated through an ethanol-propylene oxide series to 100 percent propylene oxide. Then a drop of propylene oxide- epoxy resin (50/50 mix) was applied to the exposed surfaces of the coupons to impregnate corrosion deposits. After 24 hours, a drop of 100 percent epoxy resin was applied to the coupon surfaces and allowed to cure at 60 ^{o}C for 48 hours. The impregnated corrosion deposits were subsequently removed by differential cooling in liquid nitrogen, and embedded in epoxy resin to obtain thin-sections perpendicular to the steel surface.

Specimens prepared for the SEM were examined before and after gold sputter coating using a Hitachi S-2500 SEM operating at 15 kV. The SEM was equipped with a Tracor Northern energy dispersive X-ray spectrometer. Energy dispersive X-ray spectroscopy (EDS) was conducted in the selected area electron beam raster mode, and spectra were obtained by collecting counts for up to 200 seconds (live time). Transmission electron microscopy was done using a Philips EM 400T equipped with a LINK Analytical LZ-5 energy dispersive X-ray spectrometer. The TEM was operated at 100 kV with a liquid nitrogen-cooled anticontamination device in place at all times. Electron beam spot sizes of 400 nm or less were used for EDS, and counts were collected for 100 seconds (live time). Selected area electron diffraction (SAED) was used to identify amorphous and crystalline corrosion deposits. The d-spacings of SAED patterns was calculated with evaporated aluminum as a standard for camera length determinations.

4.0 RESULTS

4.1 Bacterial Surface Colonization

In the first four weeks before treatment started in both experimental runs, all test lines were colonized to approximately 10^6 SRB per cm^2 (Figure 1). The APB counts ranged from 10^2 to 10^3 per cm^2. These numbers

© 1991 NOVA HUSKY RESEARCH CORPORATION

are lower than those obtained during the most recent investigation at the field test facility (see comparative data in Figure 1); however, data from an earlier study does compare favorably with the observed extent of bacterial surface colonization. These fluctuations in size of attached bacterial populations can be explained by changes in injection water chemistry (i.e., nutrient availability for bacterial growth). Distinct differences in biocide performance occurred during the first experimental run. With the cocodiamine based biocide, SRB counts declined slowly after injection started at week four then increased at week 8 (Figure 2). No clear differences were apparent between the two cocodiame injection protocols. Conversely, the two bromonitropropane-diol biocides was not effective against SRB at any point in time after treatment began. None of the biocides had a clear inhibitory effect on APB as counts fluctuated over 3 orders of magnitude during treatment (Figure 3). In all cases, biocide treatment inhibited sulfate-reduction activity (Figure 4).

Biocide treatment sulfate-reduction activity (Figure 4).

In the second experimental run, SRB counts decreased in all lines after week four when biocide and scale inhibitor injection began (Figure 5). Numbers decreased until week 8, then increased slightly thereafter; however, a slight inhibitory effect was apparent at week 12 for the two cocodiamine based biocides and scale inhibitor. Again, none of the chemicals had a clear inhibitory effect on APB as counts generally remained between 10^2 and 10^3 (Figure 6). Similarly, sulfate-reduction activity was not clearly impacted by treatment as the production of hydrogen sulfide generally paralleled transitions in SRB counts (Figure 7).

4.2 Corrosion Rates

Measurements of corrosion rates in each test line varied considerably before chemical treatment in the two experimental runs (Table 2). The mean corrosion rate values from week 4 data of the first experimental run were 14 to 26 times higher than those of the second experimental run. Similar variations in corrosion measurements at the field test facility have been noted before. They can be attributed to a number of factors, including turbulent flow conditions which can give rise to cavitation effects and gas break-out around corrosion probe electrodes. These processes disturb electrical potential differences between electrodes and effectively prevent precise determinations of corrosion rates from current densities. Accordingly, corrosion rates measured in each test line after the start of chemical injection were normalized by corresponding week four values to obtain proportional ratios. These ratios indicate how corrosion rates changed during chemical treatment.

In the first experimental run, general corrosion rates increased approximately 2 times in the control line during the corresponding 8 week period of biocide treatment (Figure 8). Similarly, control line pitting tendency rates increased by a factor of 1.5 times (Figure 9). Treatment with the cocodiamine biocide roughly

© 1991 NOVA HUSKY RESEARCH CORPORATION

paralleled the control line with respect to changes in general corrosion rates, while a 2 to four fold increase in pitting tendency rates occurred. On the other hand, general corrosion and pitting tendency rates decreased with the 10 % active ingredient bromonitropropane- diol biocide in comparison to the control line. In the case of the 17 % active ingredient bromonitropropane-diol biocide, general corrosion rates increased by approximately 3.5 times after 8 weeks of treatment, whereas pitting tendency rates increased to the same extend as the control.

During the second experimental run, control line general corrosion and pitting tendency rates increased approximately 7 times over the 8 week treatment period (Figures 10 and 11). The two cocodiamine biocides allowed general corrosion rates to increase by only a factor of 2, while the scale inhibitor was less effective with nearly a 5-fold increase. Pitting tendency actually decreased somewhat upon initial treatment with the cocodiamine biocides; however, by week 12 the pitting tendency rates had increased 1 to 4 times with the 35 % active ingredient and 50 % active ingredient cocodiamine biocides, respectively. Again, the scale inhibitor was less effective than the biocides with a steady 4-fold increase in pitting tendency rates over the 8 week treatment period.

4.3 Injection Water Chemistry and Bacterial Populations

As expected, the injection water chemistry was highly variable during both experimental runs. To illustrate these changes in water chemistry, all data was normalized by corresponding week 2 measurements of major cations, anions, and water quality parameters (Table 3). The ratios obtained by normalization of the data provide an indication of how injection water chemistry changed during each experimental run.

In the first experimental run, concentrations of sodium, potassium, calcium, and manganese remained at a constant level (Figure 12). Magnesium concentrations increased sharply at week 4, then decreased slowly thereafter. Similarly, iron concentrations increased steadily to 15 times the original level at week 10 before retreating somewhat. While chloride levels remained relatively constant, phosphate and sulfide concentrations alternately increased and decreased by factors of up to 5 times (Figure 13). Nitrate levels went through a dramatic 3 orders of magnitude increase and decrease over the first 8 weeks of the experimental run, whereas sulfate concentrations increased almost 500 times over the last two weeks of monitoring (Figure 14). In terms of water quality, alkalinity remained virtually unchanged. Conversely, the concentration of total suspended solids decreased marginally as levels of total organic matter fluctuated slightly (Figure 15).

Injection water chemistry was slightly less variable during the second experimental run. Concentrations of sodium, potassium, calcium, magnesium, and manganese remained relatively constant (Figure 16). An

© 1991 NOVA HUSKY RESEARCH CORPORATION

increase in the level of iron started at week 4 and continued until week 12 when a greater than 20-fold increase was measured. Of the various anions that were monitored, only sulfide concentrations changed significantly with a 5 times increase at week four (Figure 17). This was followed by a progressive 6-fold decrease in concentration which persisted up to week 12. Again, alkalinity remained virtually unchanged while a slight overall increase in total suspended solids and total organic matter occurred (Figure 18).

The influence of injection water chemistry on attached bacteria was assessed by plotting viable SRB and APB counts against concentrations of highly variable cation, anion, and water quality parameters. These include iron, magnesium, sulfate, phosphate, nitrate, sulfide, total suspended solids, and total organic matter. Of the cations, only iron concentrations varied significantly in the two experimental runs. Sulfide, total suspended solids, and total organic matter also exhibited changes in concentration during each experiment.

Although iron levels changed considerably in both experimental runs, no obvious correlation with bacterial counts was found in the corresponding scatter plots (Figures 19 to 22). In contrast, a slight trend towards decreasing numbers of bacteria with increasing magnesium concentrations was evident from data obtained during the first experiment (Figures 23 and 24). The implication is magnesium concentrations increased to such an extent that the cation had an inhibitory effect on the SRB and APB.

A positive correlation between SRB counts and sulfate concentrations was established with data from the first experimental run (Figure 25). From the scatter plot, an increase of 1 to 2 orders of magnitude in bacterial counts corresponds roughly to a 450 times increase in sulfate levels. No distinct trend was evident in the plot of APB counts and sulfate levels (Figure 26). Similarly, no correlations were found between bacterial counts and phosphate levels (Figures 27 and 28).

The increase in nitrate concentrations during the first experimental run had a slight inhibitory effect on SRB as . numbers appear to decline with increasing levels of nitrate (Figure 29). This effect was not obvious for APB (Figure 30). While sulfide concentrations over the first experiment did not influence bacterial counts (Figures 31 and 32), a modest stimulative result was evident from data acquired during the second experimental run (Figures 33 and 34). This might be related to the lower concentrations of sulfide that prevailed as the second experiment progressed.

There were no distinct trends evident in scatter plots of total suspended solids and bacterial counts (Figures 35 to 38); however, some of the lower bacterial counts were associated with higher concentrations of total suspended solids. This suggests that surface scouring by particulate matter might be a factor in controlling the size of attached bacterial populations.

© 1991 NOVA HUSKY RESEARCH CORPORATION

In both experimental runs, maximum SRB counts were associated with concentrations of 15 to 20 ppm total organic carbon (Figure 39 and Figure 41). The same type of relationship is somewhat obvious for APB in the second experiment, but not in the first experiment (Figure 40 and 42). These results imply that a optimum concentration of organic carbon may exist in the range of 15 to 20 ppm for bacterial growth in the field.

4.5 Transition of Bacterial Field Populations

The installation of bull plugs from various water injection facilities in the Wainwright oil field at the field test facility caused some major changes in numbers of attached SRB and APB (Figures 43 to 47). On bull plugs from Unit # 1 waterplant (WP) and free water knockout (FWKO), SRB counts increased 4 orders of magnitude at the field test facility (Figure 43). In contrast, numbers of APB remained relatively constant or decreased slightly. A similar trend in SRB and APB counts was evident with bull plugs from Unit # 28 WP and FWKO (Figure 44), Unit # 6 FWKO (Figure 45), and Wildmere Washtank (Figure 45).

At Unit # 5, high numbers of SRB were detected at the WP and FWKO (Figure 46). The SRB counts remained as high (in the case of the WP) or increased (in the case of the FWKO) at the field test facility. In contrast, the high numbers of APB detected at Unit # 5 WP decreased 4 orders of magnitude at the field test facility. At the same time, APB counts on bull plugs from the FWKO (which were low in comparison to WP APB counts) increased 10-fold at the field test facility.

The numbers of SRB on bull plugs from Unit # 14 WP decreased by 4 orders of magnitude at the field test facility (Figure 47). Conversely, SRB counts for FWKO bull plugs at the field test facility increased by almost the same amount. Numbers of APB remained the same on WP bull plugs, and decreased about 2 orders of magnitude on FWKO bull plugs.

4.6 Corrosion Deposit Structure and Composition

An uneven distribution of corrosion deposits was found on the surfaces of sample coupons prepared for SEM. Most of the exposed surface area on the sample coupons was covered by a thin corrosion deposit layer (Figure 48). Thicker deposits with a caked appearance occurred at random on the coupon surfaces. These deposits typically generated Fe, S, Cl, Ca, P, and Si peaks in corresponding EDS spectra (Figure 49). There were no differences in the morphology or composition of the corrosion deposits among the various treatment protocols used in the two experimental runs.

Most of the thicker deposits exhibiting a caked appearance were relatively smooth, whereas peripheral or cracked regions tended to be porous with a sponge-like texture. The elemental composition of the different

© 1991 NOVA HUSKY RESEARCH CORPORATION

regions on the corrosion deposits were generally the same; however, bacterial cells were commonly observed in porous areas of the deposits (Figure 50). No bacteria were found in any of the thinner deposits on the sample coupons. As is evident in Figure 50, individual cells with a curved (i.e., vibroid) shape characteristic of *Desulfovibrio* species were easily discerned. In addition, other types of cellular morphologies (e.g., filamentous bacteria) were observed as expected for a complex biofilm community.

In thin-sections of the corrosion deposits examined by TEM, a variety of morphologically diverse bacteria were found embedded in the corrosion deposit matrix (Figure 51). Vibroid-shaped cells were prominent among the bacteria, as would be anticipated from the SEM observations. The bacteria were mostly concentrated near the outer surface of the corrosion deposits. Intact cells were found deeper within the corrosion deposits along with heavily mineralized cellular ghosts (Figure 52).

The bulk of the corrosion deposit matrix consisted of an amorphous chlorine-rich iron sulfide phase, as determined by SAED and EDS (Figure 53); however, in some areas the matrix exhibited a platy habit implying some degree of crystallinity (cf. Figure 52). These crystalloids contained significantly less chlorine, and more iron and sulfur than amorphous parts of the matrix (Figure 54). From d-spacings of 0.29, 0.23, 0.18, and 0.16 nm in SAED patterns, the crystalloids were identified as poorly ordered mackinawite (FeS0.9). Based on the frequency of observations by EDS and SAED, the corrosion deposit matrix consisted of approximately 90 percent amorphous material, and 10 percent mackinawite.

5.0 DISCUSSION

Bacterial surface colonization has been known since Zobell described the attachment and growth of marine bacteria on glass slides (Zobell and Allen, 1933; Zobell, 1943). It is know recognized as a basic growth strategy in nature which depends fundamentally on a combination of adhesion by means of extracellular polymers and sustained growth by attached bacterial cells (Costerton *et al.*, 1978; Caldwell *et al.*, 1981). This results in the formation microcolonies of morphologically identical cells which eventually coalesce with other microcolonies to establish complex biofilm communities similar to those occurring on internal pipe surfaces of oil field water injection systems.

The availability of nutrients plays an important role in the colonization of solid surfaces by bacteria. Salas and Geesey (1983) have shown that surface colonization rates and the adhesiveness of bacterial cells are usually diminished under starvation conditions. In addition, cells tend to slough from established biofilms in response to nutrient depletion (Delaquis *et al.*, 1989; Characklis and Cooksey, 1983). In view of these considerations, it is highly likely that a poorer supply of nutrients contributed to the comparatively low

© 1991 NOVA HUSKY RESEARCH CORPORATION

numbers of SRB and APB observed during this investigation and previous studies at the field test facility.

The results of this study indicate that inactivation of attached bacteria by chemical treatment was not solely related to the dosage level of a biocide. When comparisons were made on the basis of injection concentration and exposure time, no clear differences in performance against SRB and APB was discerned with the cocodiamine biocides. The implication is that, when a biocide is used at bactericidal levels, penetration into a biofilm (i.e., mass transfer) is an important rate limiting step (LeChevallier *et al.*, 1988; Ferris, 1990). Additional evidence in support of this concept comes from the better performance of the 35 % active ingredient cocodiamine biocide against SRB and APB than either of the two bromonitropropane-diol biocides. Presumably, the cocodiamine effectively penetrated the biofilms whereas the bromonitropropane-diol was excluded when the biocides were injected at approximately equal dosage levels.

The application of electrochemical techniques to measure corrosion rates in field operations is becoming increasing popular. While the use of weight-loss coupons is commonly used in long-term corrosion studies lasting days or weeks, an electrochemical measurement requires at most several hours to complete (EC&G Applied Instrument Group, 1982). A drawback of electrochemical corrosion rate determinations is that any perturbation of electrical potential difference and current flow between probe electrodes can cause significant deviations in measured values (Patton, 1979). For example, under turbulent flow conditions cavitation or gas break-out may occur around electrodes. This effectively decreases the working area of the electrodes and alters surface current density. On the other hand, the formation of electrically conductive iron sulfide films not only increases the working area of electrodes, but also generates galvanic coupling effects which can stimulate corrosion (Barnartt, 1976). These kinds of events, alone or in combination, provide an explanation for the difference in corrosion rates between the two experimental runs.

Normalization of corrosion rates measured after the start of chemical treatment by corresponding week four values facilitated a direct comparison of the various treatment protocols. In general, the cocodiamine biocides and scale inhibitor exhibited a tendency to retard increases in corrosion rates. At the same time, bacterial counts decreased somewhat. These data suggest that chemical inactivation of attached SRB and APB on steel surfaces can sustain lower corrosion rates. Exceptions to this situation occurred with the two bromonitropropane-diol biocides. In one case, corrosion rates actually decreased while, in the other instance, corrosion rates increased. These effects are difficult to understand, particularly as the biocides performed poorly against surface attached bacteria.

Water produced with oil is commonly injected back underground to maintain reservoir pressure and enhance recovery by sweeping residual oil towards producing wells (Ostroff, 1979). As the volume of oil available for production decreases, requirements for water increase. In order to satisfy the additional demands for water,

© 1991 NOVA HUSKY RESEARCH CORPORATION

other sources are utilized (e.g., lakes, rivers, or wells). At the same time, a variety of chemicals like oxygen scavengers, corrosion inhibitors, and scale inhibitors are added to water at oil field production facilities. Thus, it is not surprising that the injection water chemistry at the field test facility was found to be highly variable over both experimental runs.

Despite the variability in composition, values obtained for injection water chemistry at the field test facility were typical of oil production operations. Most produced waters tend to be highly saline, and may contain upwards of 220,000 ppm of dissolved solids, suspended solids, and organic carbon (i.e., oil, grease, and other organic molecules) (Ostroff, 1979). Sodium and chloride are generally the ions present in the largest amounts. Other ions commonly encountered in injection water include potassium, calcium, magnesium, sulfate, bicarbonate, and carbonate. The later two of these contribute to alkalinity (reported as ppm $CaCO_3$), while the presence of sulfide is generally be attributed to SRB. Nitrate, phosphate, iron, and manganese are less common constituents of injection water; however, both of these anions were detected in water from the field test facility suggesting introduction from an external source (e.g., surface derived make-up water). On the other hand, iron and manganese can be derived from corrosion of steel pipes, tubulars, and tanks.

Of the various chemical constituents in the injection water at the field test facility, sulfate is notable in that it serves as the primary electron acceptor for sulfate reducing bacteria. These bacteria derive energy for growth through anaerobic respiration during which the oxidation of simple carbon compounds (e.g., acetate or lactate) is coupled to the reduction of sulfate (Hamilton, 1985). Conversely, APB are generally fermentative microorganisms that simultaneously oxidize and reduce organic molecules. These basic physiological traits of SRB and APB explain why a strong positive correlation was found between viable SRB counts and sulfate levels in the injection water, whereas APB were largely uneffected. Furthermore, this provides compelling evidence which indicates that the availability of sulfate is a key parameter for corrosion involving SRB in oil field water injection systems.

An inhibitory effect on bacteria was noted with both magnesium and nitrate. In the case of magnesium, SRB and APB were adversely influenced by exceptionally high concentrations of the cation. The precise reason for this is not known as magnesium is required for the assembly, stability, and functioning of the plasma membrane in bacteria (Collins and Stotzky, 1989); however, it is possible that the normal calcium-magnesium exchange processes which occur across the plasma membrane of bacterial cells was disrupted by high levels of magnesium ions (Sprott, 1989). On the other hand, nitrate is known to exchange with sulfate and suppresses SRB growth by acting as an inefficient electron acceptor analogue. From this, it follows that nitrate did not effect APB.

There are two possible explanations for the positive correlation between SRB counts and sulfide

© 1991 NOVA HUSKY RESEARCH CORPORATION

concentrations obtained with data from the second experimental run. In the first case, increasing sulfide levels generally enhance and sustain the development of anaerobic conditions which favor the growth of SRB. Alternatively, one would anticipate the evolution of elevated concentrations of sulfide from actively growing populations of SRB, particularly when sulfate is present in sufficient quantities. The second interpretation conforms with the Monod equation which delineates nutrients effects on microbial growth (Dawes and Sutherland, 1976). Also, it is consistent with data from the first experimental run which suggested that no relationship existed between SRB and sulfide. In this situation, sulfate levels (which were higher than in the second experiment) probably exceeded SRB requirements so sulfide concentrations remained unchanged.

The peculiar correlation between bacterial counts and total organic carbon infers that SRB and APB growth occurs optimally over a narrow concentration range (15 to 20 ppm). Below this range, bacterial growth is presumably limited by a poor supply of organic nutrients. Conversely, the formation and accumulation of production of inhibitory metabolic waste products within biofilms is likely to be a problem when organic nutrients are present in excess amounts. This effect relates to the mass transfer and diffusion limitations imposed on biocides by biofilms. Similar constraints presumably exist in biofilms for the outward diffusion of toxic metabolic products formed by attached bacteria.

The importance of injection water chemistry for microbial growth in oil field production operations is emphasized by the results from the bull plug test line. Established populations of SRB and APB clearly changed with respect to numbers and distribution when exposed to injection water at the field test facility. In most cases, SRB counts increased or remained steady while numbers of APB generally declined. This indicates that conditions at the field test facility not only enhanced the growth of SRB over APB, but also were more favorable for SRB relative to other production operations in the Wainwright oil field. An interesting exception to this general trend occurred with bull plugs from Unit # 14 WP. In this case, SRB counts declined suggesting that an extremely unique site specific population existed at Unit # 14 WP. All of these data imply that injection water chemistry is extremely important for the development and growth of attached populations of corrosion enhancing bacteria under field conditions. Further research is needed to more accurately determine how injection water chemistry and microbial population distributions relate to corrosion problems in oil field production systems.

As in an earlier investigation, direct examination of sample coupons from the field test facility by SEM revealed a variety of bacteria including vibroid cells reminiscent of *Desulfovibrio* species. The bacteria were commonly exposed in porous regions of corrosion deposits which predominantly consisted of iron, sulfur, and chlorine. In some cases, bacterial cells were partly entrained within the corrosion deposit matrix and appeared to be mineralized by iron sulfide. Epitaxial nucleation and crystal growth of such inorganic

© 1991 NOVA HUSKY RESEARCH CORPORATION

mineral precipitates on bacterial surfaces is well documented (Beveridge *et al.*, 1983; Beveridge *et al.*, 1989; Ferris *et al.*, 1987; Ferris *et al.*, 1989). It occurs as anionic structural polymers in the cell walls of bacteria bind metallic ions which then precipitate at the cell surface by reaction with counterions in solution. Further growth of these deposits can proceed via homogenous crystal nucleation reactions (Berner, 1980). These kinds of processes explain the mineralization of bacteria on sample coupons from the field test facility. Presumably, dissolved iron arising from the corrosion of the steel sample coupons was complexed by surface polymers of attached bacteria. Then the bound iron reacted with bacteriogenic or indigenous sulfide in the injection water to precipitate the iron sulfide corrosion deposits.

While SEM revealed surface topology of the corrosion deposits, TEM exposed internal structure. In thin-sections, a highly porous matrix containing bacteria was easily discerned. Corrosion deposit porosity must play an important role in terms of permeability which controls the inward or outward movement of biocides, nutrients, and metabolic waste products from bacteria. Permeability is defined as the ability of a porous matrix to let fluid molecules flow through an interconnected pore network (Baijal, 1982). Meager permeability arises when there is little interconnection between pores, so the geometry of porous structure is a critical factor. Given the complex pore geometry of the corrosion deposits, it is not difficult to appreciate that permeability constraints for fluid molecules exist within biofilms of corrosion enhancing bacteria.

The TEM examination of corrosion deposits also permitted a more detailed analysis of mineral and elemental composition by EDS and SAED. In terms of bulk composition, at least 90 % of the corrosion deposit matrix consisted of an amorphous chlorine-rich iron sulfide phase. Trapped clay particles and poorly ordered crystalloids of mackinawite (i.e., $FeS_{0.9}$) made-up the remainder. These data have important implications for the mechanisms of microbial corrosion. The classical theory of von Wolzogen Kuhr (von Wolzogen Kuhr and van der Vlugt, 1939) infers that hydrogen-consuming bacteria accelerate corrosion by removing cathodic hydrogen from steel (i.e., depolarize cathodic surfaces); however, efforts to demonstrate this in the laboratory using pure cultures of bacteria have largely failed to arrive at corrosion rates equivalent to those experienced in the field (Jack *et al.*, 1986). This consideration implies that microbial corrosion is a more complex process. In other studies, chemically synthesized or biogenically formed iron sulfides have been shown to enhance corrosion rates which later decrease as the sulfide matrix becomes polarized by cathodic hydrogen (King and Wakerly, 1973; Smith and Miller, 1975). If hydrogen-consuming bacteria are added to such systems, high rates of corrosion are sustained (Jack *et al.*, 1986). These results suggest that bacteria enhance corrosion by removing cathodic hydrogen from iron sulfides galvanically coupled to steel surfaces. King and Wakerley (1973) recognized this possibility and proposed that a series of reactions occur in the presence of bacteria, as follows:

© 1991 NOVA HUSKY RESEARCH CORPORATION

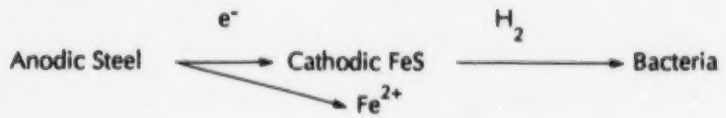

The presence of bacteria embedded in iron sulfide corrosion deposits as observed by SEM and TEM is consistent with this modified version of the cathodic depolarization theory for microbial corrosion; however, the iron-sulfur-chlorine stoichiometry (approximately $FeS_{0.5}Cl$) of the amorphous corrosion deposit phase is highly unusual. If the oxidation states of ferrous iron and sulfide are taken into account, it would appear that chloride ions maintain charge balance instead of expected hydroxyl ions. Presumably, chloride ions are favored because of their abundance in injection water. On the other hand, sulfur deficiency conforms with the cathodic depolarization theory and the following cyclical reaction sequence involving SRB:

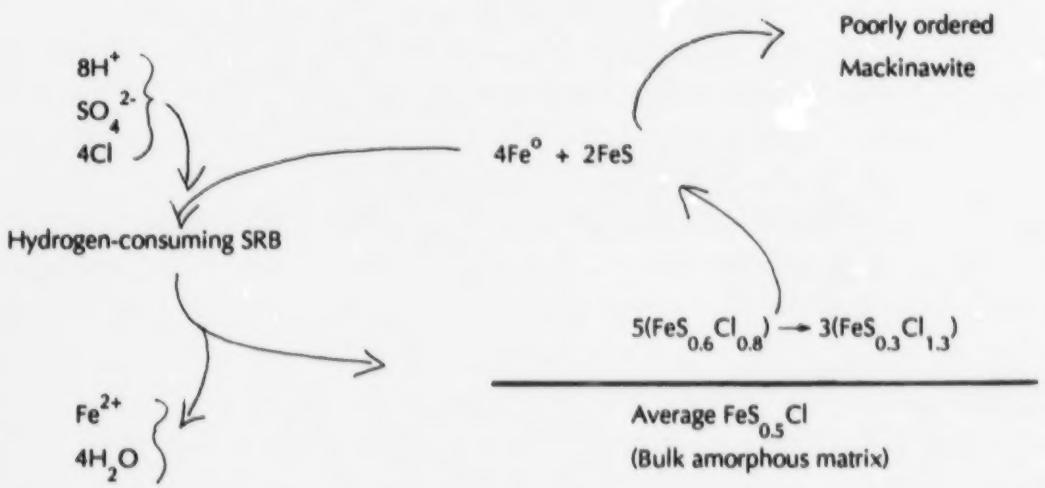

In this series of reactions, sulfate reduction is coupled to oxidation of iron and formation of cathodic hydrogen in association with the iron sulfide matrix. Chloride ions are derived from the water phase, whereas protons probably arise from the oxidation of organic carbon substrates by SRB (Odom and Peck, 1984). When the cathodic hydrogen is removed or disbonded from the iron sulfide matrix by the SRB, sulfate is reduced. A cationic sulfur deficient iron sulfide phase is precipitated that requires chloride ions to balance charge. At the same time, ferrous iron is liberated from the anodic site. As the cycle repeats, an amorphous corrosion deposit with an average composition of $FeS_{0.5}Cl$ develops. When bacterial activity ceases, poorly ordered mackinawite forms within the amorphous corrosion deposit matrix. The precise manner in which iron sulfides contribute to cathodic hydrogen forming reactions is not known; however, the crystal structure of iron sulfides gives rise to metallic properties which apparently make these compound easily polarizable (Cotton and Wilkinson, 1962; King and Wakerley, 1973; Smith and Miller, 1975). This might occur through

© 1991 NOVA HUSKY RESEARCH CORPORATION

the generation of interstitial cathodic hydrogen, or by the formation of H-S bonds within the sulfide matrix (King and Wakerley, 1973). In any event, removal or disbonding of this polarizing hydrogen by SRB not only sustains high rates of corrosion (Jack *et al.*, 1986), but also provides a source of energy for bacterial growth (Odom and Peck, 1984). These consideration provide a reasonable explanation for the preferential growth of bacteria within amorphous iron sulfide corrosion deposits.

6.0 CONCLUSIONS

- The extent to which steel surfaces are colonized by corrosion enhancing bacteria depends strongly on injection water chemistry (i.e., nutrient availability). Numbers of attached bacteria tend to decrease when nutrient limitations arise as a result of variable injection water chemistry.

- Diffusion rates in biofilms seem to determine the efficacy of chemicals against attached bacteria populations. Active ingredients used in biocides differ in their ability to penetrate biofilms and inactivate bacteria.

- Chemical treatments to inactivate sessile bacteria on steel surfaces generally prevent increases in corrosion rates; however, some bactericidal chemical formulations (regardless of active ingredient) are more effective at retarding corrosion rates than others.

- Water chemistry at the field test facility was highly variable. Of the various chemical constituents present in the injection water, sulfate had a profound stimulative effect on SRB. Nitrate was inhibitory, whereas sulfide exhibited a positive correlation with SRB. While high concentrations of magnesium constrained SRB and APB, high bacterial counts coincided with an optimal range of 15 to 20 ppm total organic carbon.

- Conditions at the field test facility enhanced the growth of SRB over APB, and favored SRB relative to other production operations in the Wainwright oil field. Relationships between injection water chemistry, microbial population distributions, and corrosion problems in oil field production systems remain to be determined.

- The permeability of biofilms on steel surfaces is controlled to a large extent by corrosion deposit porosity. Complex pore geometries contribute to meager permeability which constrains the inward and outward movement of fluid molecules, including biocides and metabolic waste products from bacteria.

© 1991 NOVA HUSKY RESEARCH CORPORATION

- Amorphous iron sulfide corrosion deposits that develop in association with biofilms on steel surfaces contribute to corrosion by coupling entrained bacteria to cathodic reactions. As hydrogen-consuming SRB depolarize the iron sulfide matrix and reduce sulfate, high rates of corrosion are sustained. This results in the precipitation of a cationic sulfur deficient iron sulfide phase that, at the field test facility, incorporates chloride ions to balance electrical charge.

7.0 REFERENCES

Barnartt, S. 1979 *In* Proceeding of NACE Symposium on Electrochemical Techniques for Corrosion Control (R. Baboian, ed.), NACE, Houston.

Berner, R.A. 1980. Early Diagenesis: a theoretical approach. Princeton University Press, Lawrenceville.

Berveridge, T.J., D.J. Meloche, W.S. Fyfe, and R.G.E. Murray. 1983. Appl. Environ. Microbiol. 45: 1094-1108.

Beveridge, TJ. 1989. Ann. Rev. Microbiol. 43: 147-171.

Caldwell, D.E., D.K. Brannan, M.E. Moaris, and M.R. Betlach. 1981. Microb.Ecol. 7: 1-11.

Characklis, W.G. and K.E. Cooksey. 1983. Adv.Appl.Microbiol. 18: 93-138.

Chen, E.Y. and R.B. Chen. 1984. J.Petrol.Technol. 36: 1171-1176.

Collins, Y.E. and G. Stotzky. 1989. p.31-90. *In* Metallic Ions and Bacteria (T.J. Beveridge and R.J. Doyle, eds.), John Wiley and Sons, New York.

Costerton, J.W., G.G. Geesey, and K.J. Cheng. 1978. Sci.Am. 238: 86-95.

Cotton, F.A. and G. Wilkinson, 1962. Advanced Inorganic Chemistry, John Wiley and Sons, New York, 959 pp.

Dawes, I.W. and I.W. Sutherland. 1976. Microbiol.Physiology, Backwell Scientific, London. 185 pp.

© 1991 NOVA HUSKY RESEARCH CORPORATION

Delaquis, P.J., D.E. Caldwell, J.R. Lawrence, and A.R. McCurdy. 1989. Microb. Ecol. 18 : 199-210.

EG & G Princeton Applied Research, Applied Instrument Group. 1982. Application Note Corr 1, 12 pp.

Ferris, F.G. 1989. Evaluation of Biocorrosion in Pipelines, Final Report to CANMET, Contract Serial No. 23440-8-9186/01-SQ.

Ferris, F.G., W.S. Fyfe, and T.J. Beveridge. 1987. Chem. Geol. 63 : 225-232.

Ferris, F.G., K. Tazaki, and W.S. Fyfe. 1989. Chem. Geol. 74 : 321-330.

Ferris, F.G., 1990. Internal Biocorrosion of Steel Pipes, Final Report to CANMET, Contract Serial No. 23440-9-9006/01-SQ, 48 pp.

Hamilton, W.A., 1985. Ann. Rev. Microbiol. 39 : 195-217.

Jack, T.R., M.McD. Francis, and R.G. Worthingham. 1986. p. 339-350 *In* Proceedings of the International Conference on Biologically Induced Corrosion (S.C. Dexter, ed.), NACE, Houston.

King, R.A. and D.S. Wakerley, 1973. Br. Corros. J. 8 : 41-45.

LeChevallier, M.W., C.D. Cawthorn, and R.G. Lee. 1988. Appl. Environ. Microbiol. 54 : 2492-2499.

Odom, J.M. and H.D. Peck. 1984. Ann. Rev. Microbiol. 38 : 551-592.

Ostroff, A.G. 1979. Introduction to Oilfield Water Technology, NACE, Houston. 394 pp.

Patton, C.C. 1979. Corrosion Control in Petroleum Production. NACE, Houston, 101 pp.

Postgate, J.R. 1984. The Sulfate-reducing Bacteria, 2nd ed., Cambridge University Press, Cambridge.

Ruseska, I., J. Robbins, and J.W. Costerton. 1982. Oil and Gas Journal, March 8, p. 253-264.

Salas, S.D. and G.G. Geesey, 1983. Microb. Ecol. 9 : 307-315.

Sprott, G.D. 1989. p. 91-120. *In* Metallic Ions and Bacteria (T.J. Beveridge and R.J. Doyle, eds.), John

© 1991 NOVA HUSKY RESEARCH CORPORATION

Wiley and Sons, New York.

Smith, J.S. and J.D.A. Miller. 1975. Br. Corros. J. 10 : 136-143.

von Wolzogen Kuhr, C.A.H. and L.W. van der Vlugt. 1934. Water Den Haag 16 : 147.

Zobell, C.E. 1943. J. Bacteriol. 46 : 39-54.

Zobell, C.E. and E.C. Allen. 1933. Proc. Soc. Exp. Biol. Med. 30: 1409-1411.

© 1991 NOVA HUSKY RESEARCH CORPORATION

8.0 TABLES

© 1991 NOVA HUSKY RESEARCH CORPORATION

Table 1: Treatment protocols for first and second experimental runs		
	TREATMENT PROTOCOL	
TEST LINE	FIRST EXPERIMENT	SECOND EXPERIMENT
1	Cocodiamine Biocide, 35% Active, 250 ppm, 6 hrs on, 42 hrs off	Cocodiamine Biocide, 35% Active, 250 ppm, 6 hrs on, 42 hrs off
2	Cocodiamine Biocide, 35% Active, 126 ppm, 6 hrs on, 82 hrs off	Cocodiamine Biocide 50% Active 250 ppm, 6 hrs on, 42 hrs off
3	Control (no chemical)	Control (no chemical)
4	Bromonitropropane-diol Biocide, 17% Active 120 ppm, 8hrs on, 40 hrs off	Phosphonic Acid Scale Inhibitor, 250 ppm, 6 hrs on, 42 hrs off
5	Bromonitropropane-diol Biocide, 10% Active, 200 ppm, 8 hrs on, 40 hrs off	Modified Test Line For Bull Plugs

© 1991 NOVA HUSKY RESEARCH CORPORATION

Table 2: Corrosion rates measured at week 4 (prior to chemical treatment) in first and second experimental runs

	CORROSION RATE (mpy)			
	FIRST EXPERIMENT		SECOND EXPERIMENT	
TEST LINE	GENERAL	PITTING	GENERAL	PITTING
1	1.00	23.50	0.46	15.00
2	1.60	47.00	0.07	2.40
3	0.70	27.00	0.05	1.80
4	3.30	230.00	0.09	3.30
5	5.58	400.00	-	-
MEAN	2.44	145.50	0.17	5.63
STANDARD ERROR	0.90	74.21	0.10	3.14

© 1991 NOVA HUSKY RESEARCH CORPORATION

Table 3: Injection water chemistry at week 2 of the first and second experimental runs		
	WATER CONSTITUENTS (ppm)	
PARAMETER	FIRST EXPERIMENT	SECOND EXPERIMENT
CATIONS		
Na^+	25000	24000
K^+	510	320
Ca^{2+}	2200	2000
Mg^{2+}	1000	1000
Fe^{3+}	0.24	0.37
Mn^{2+}	0.50	0.28
ANIONS		
Cl^-	53000	39000
SO_4^{2-}	0.10	0.10
NO_3^{2-}	0.10	0.10
PO_4^{2-}	0.03	0.20
S^{2-}	1.10	0.50
WATER QUALITY		
Alkalinity (as $CaCO_3$)	510	450
Total Suspended Solids	2400	210
Total Organic Matter	20	14

© 1991 NOVA HUSKY RESEARCH CORPORATION

9.0 FIGURES

© 1991 NOVA HUSKY RESEARCH CORPORATION

FIGURE 1. **Mean values of viable counts for sulfate-reducing and acid producing bacteria after four weeks of colonization at the field test facility.**

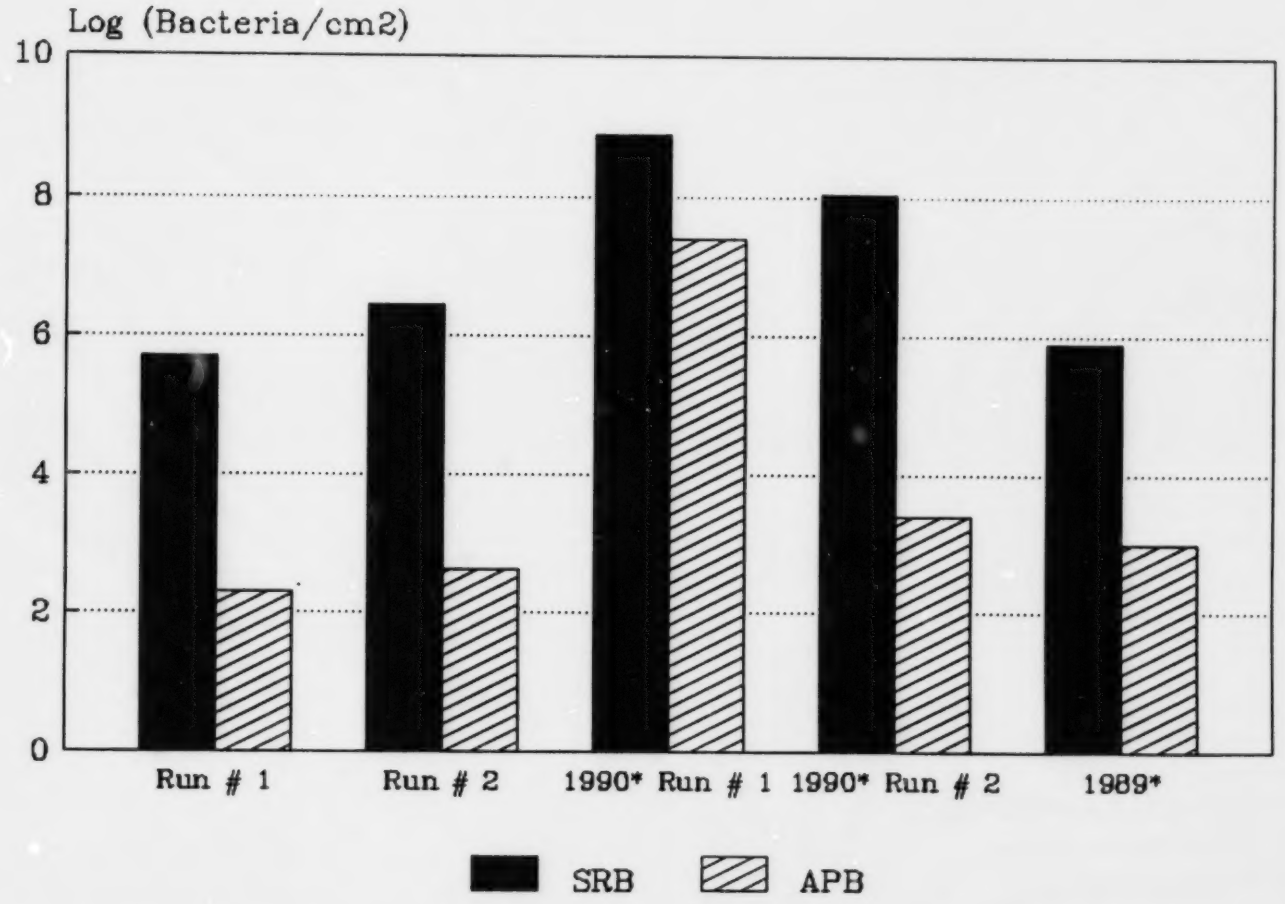

* Note: From Ferris, 1990.

© 1991 NOVA HUSKY RESEARCH CORPORATION

FIGURE 2. **Sulfate-reducing bacterial counts during the first experimental run.**

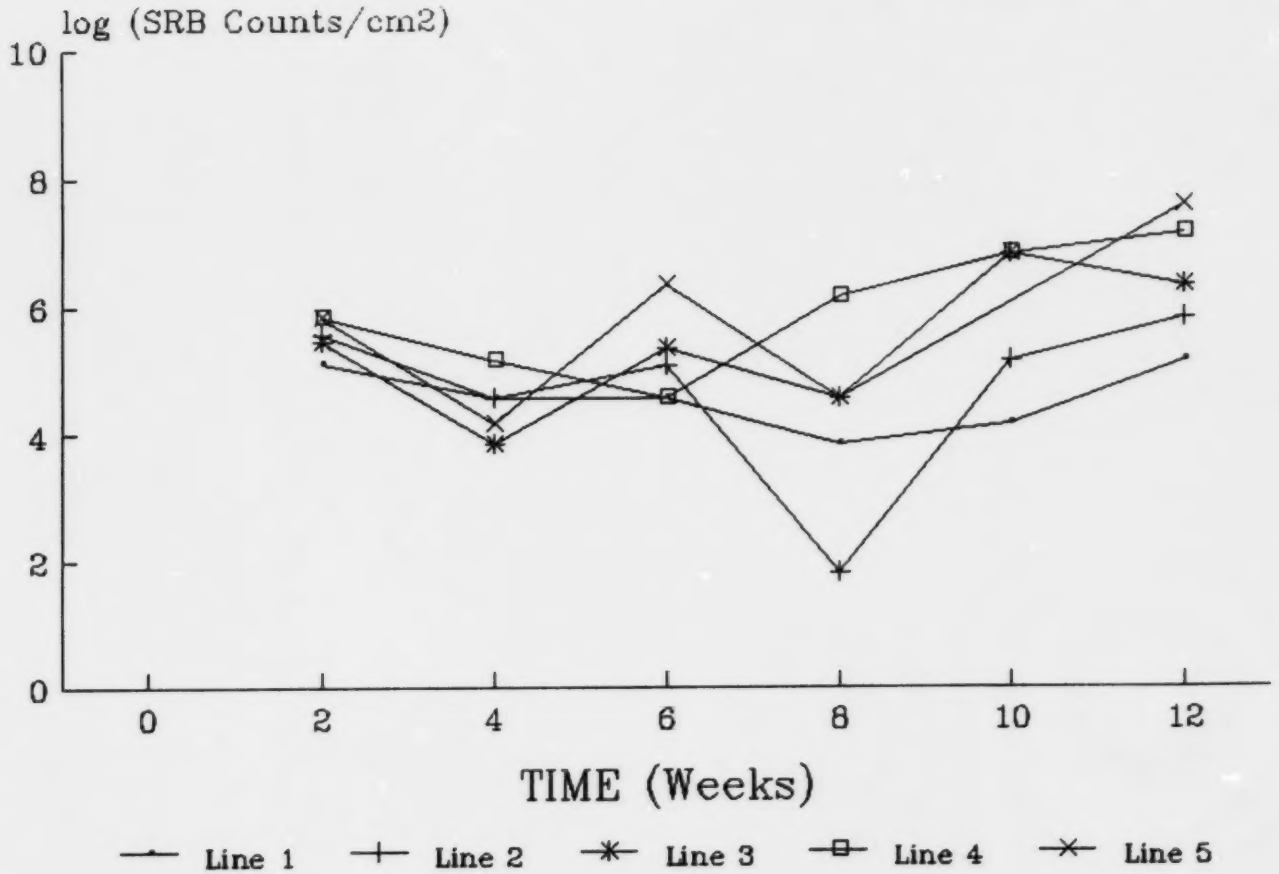

© 1991 NOVA HUSKY RESEARCH CORPORATION

FIGURE 3. **Acid-producing bacterial counts during the first experimental run.**

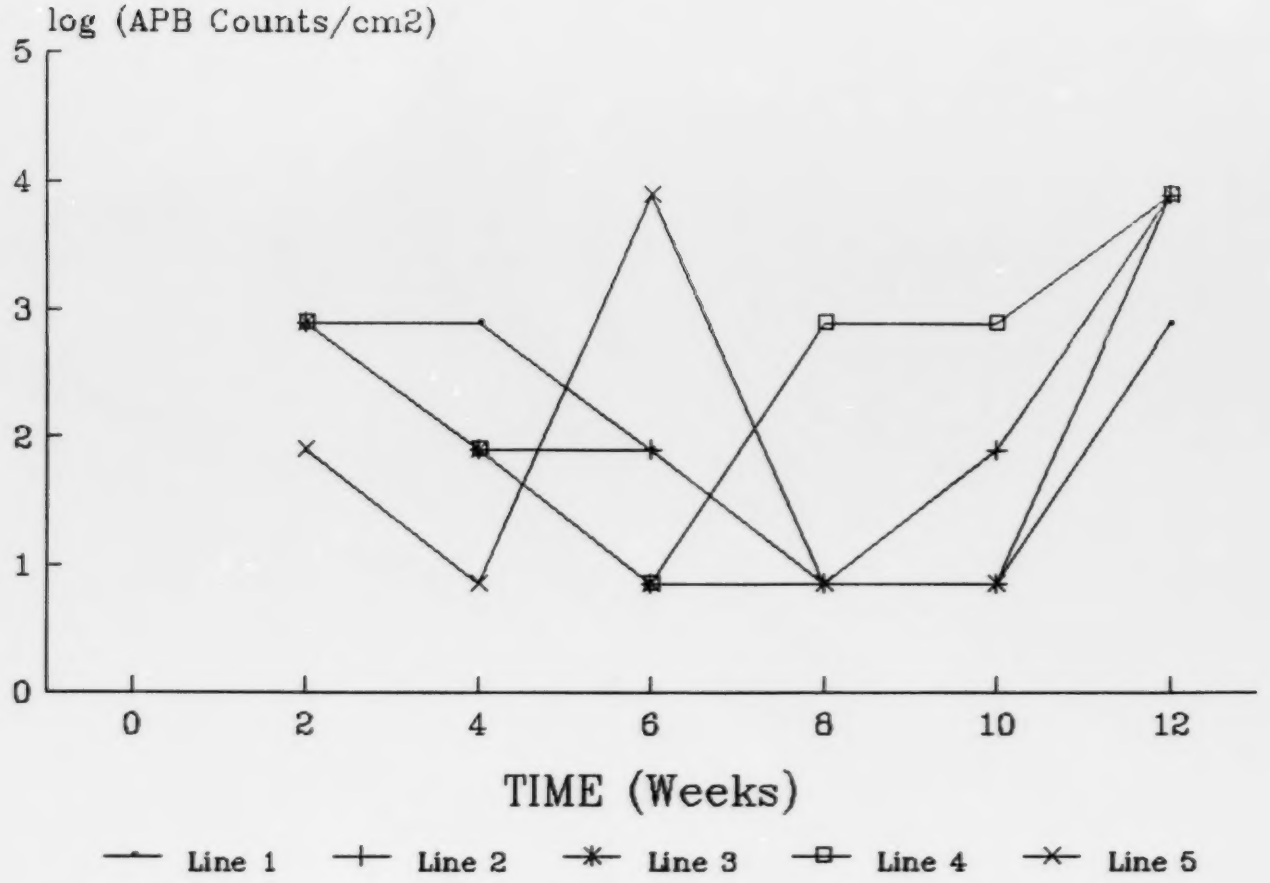

© 1991 NOVA HUSKY RESEARCH CORPORATION

FIGURE 4. Sulfate-reduction activity during the first experimental run.

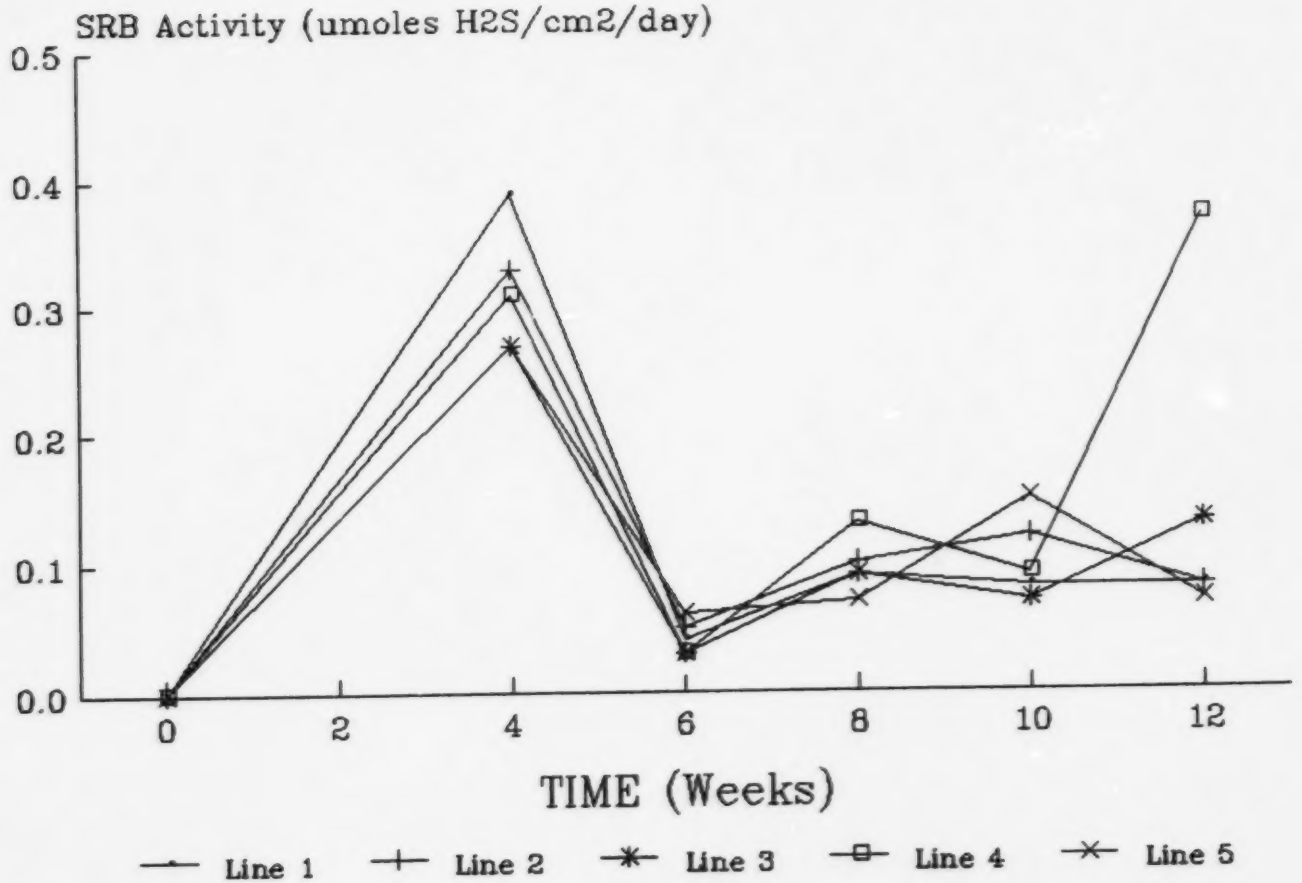

© 1991 NOVA HUSKY RESEARCH CORPORATION

FIGURE 5. **Sulfate-reducing bacterial counts during the second experimental run.**

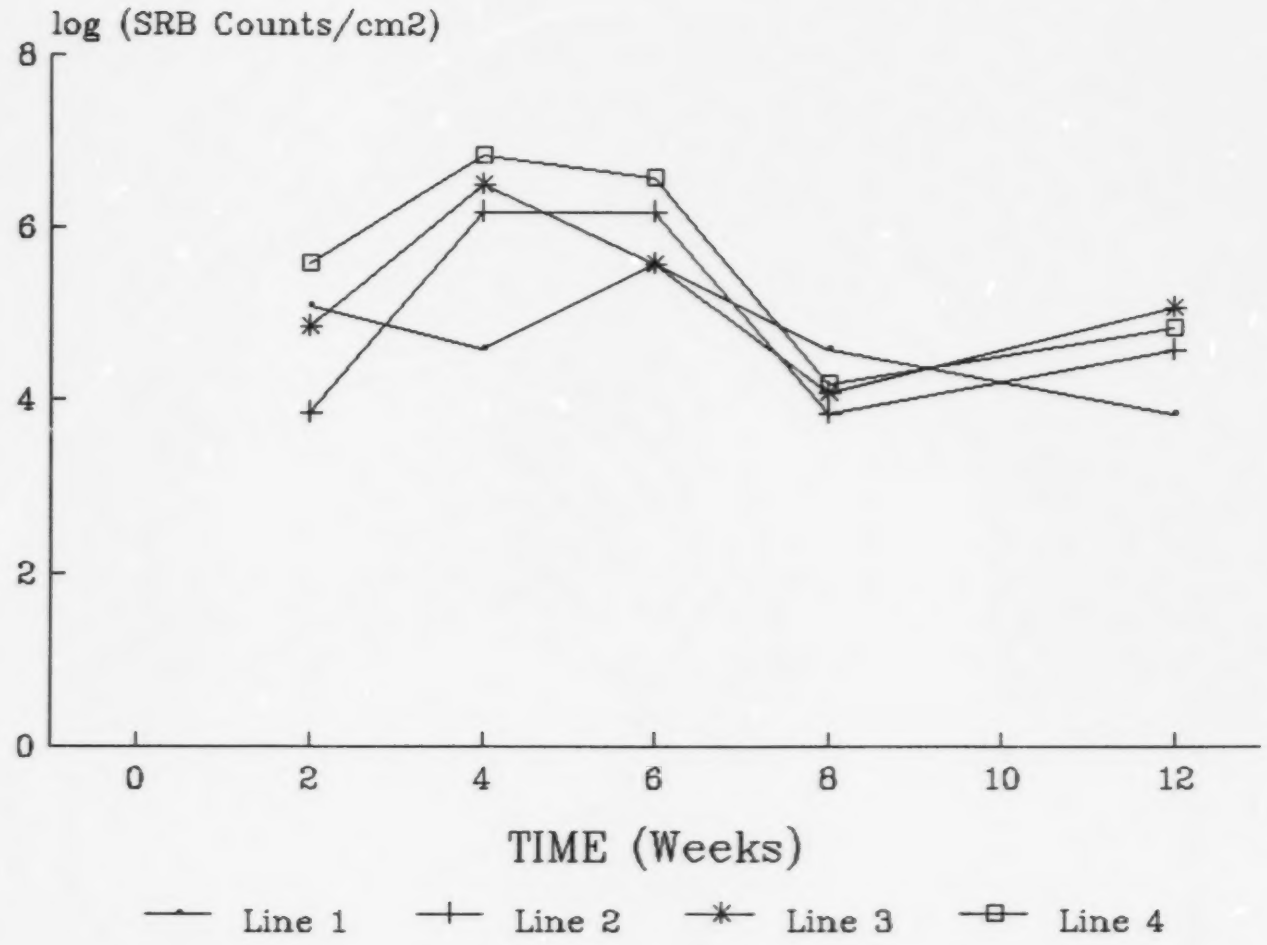

© 1991 NOVA HUSKY RESEARCH CORPORATION

FIGURE 6. Acid-producing bacterial counts during the second experimental run.

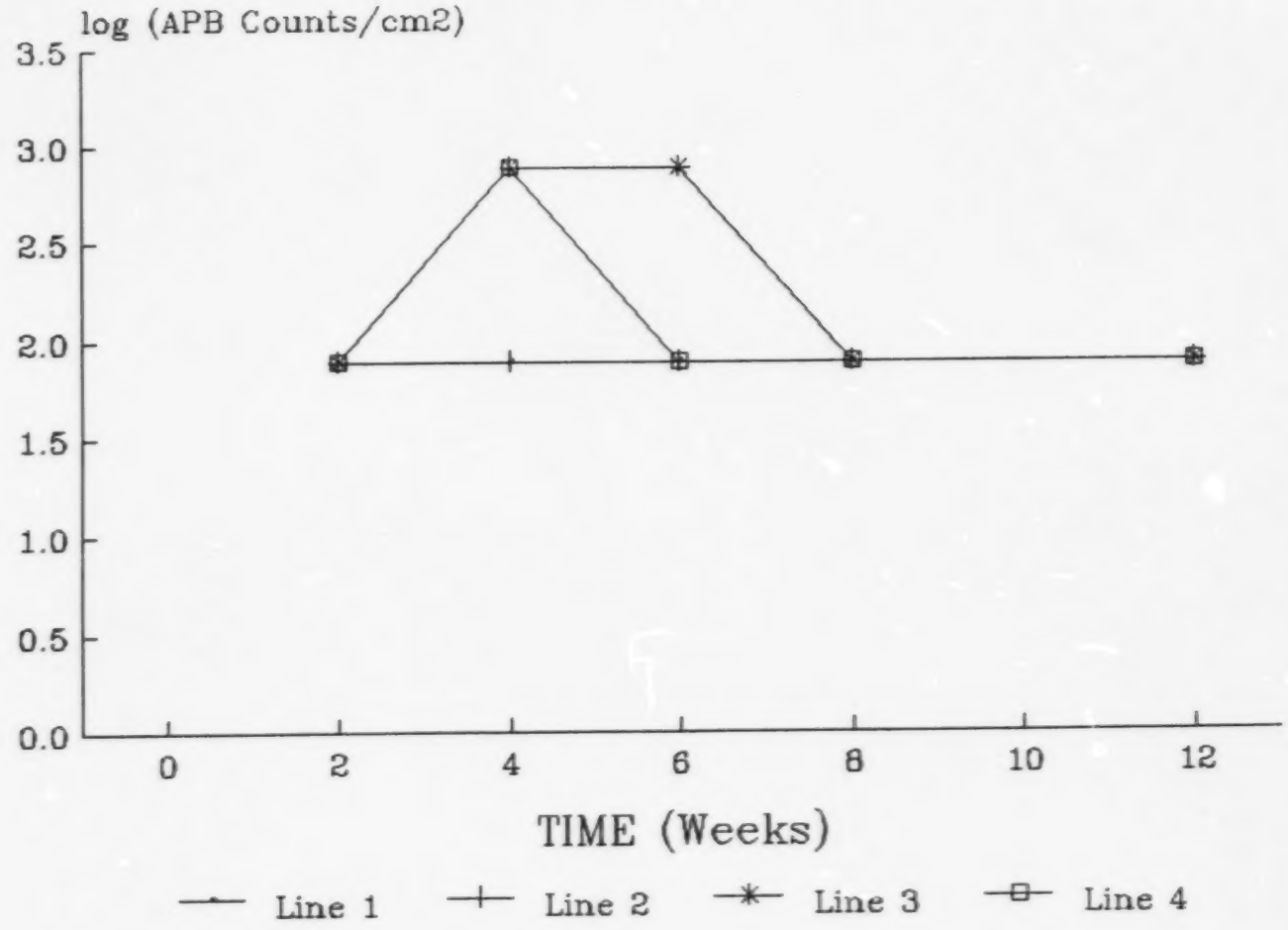

© 1991 NOVA HUSKY RESEARCH CORPORATION

FIGURE 7. Sulfate-reduction activity during the second experimental run.

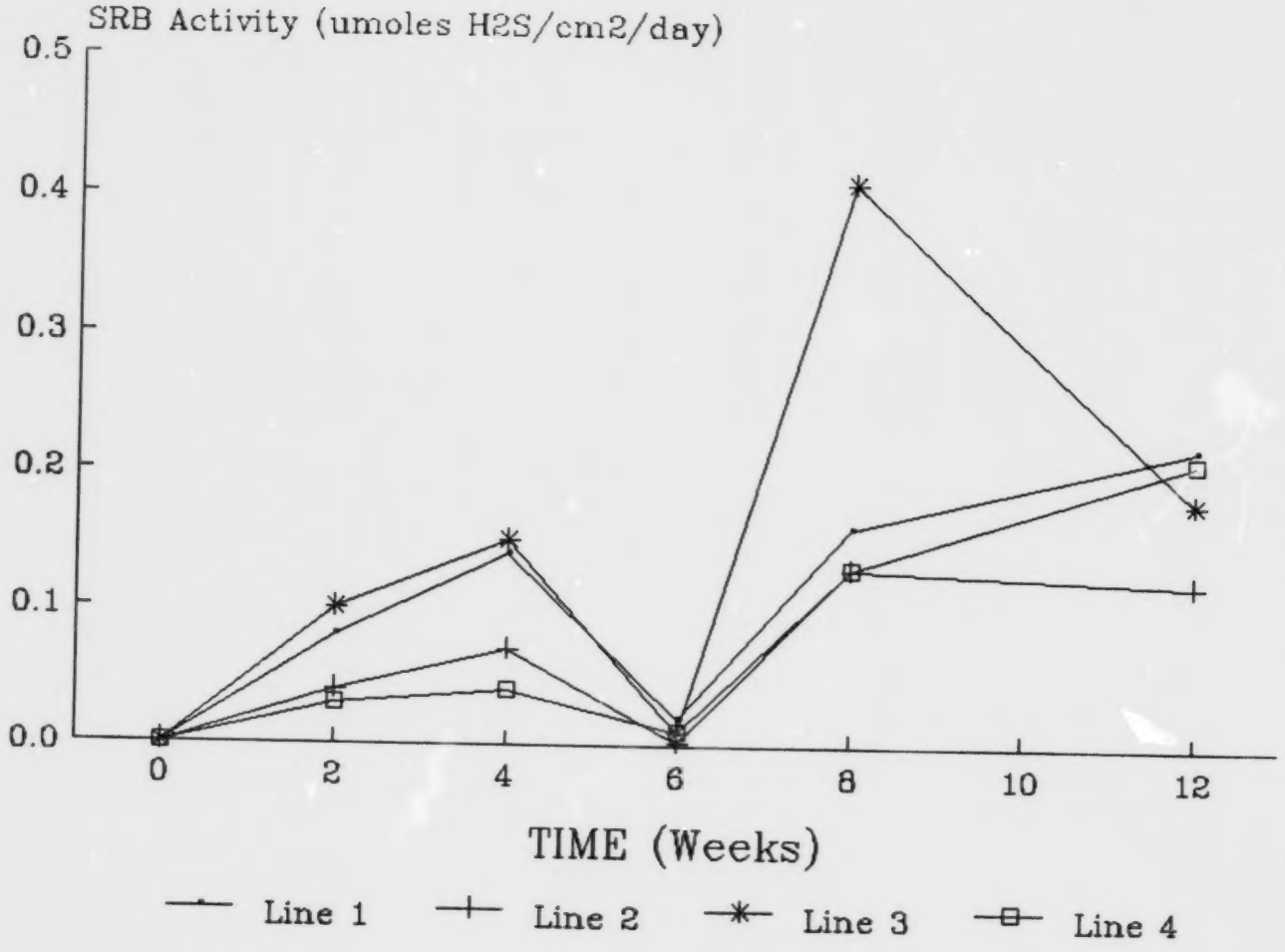

© 1991 NOVA HUSKY RESEARCH CORPORATION

FIGURE 8. **Enhancement of general corrosion rates after chemical treatment in the first experiment.**

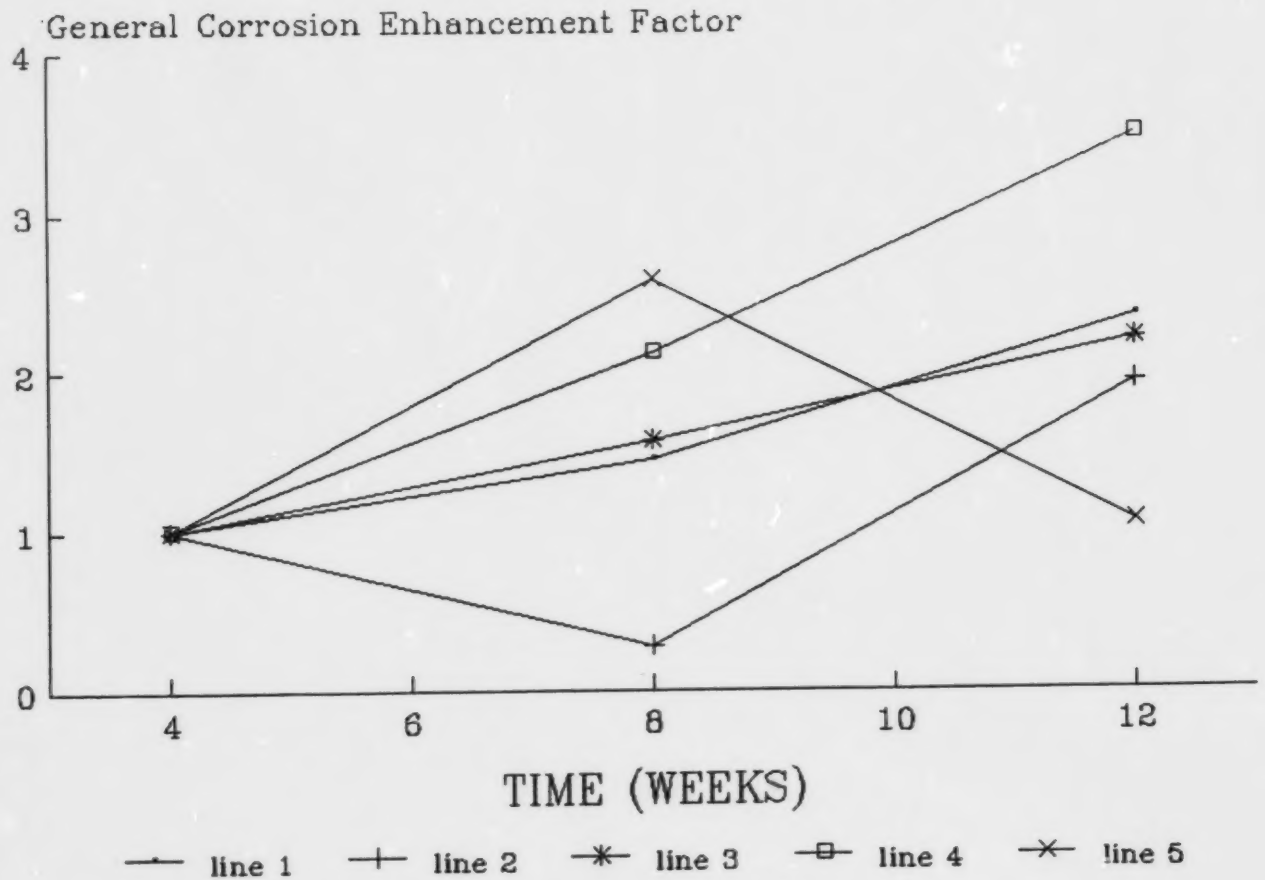

© 1991 NOVA HUSKY RESEARCH CORPORATION

FIGURE 9. **Enhancement of pitting tendency rates after chemical treatment in the first experiment.**

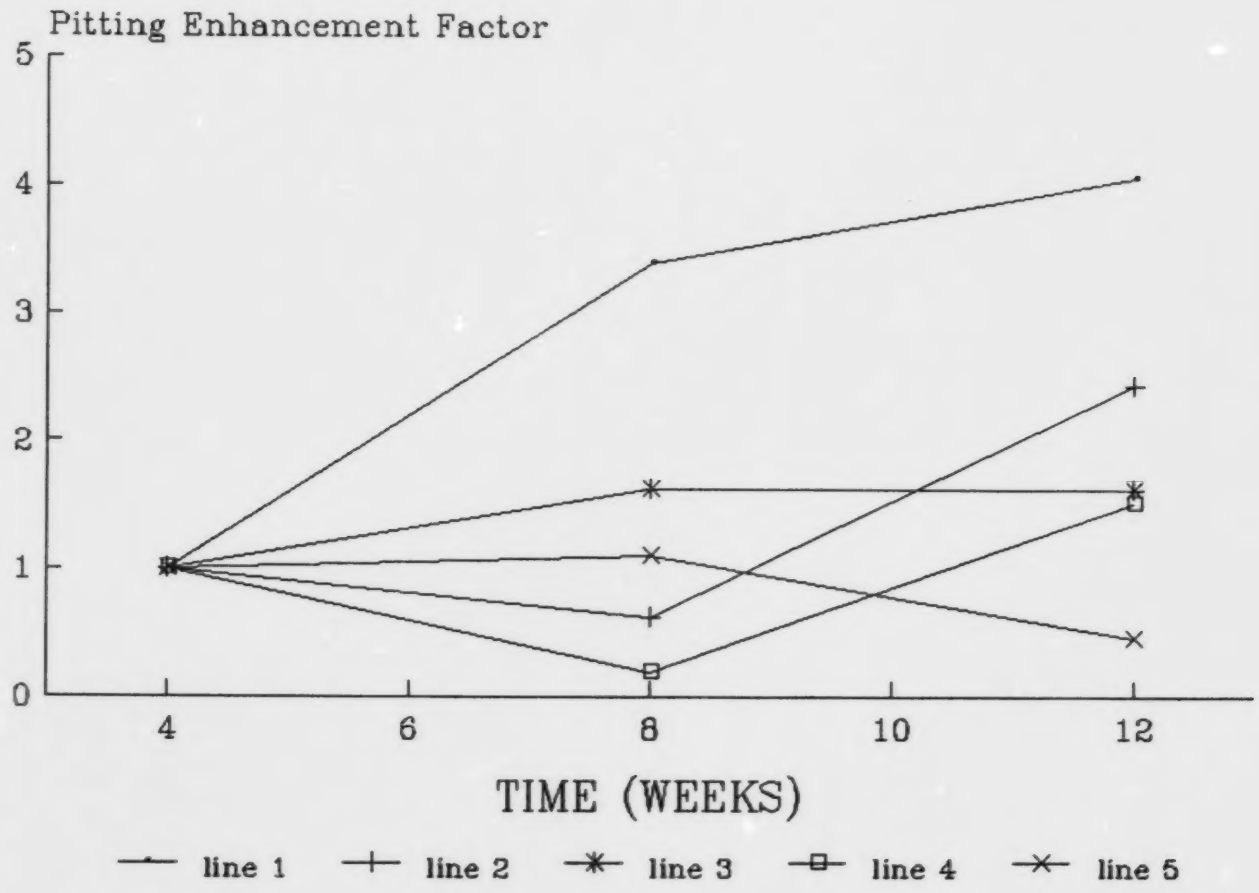

© 1991 NOVA HUSKY RESEARCH CORPORATION

FIGURE 10. **Enhancement of general corrosion rates after chemical treatment in the second experiment.**

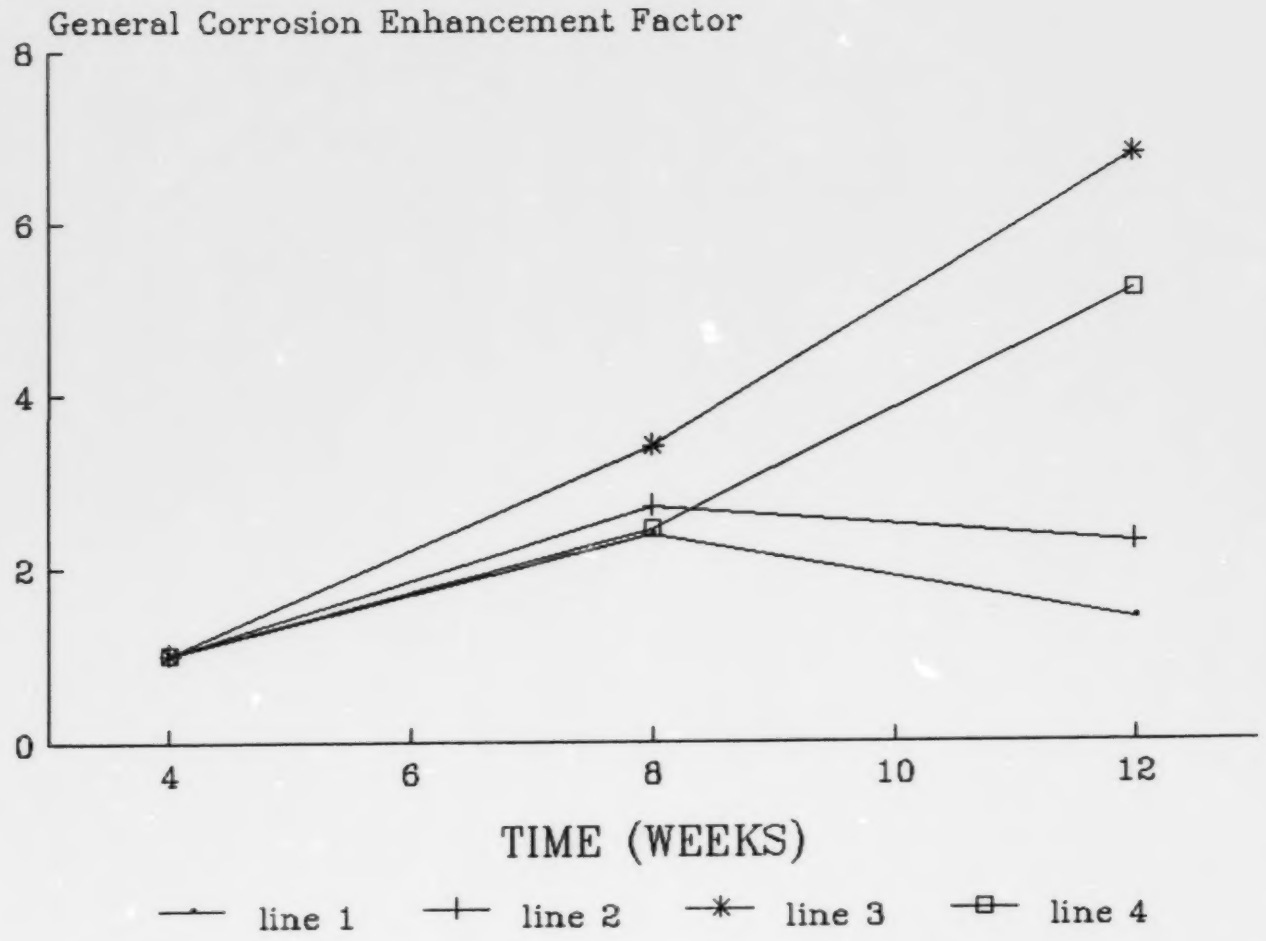

© 1991 NOVA HUSKY RESEARCH CORPORATION

FIGURE 11. **Enhancement of pitting tendency rates after chemical treatment in the second experiment.**

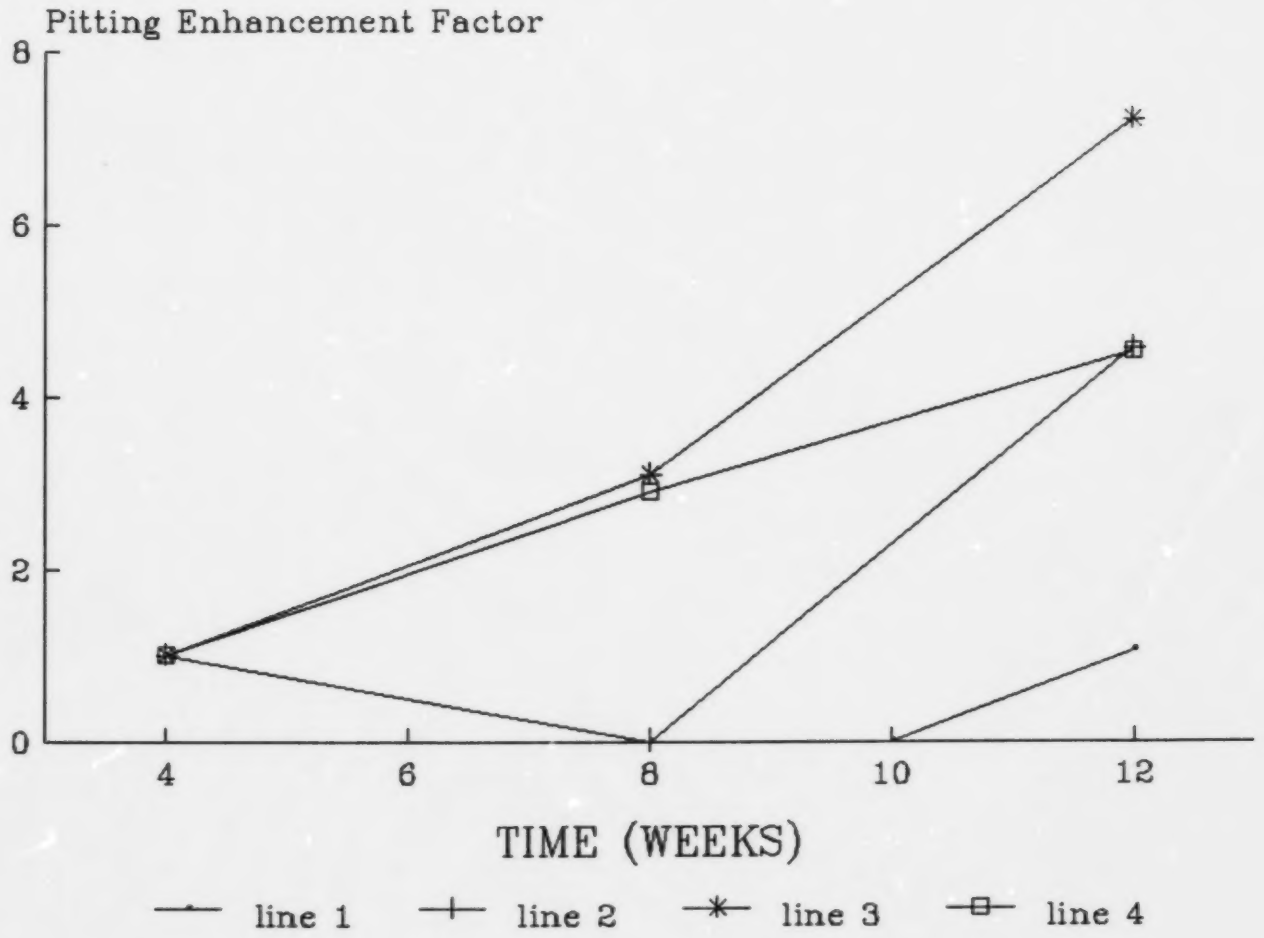

© 1991 NOVA HUSKY RESEARCH CORPORATION

FIGURE 12. Fluctuations in sodium, potassium, calcium, magnesium, iron, and manganese concentrations over the first experimental run.

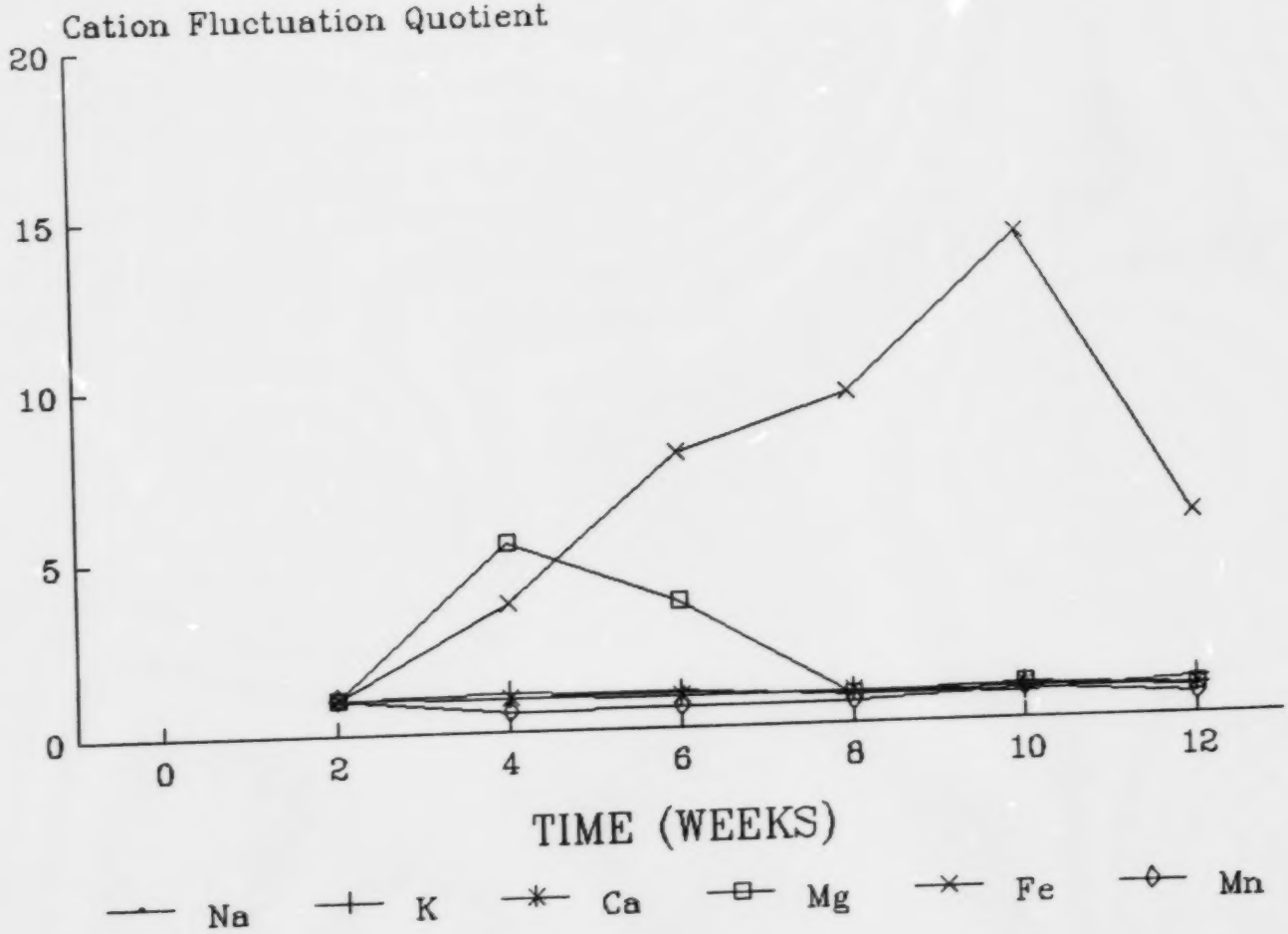

© 1991 NOVA HUSKY RESEARCH CORPORATION

FIGURE 13. Fluctuations in chloride, phosphate, and sulfide concentrations over the first experimental run.

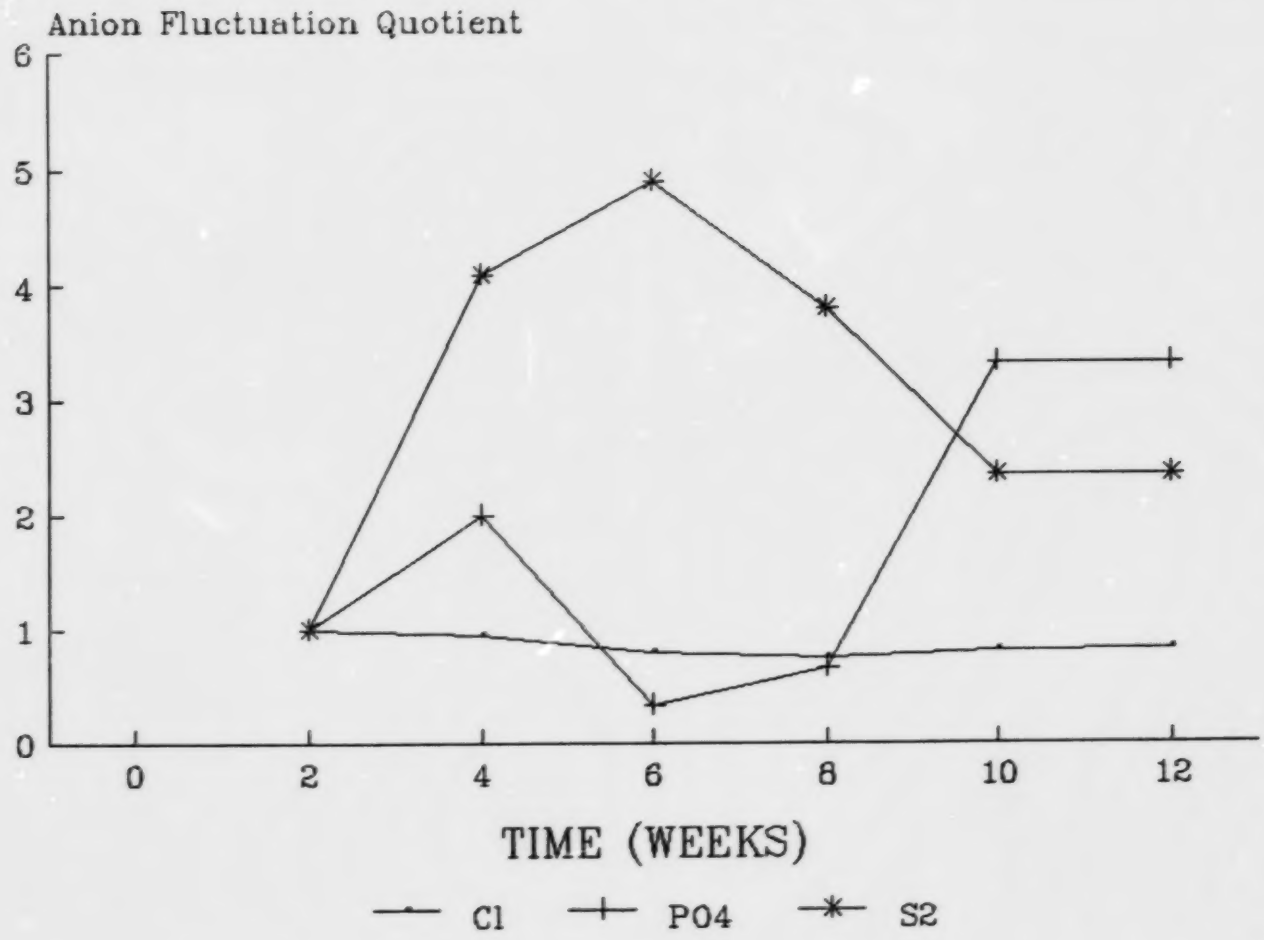

© 1991 NOVA HUSKY RESEARCH CORPORATION

FIGURE 14. **Fluctuations in sulfate and nitrate levels over the first experimental run.**

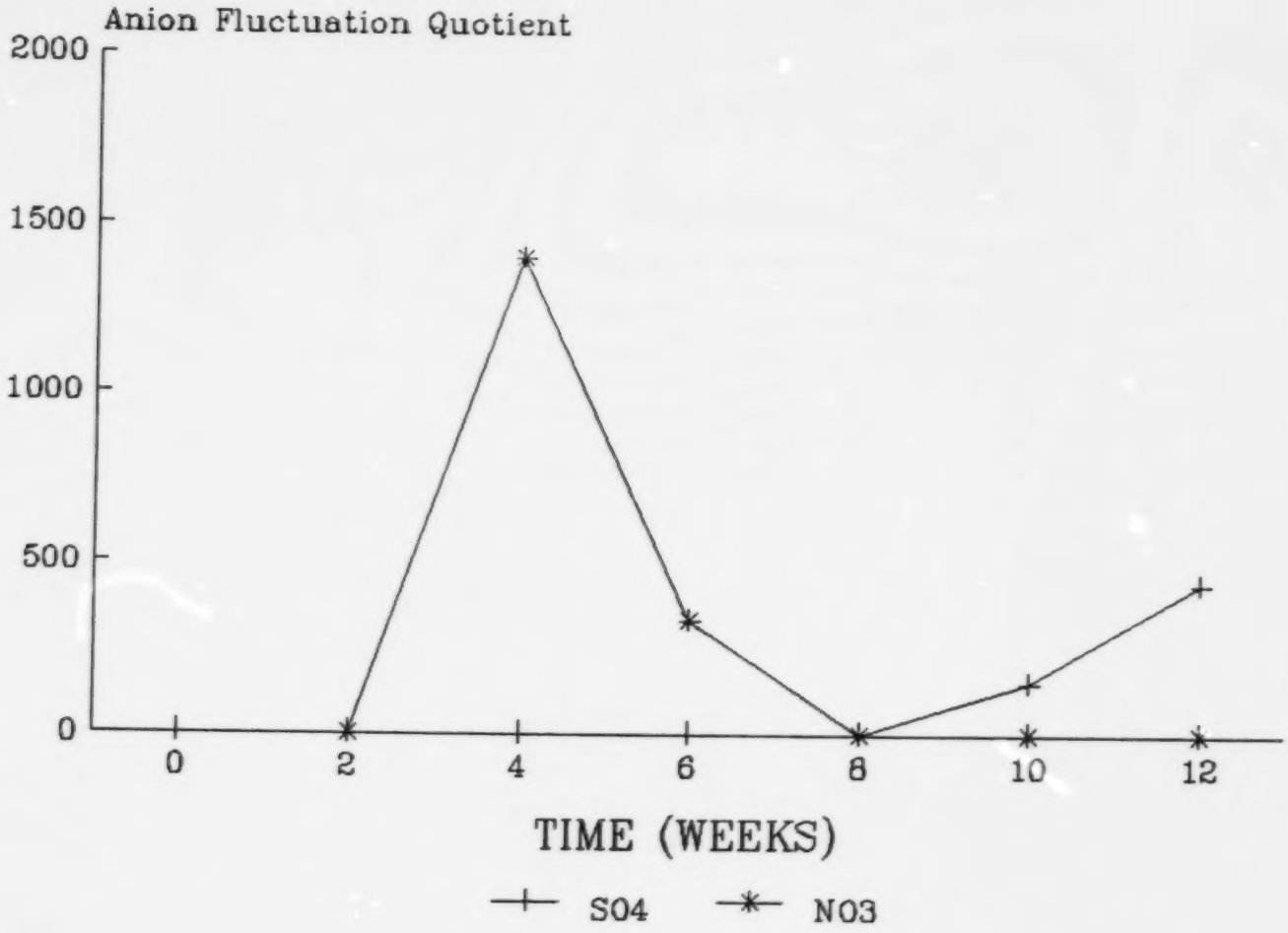

© 1991 NOVA HUSKY RESEARCH CORPORATION

FIGURE 15. **Fluctuations in alkalinity, total suspended solids, and total organic carbon over the first experimental run.**

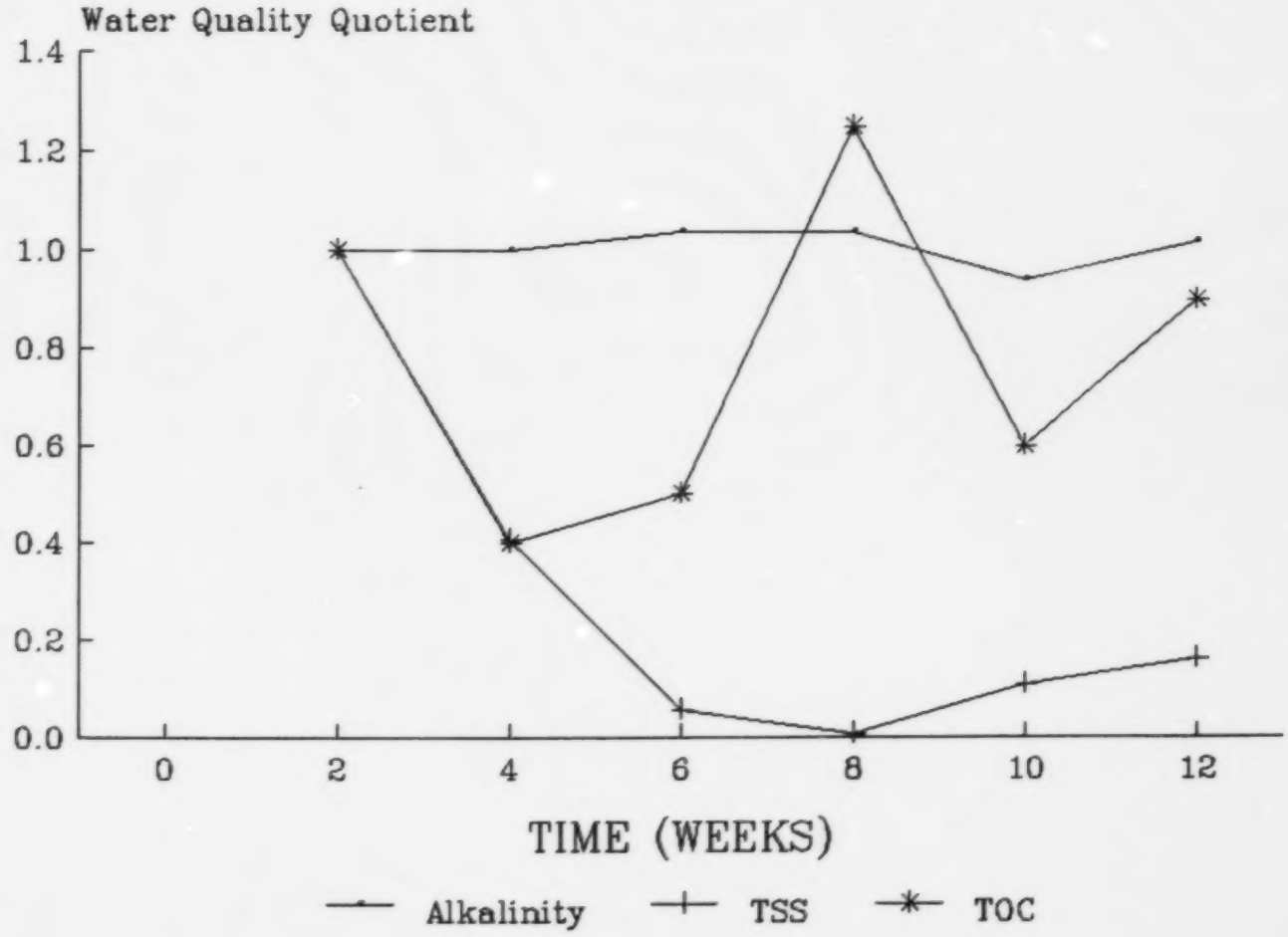

© 1991 NOVA HUSKY RESEARCH CORPORATION

FIGURE 16. Fluctuations in sodium, potassium, calcium, magnesium, iron, and manganese concentrations over the second experimental run.

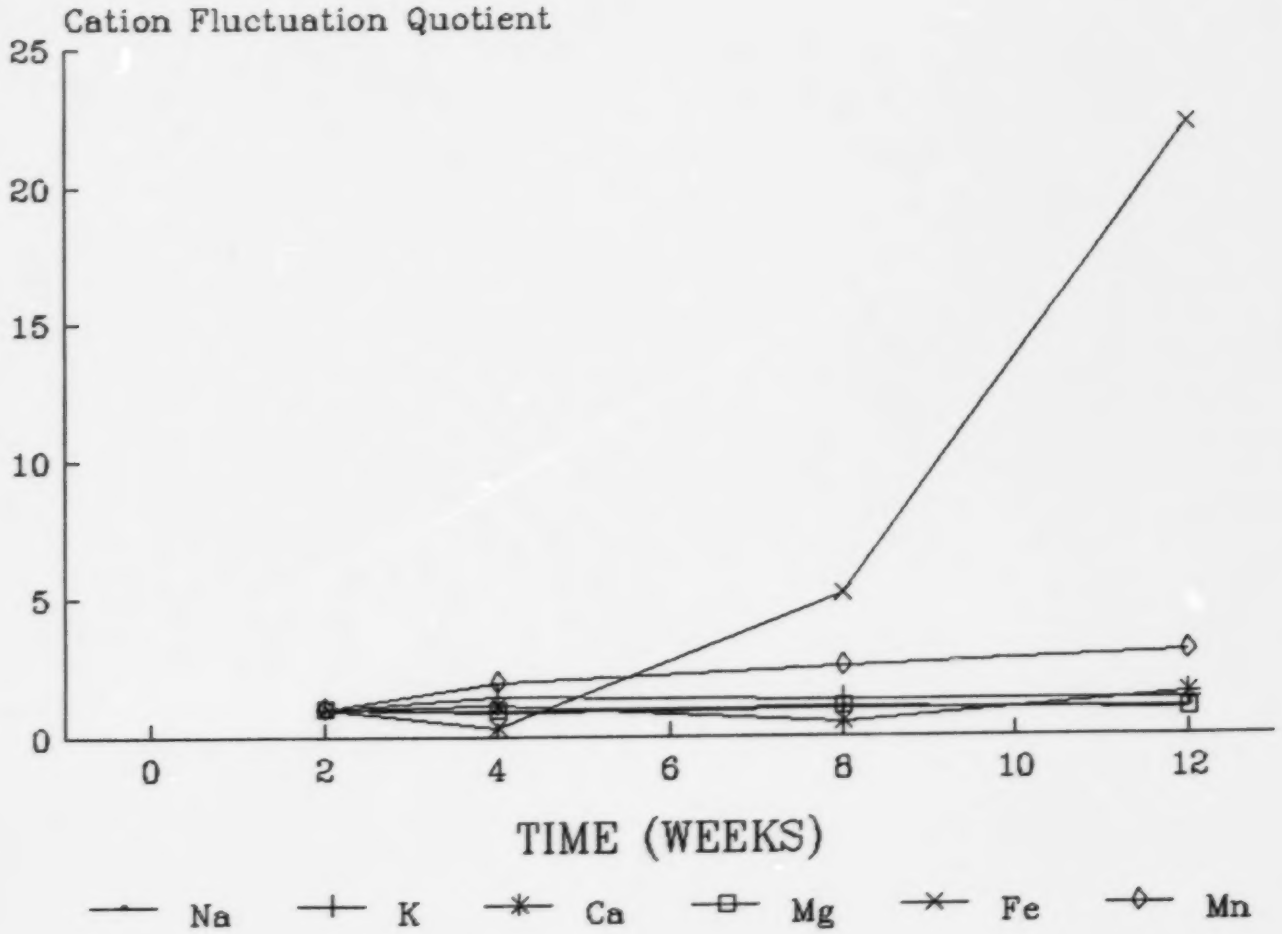

© 1991 NOVA HUSKY RESEARCH CORPORATION

FIGURE 17. Fluctuations in chloride, sulfate, nitrate, phosphate,and sulfide concentrations over the second experimental run.

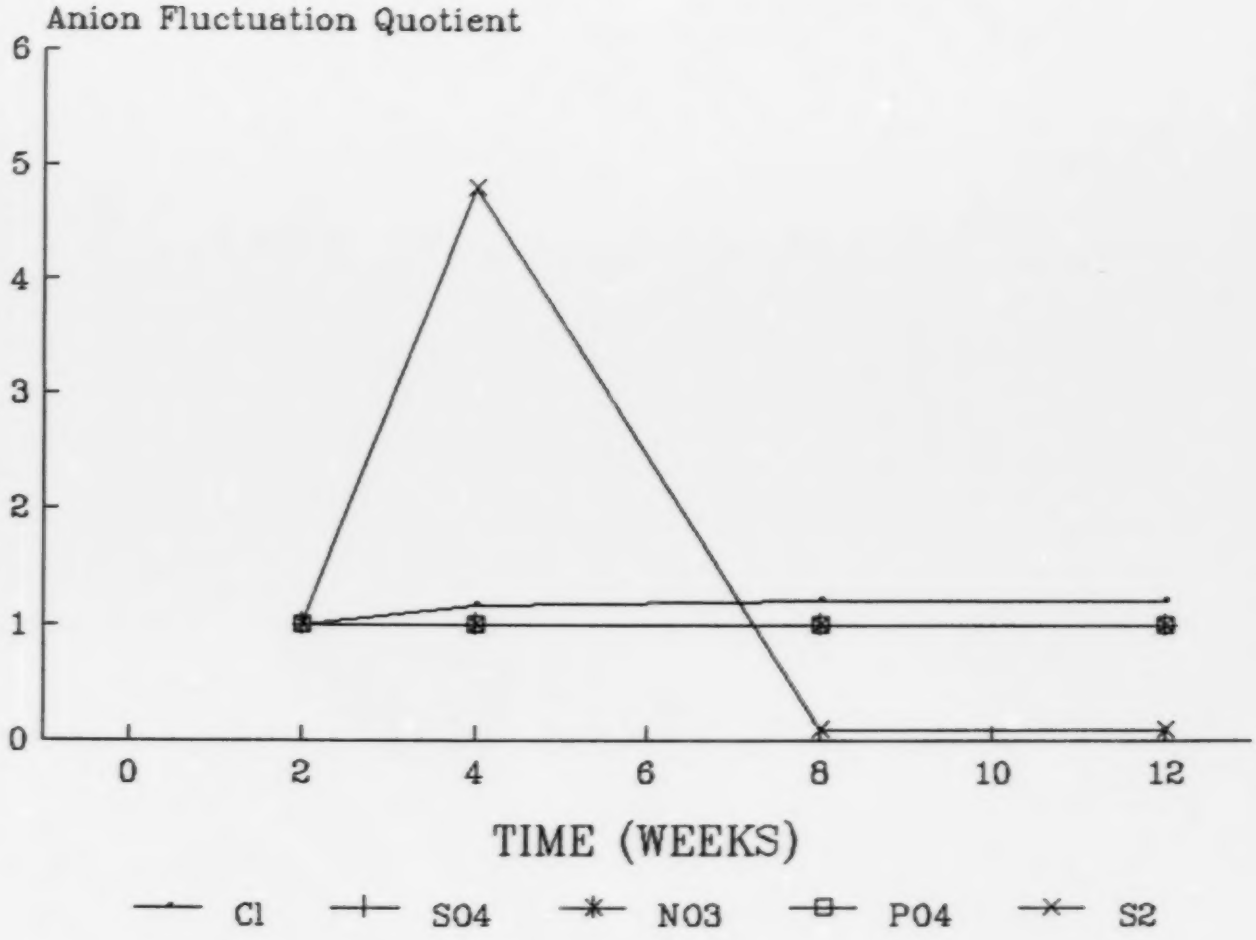

© 1991 NOVA HUSKY RESEARCH CORPORATION

FIGURE 18. Fluctuations in alkalinity, total suspended solids, and total organic carbon over the second experimental run.

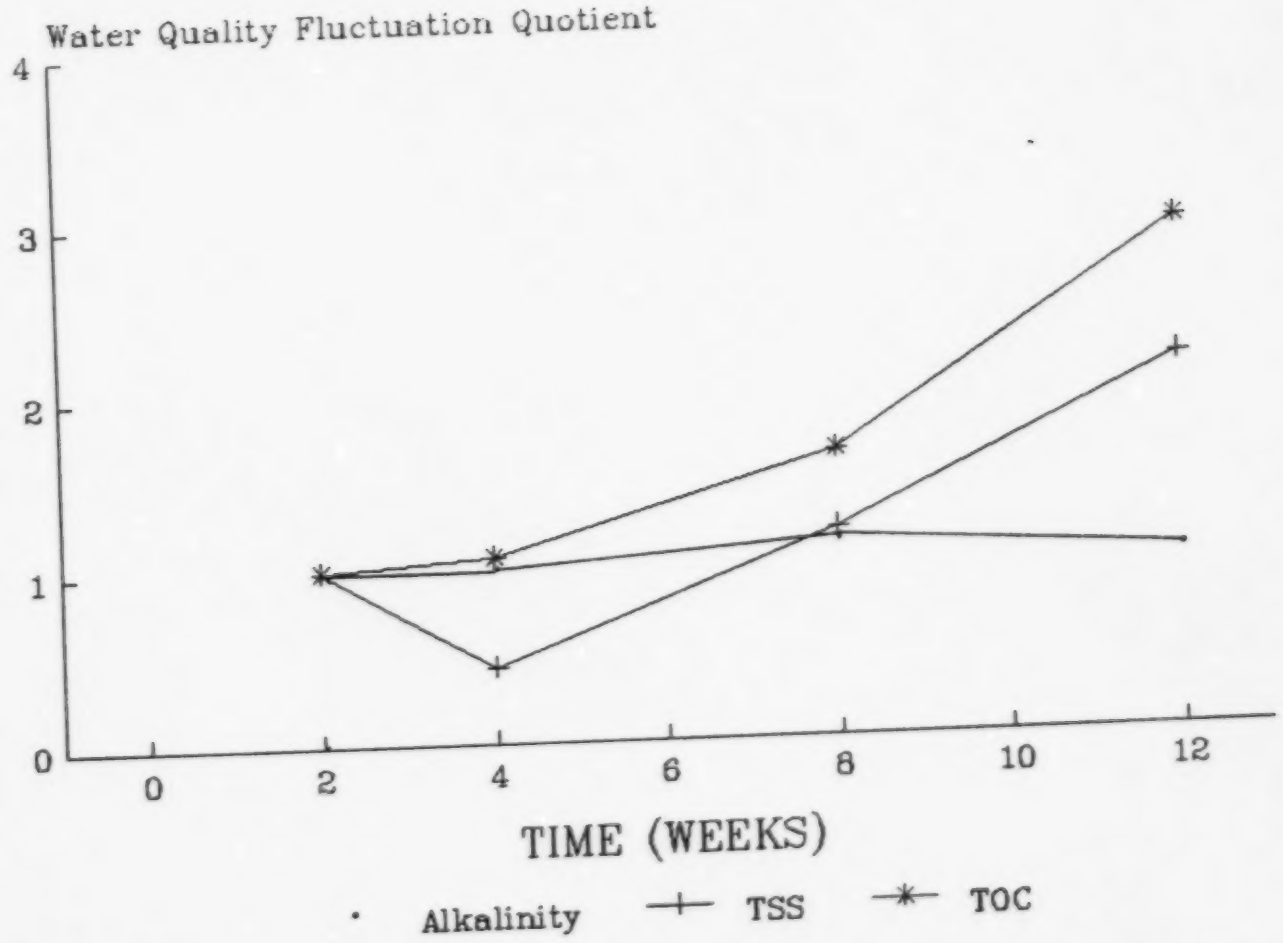

© 1991 NOVA HUSKY RESEARCH CORPORATION

FIGURE 19. Scatter plot of sulfate-reducing bacterial counts and iron concentrations in the first experiment.

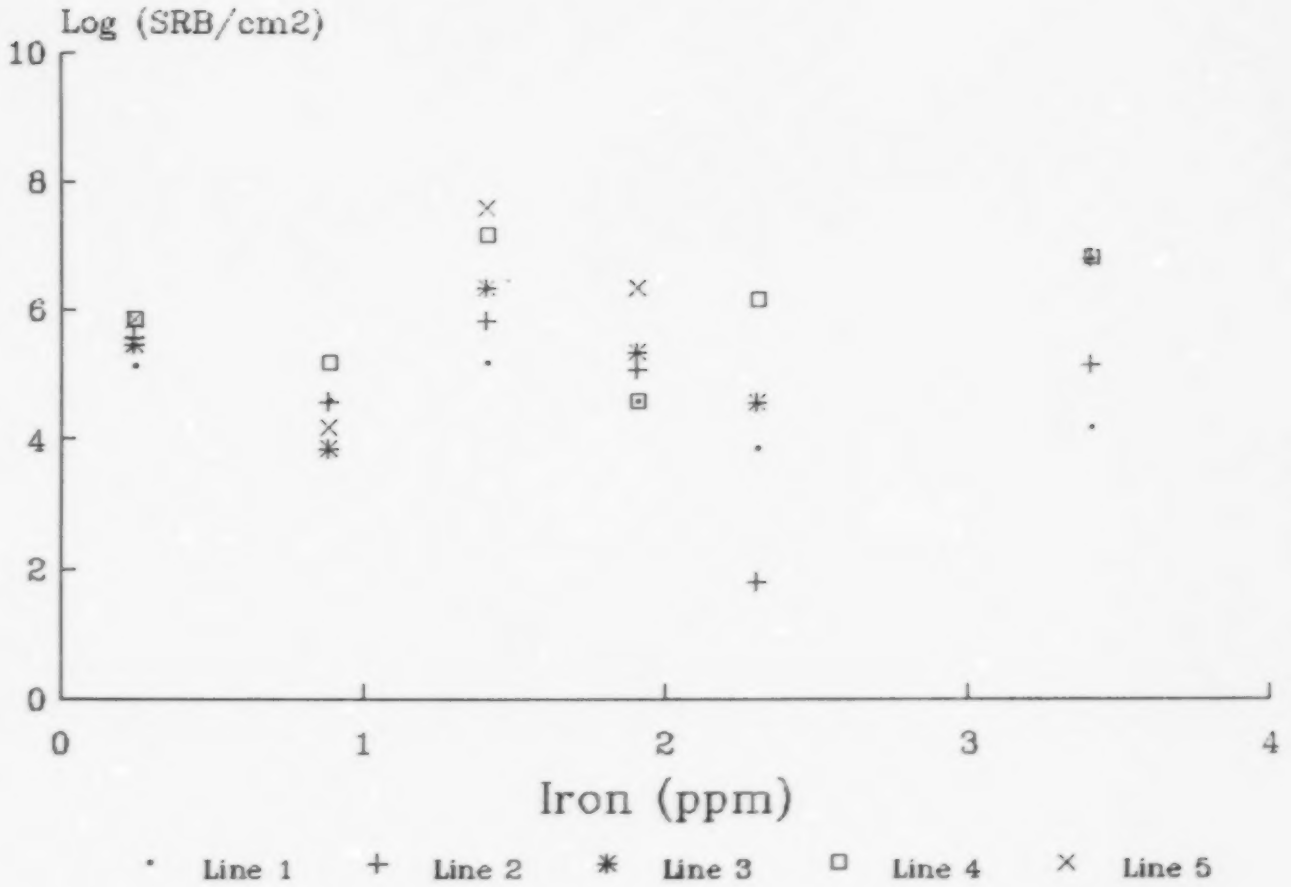

© 1991 NOVA HUSKY RESEARCH CORPORATION

FIGURE 20. Scatter plot of acid-producing bacterial counts and iron concentrations in the first experiment.

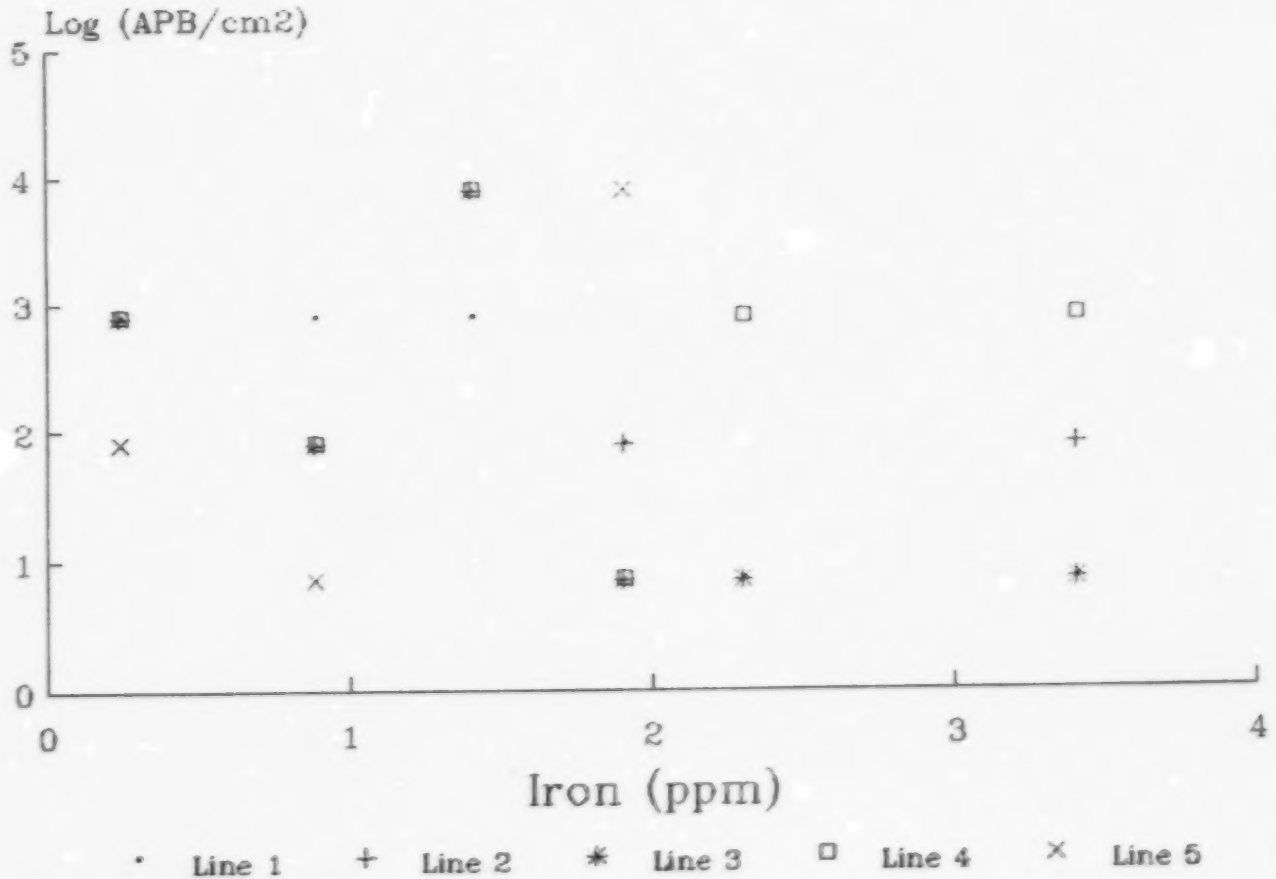

© 1991 NOVA HUSKY RESEARCH CORPORATION

FIGURE 21. Scatter plot of sulfate-reducing bacterial counts and iron concentrations in the second experiment.

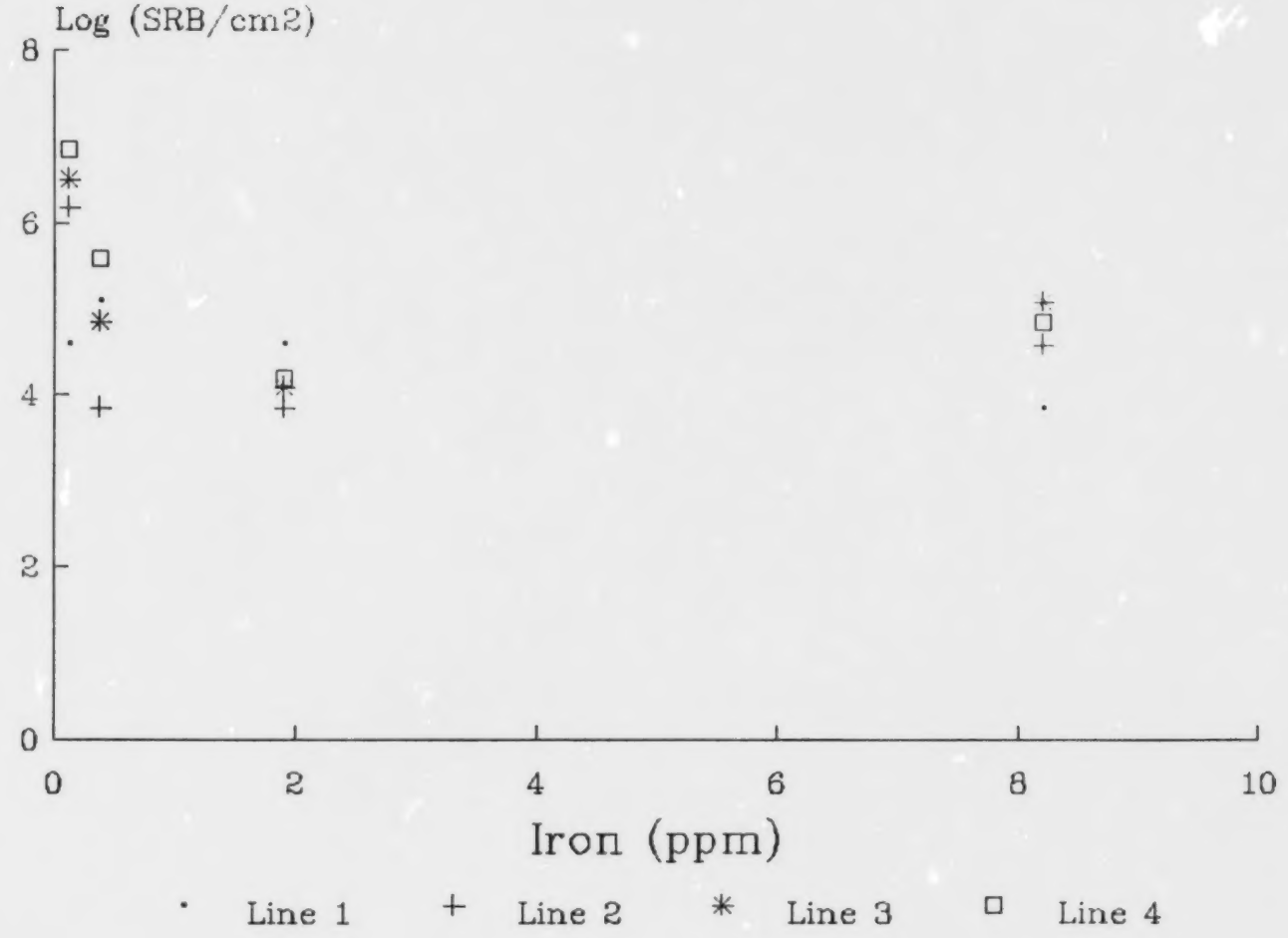

© 1991 NOVA HUSKY RESEARCH CORPORATION

FIGURE 22. Scatter plot of acid-producing bacterial counts and iron concentrations in the second experiment.

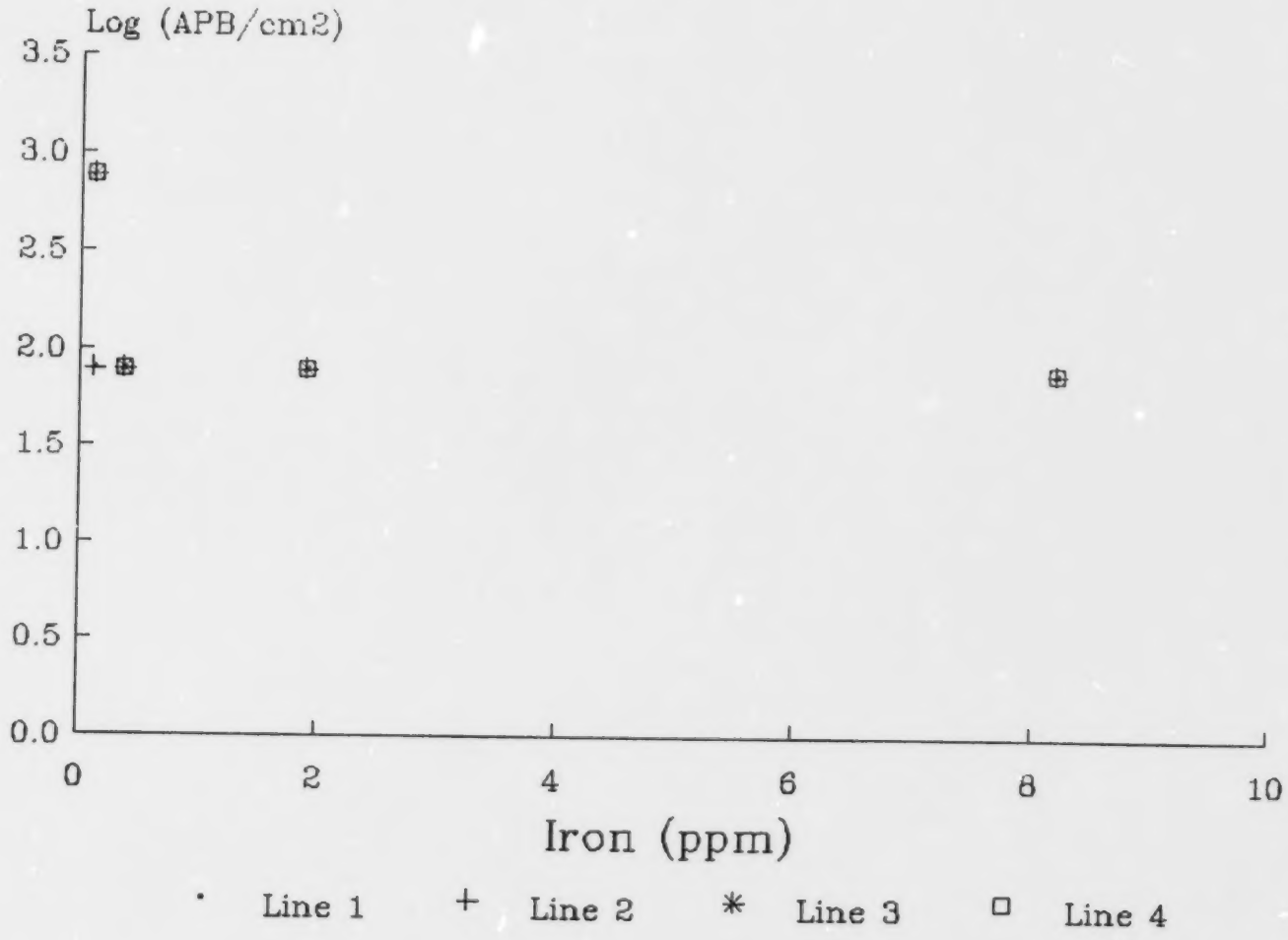

© 1991 NOVA HUSKY RESEARCH CORPORATION

FIGURE 23. Scatter plot of sulfate-reducing bacterial counts and magnesium concentrations in the first experiment.

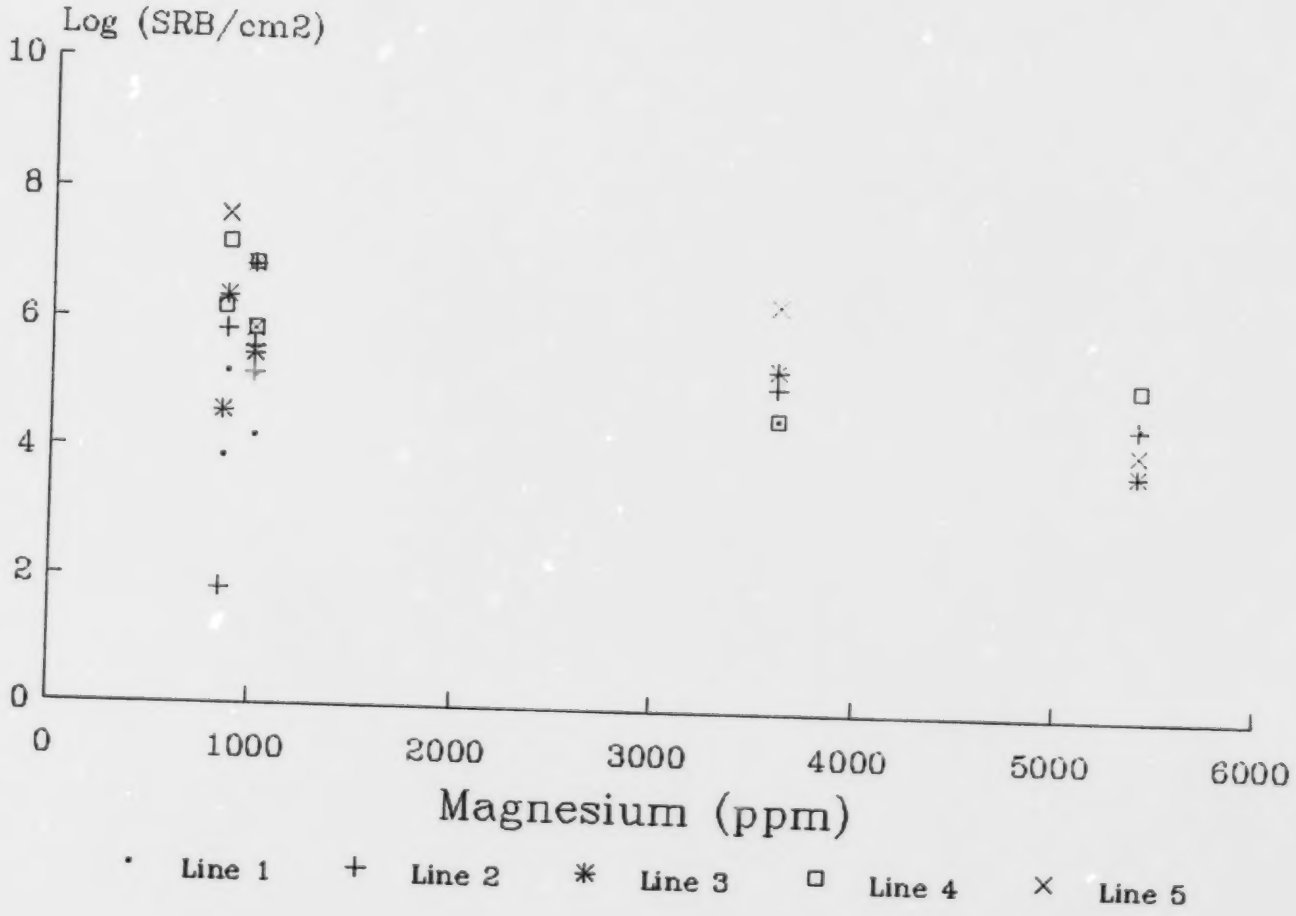

© 1991 NOVA HUSKY RESEARCH CORPORATION

FIGURE 24. Scatter plot of acid-producing bacterial counts and magnesium concentrations in the first experiment.

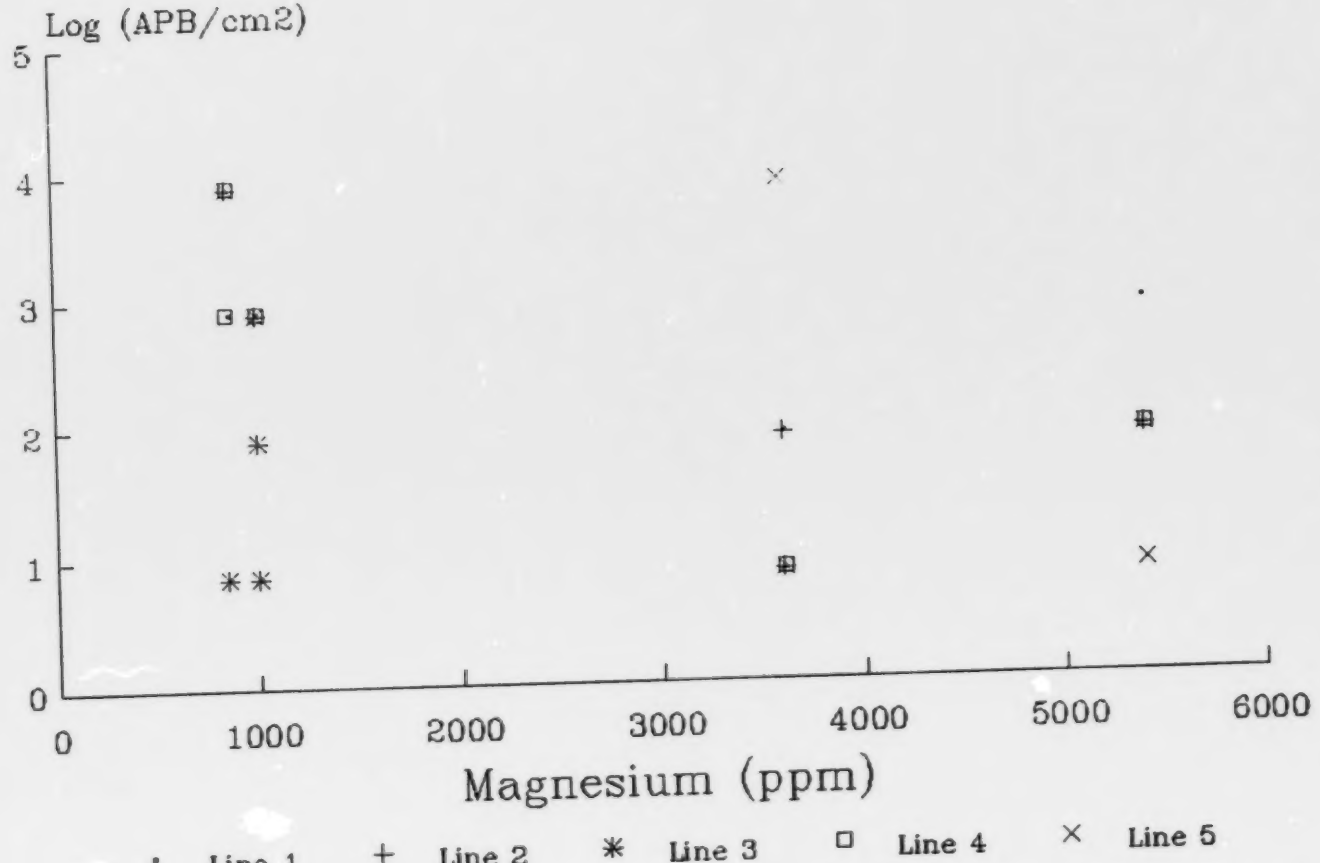

© 1991 NOVA HUSKY RESEARCH CORPORATION

FIGURE 25. Scatter plot of sulfate-reducing bacterial counts and sulfate concentrations in the first experiment.

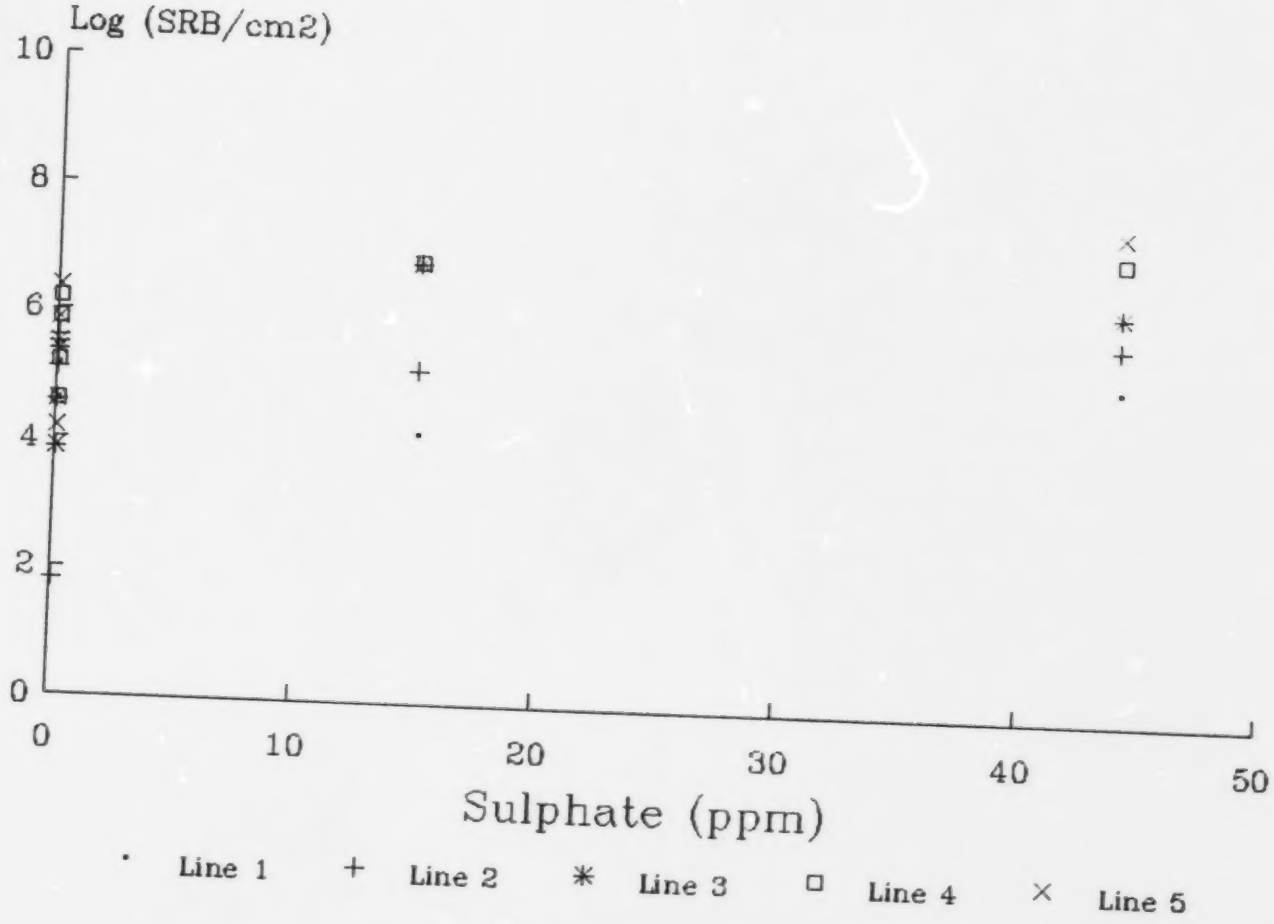

© 1991 NOVA HUSKY RESEARCH CORPORATION

FIGURE 26. Scatter plot of acid-producing bacterial counts and sulfate concentrations in the first experiment.

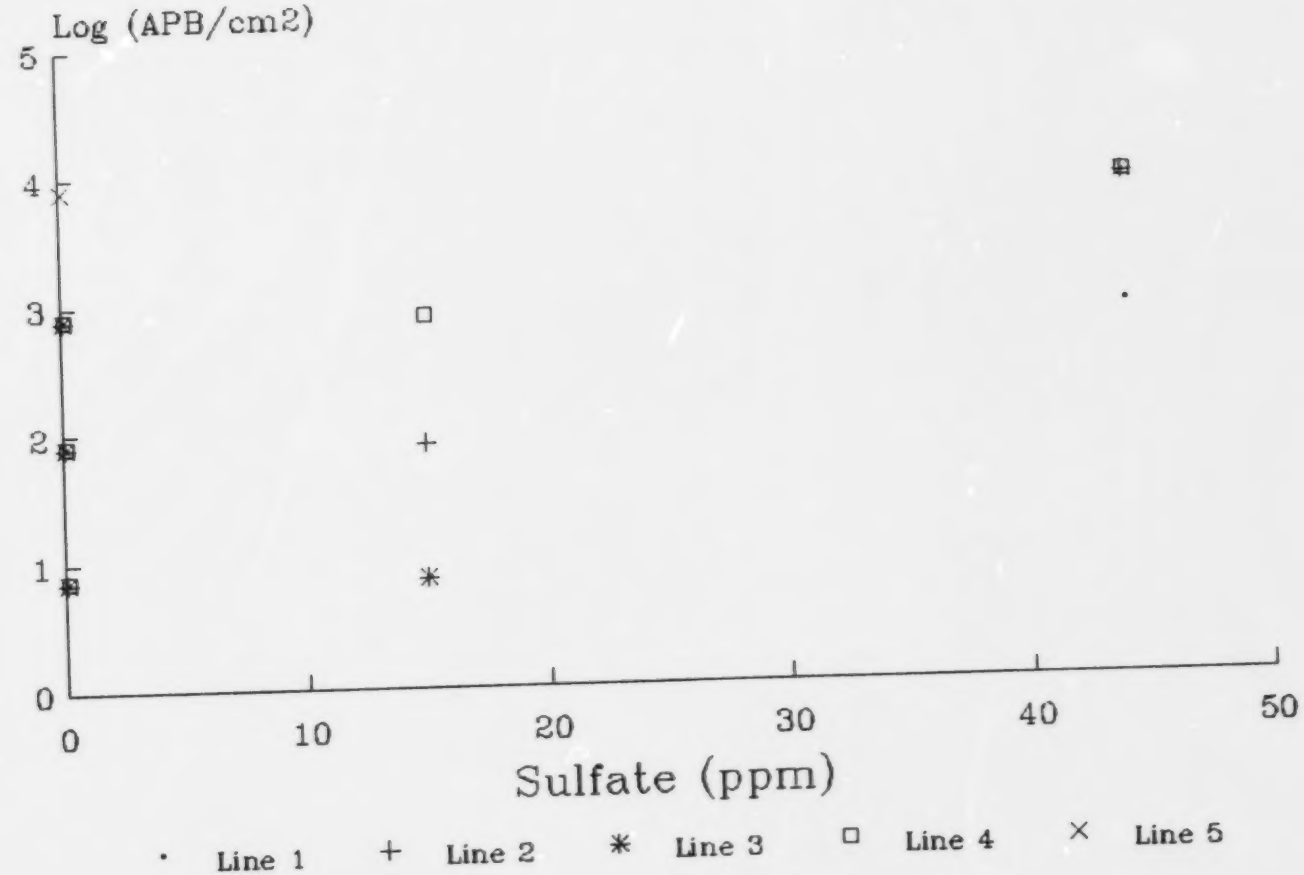

© 1991 NOVA HUSKY RESEARCH CORPORATION

FIGURE 27. Scatter plot of sulfate-reducing bacterial counts and phosphate concentrations in the first experiment.

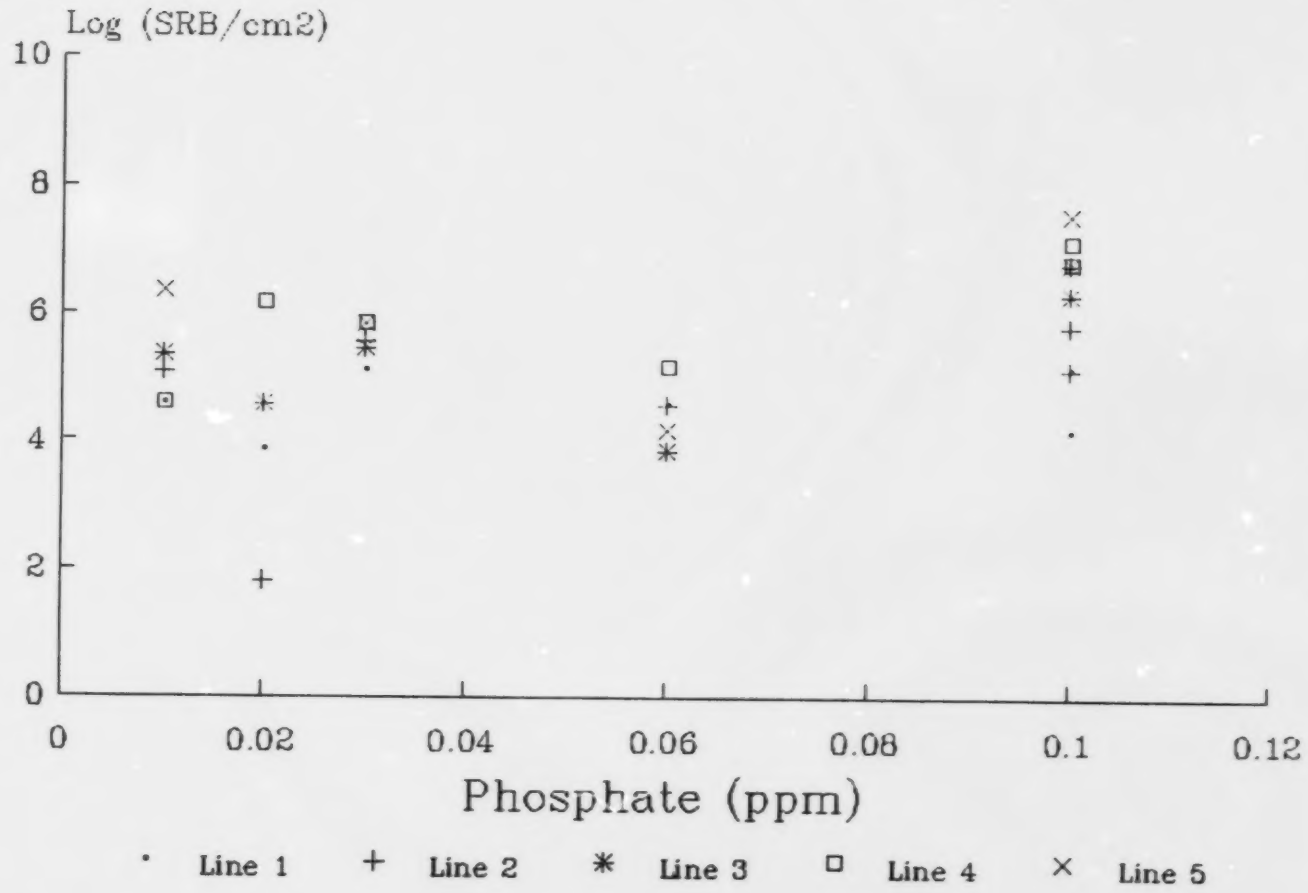

© 1991 NOVA HUSKY RESEARCH CORPORATION

FIGURE 28. Scatter plot of acid-producing bacterial counts and phosphate concentrations in the first experiment.

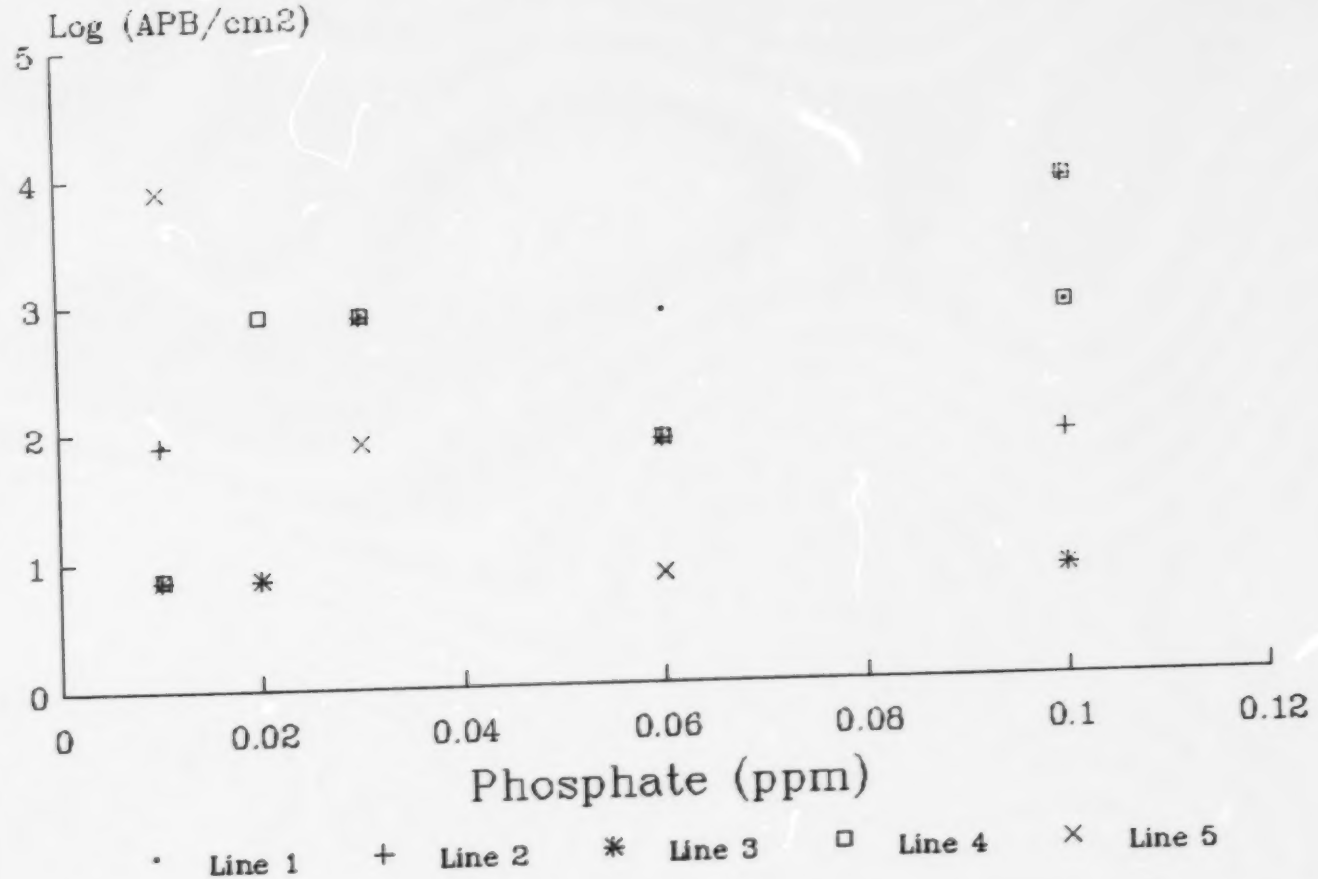

© 1991 NOVA HUSKY RESEARCH CORPORATION

FIGURE 29. Scatter plot of sulfate-reducing bacterial counts and nitrate concentrations in the first experiment.

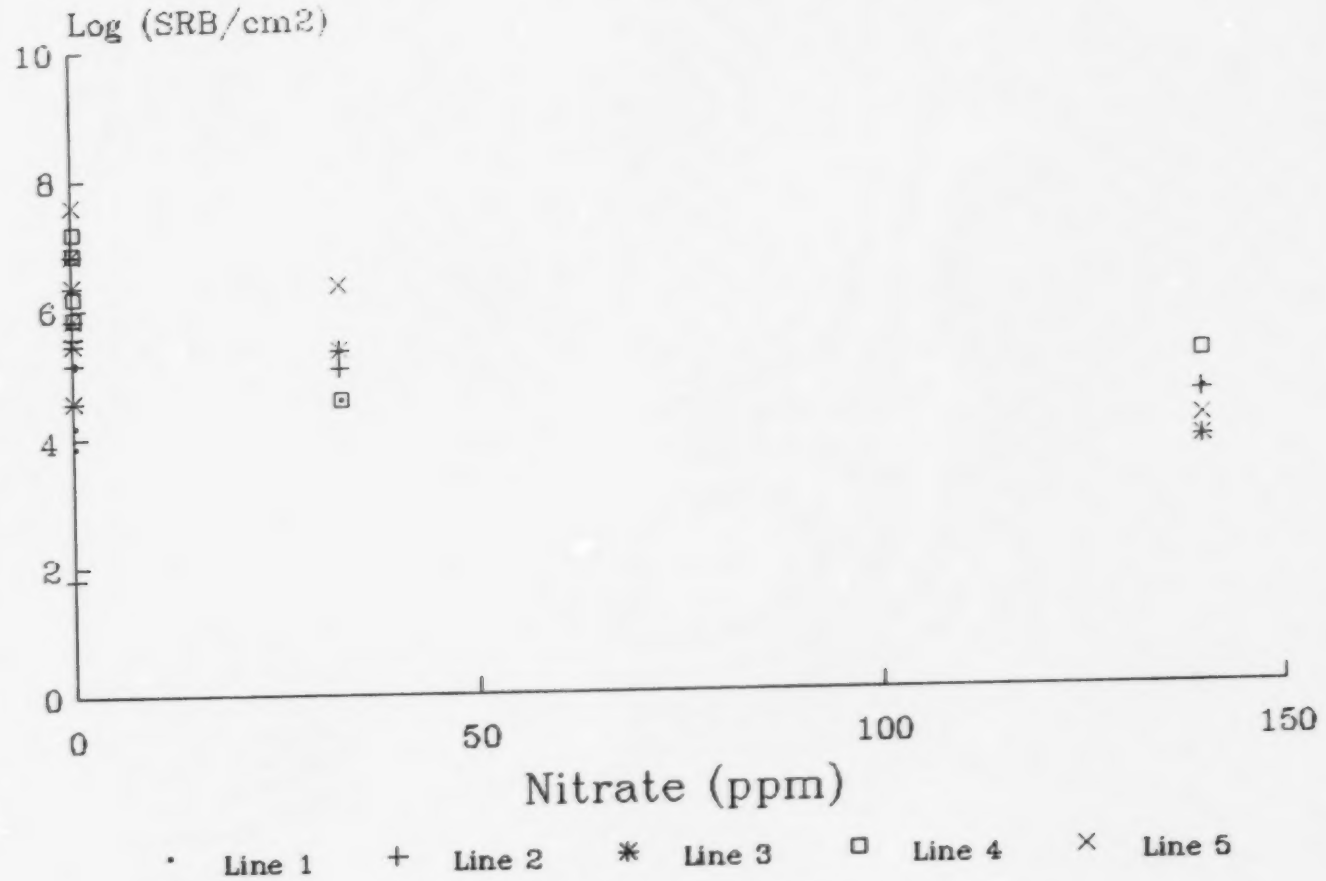

© 1991 NOVA HUSKY RESEARCH CORPORATION

FIGURE 30. Scatter plot of acid-producing bacterial counts and nitrate concentrations in the first experiment.

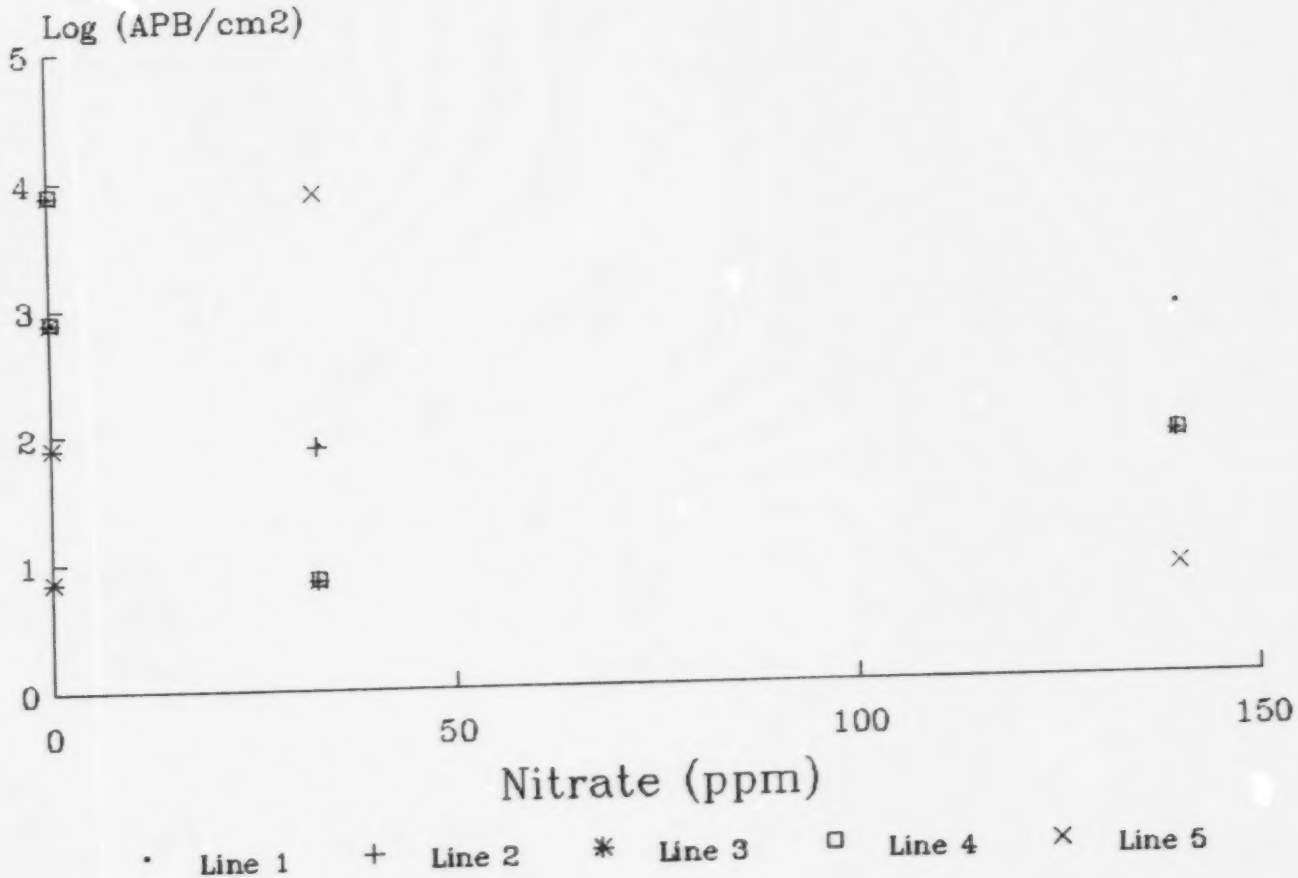

© 1991 NOVA HUSKY RESEARCH CORPORATION

FIGURE 31. Scatter plot of sulfate-reducing bacterial counts and sulfide concentrations in the first experiment.

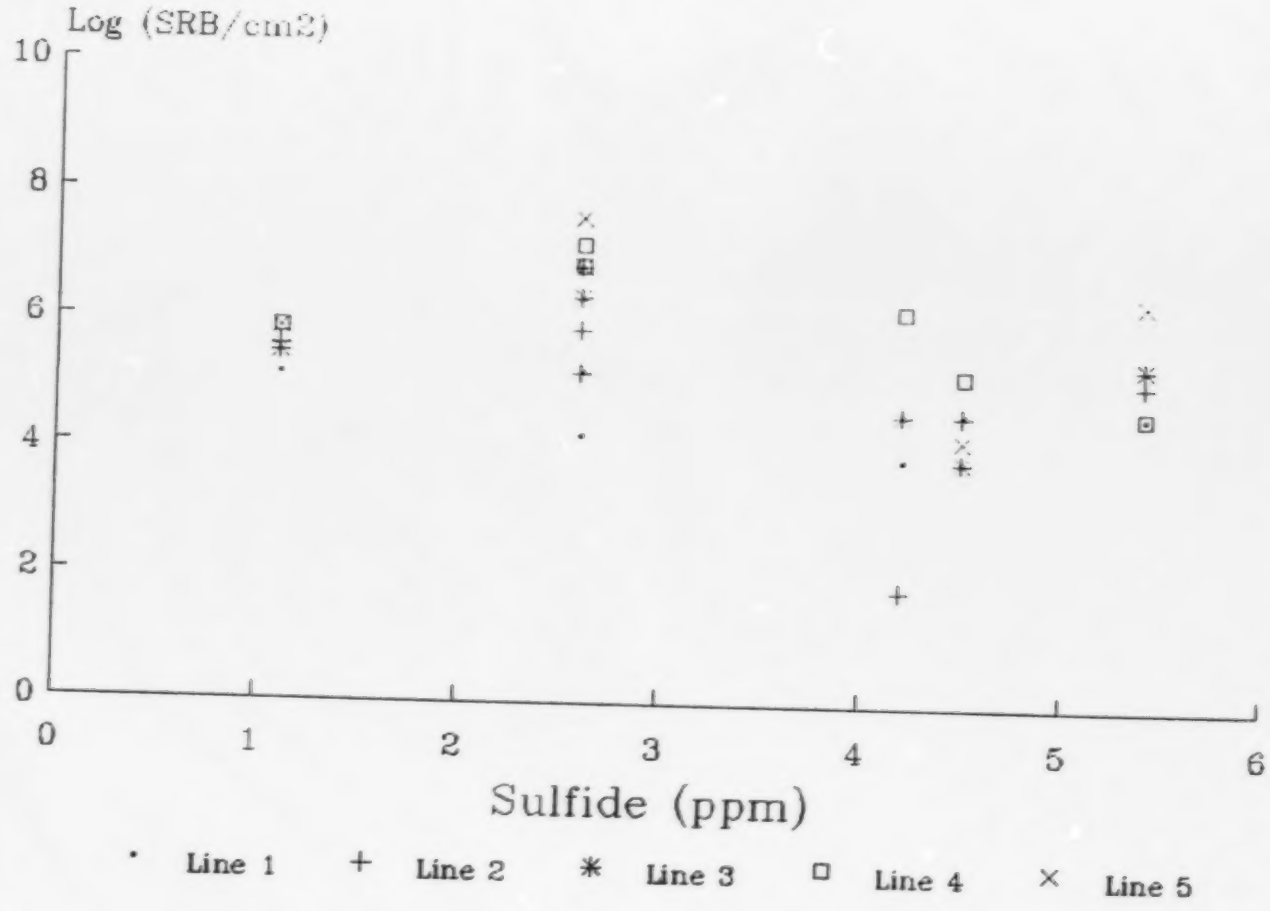

FIGURE 32. Scatter plot of acid-producing bacterial counts and sulfide concentrations in the first experiment.

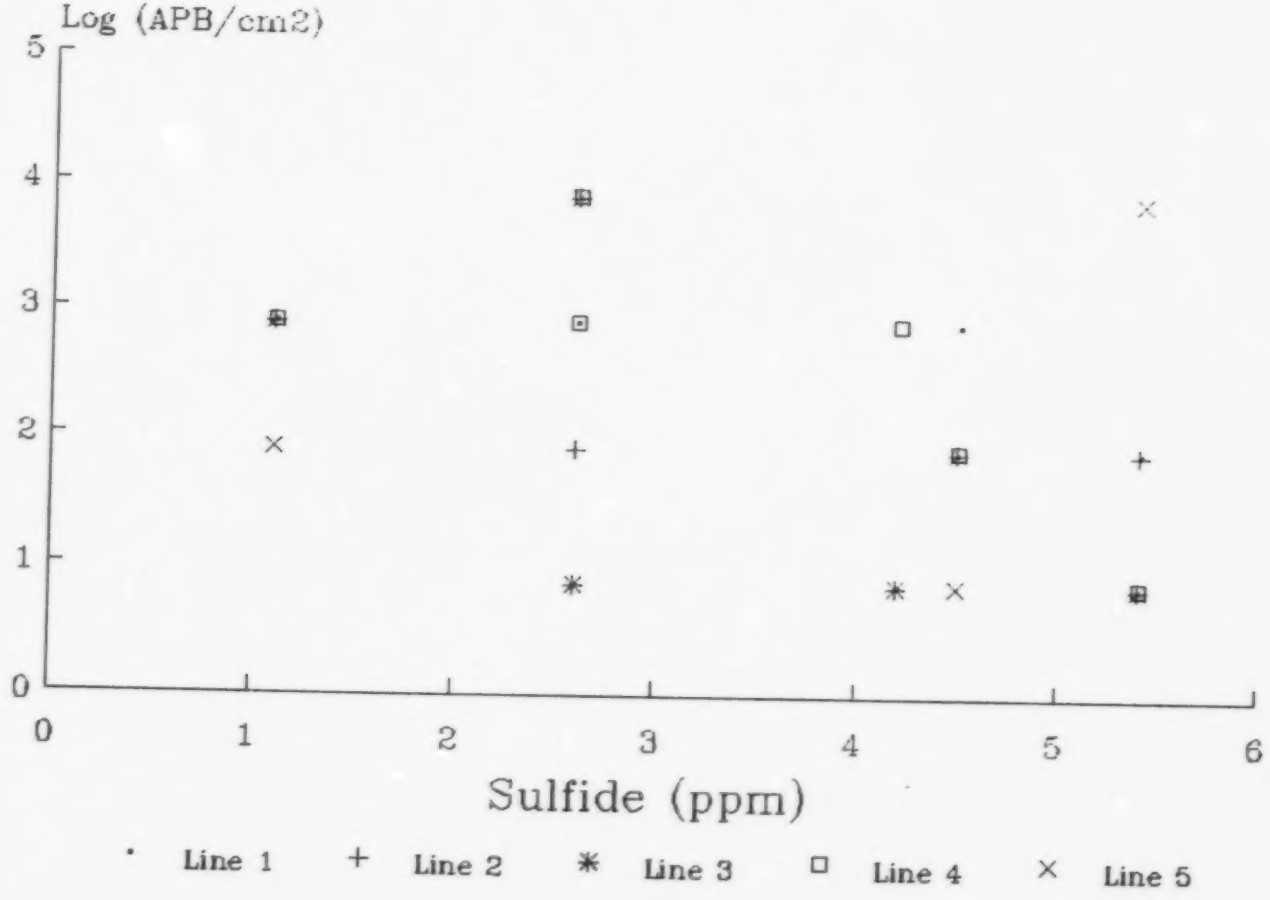

© 1991 NOVA HUSKY RESEARCH CORPORATION

FIGURE 33. Scatter plot of sulfate-reducing bacterial counts and sulfide concentrations in the second experiment.

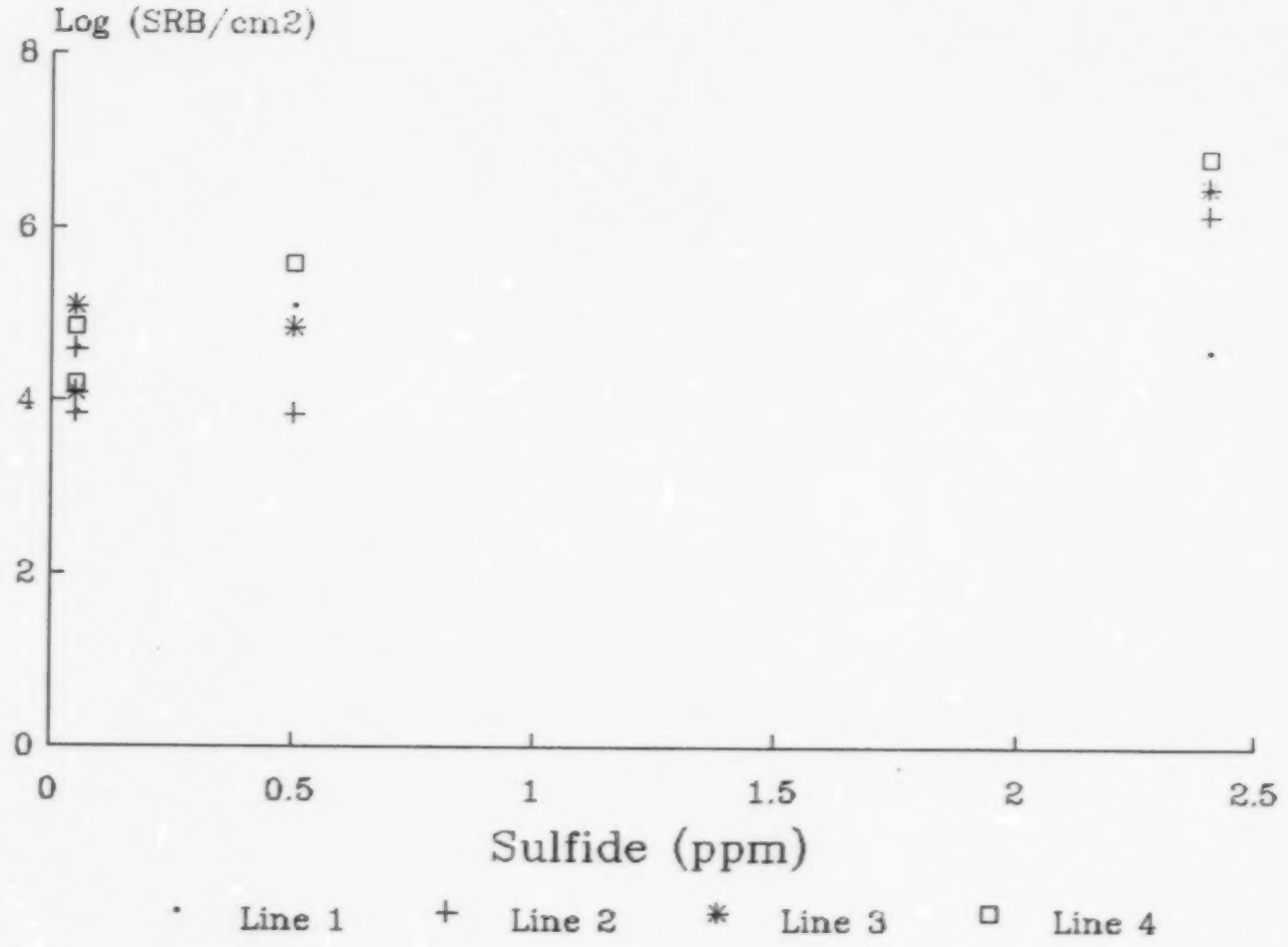

© 1991 NOVA HUSKY RESEARCH CORPORATION

FIGURE 34. Scatter plot of acid-producing bacterial counts and sulfide concentrations in the second experiment.

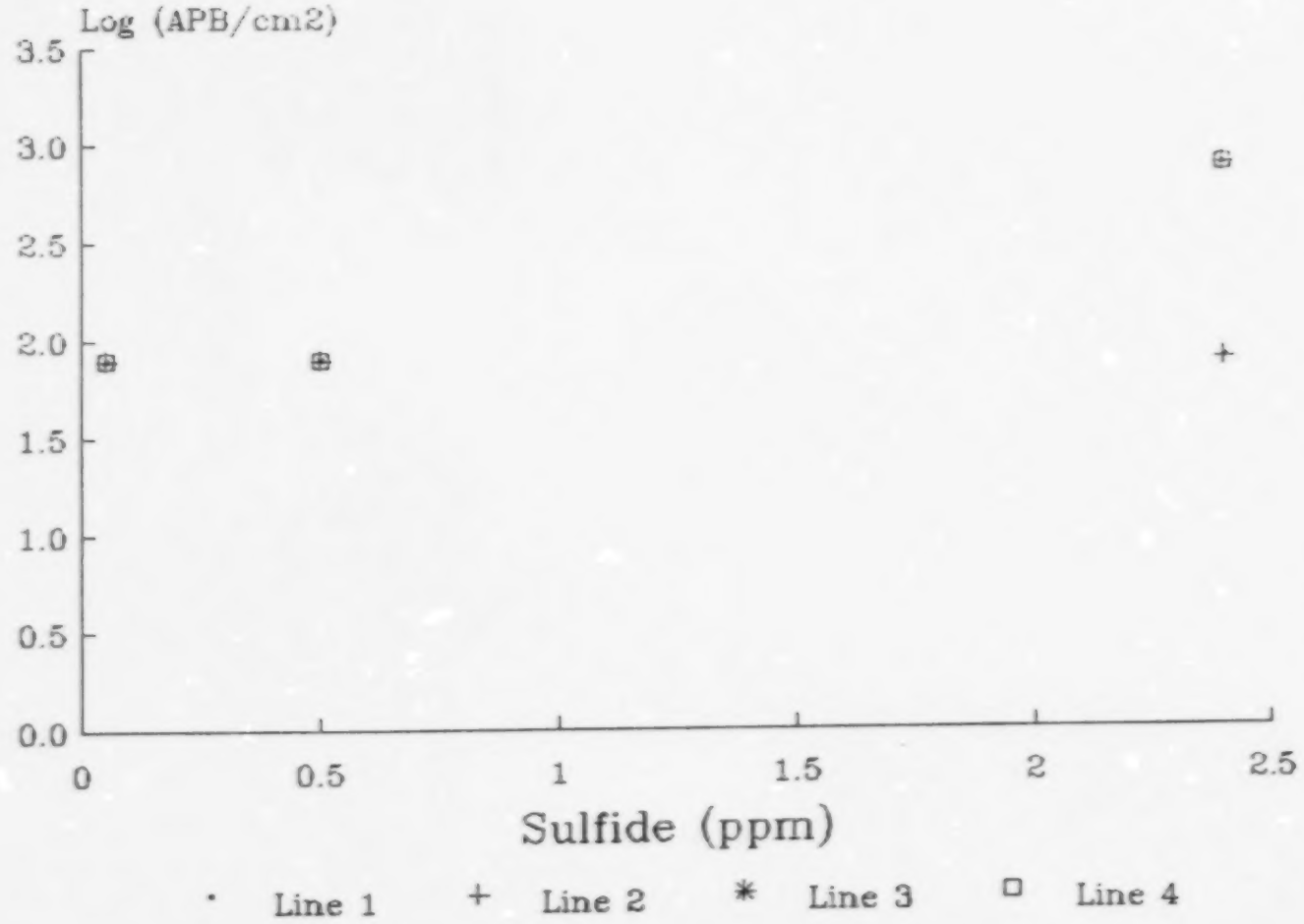

© 1991 NOVA HUSKY RESEARCH CORPORATION

FIGURE 35. Scatter plot of sulfate-reducing bacterial counts and total suspended solids in the first experiment.

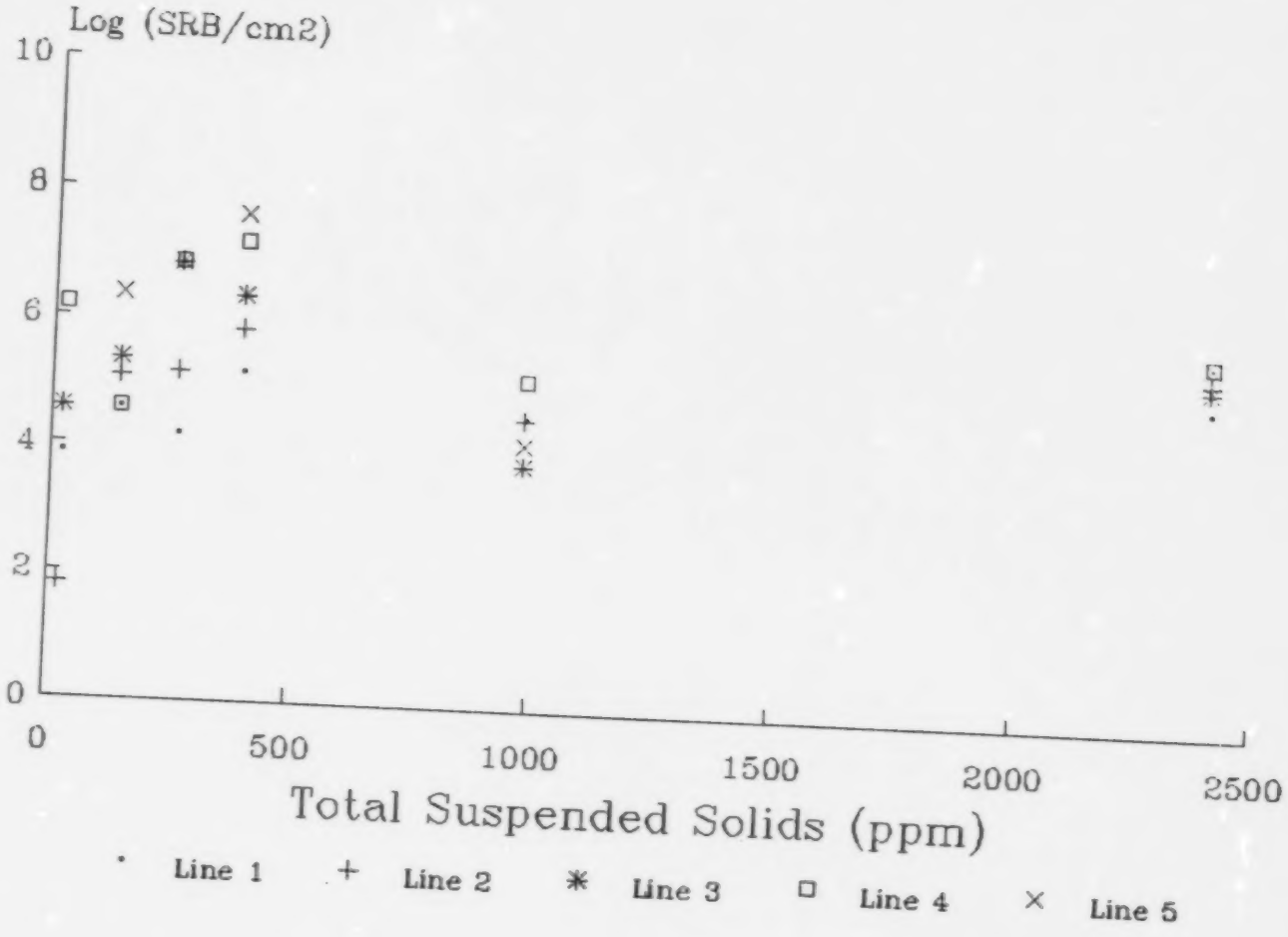

© 1991 NOVA HUSKY RESEARCH CORPORATION

FIGURE 36. Scatter plot of acid-producing bacterial counts and total suspended solids in the first experiment.

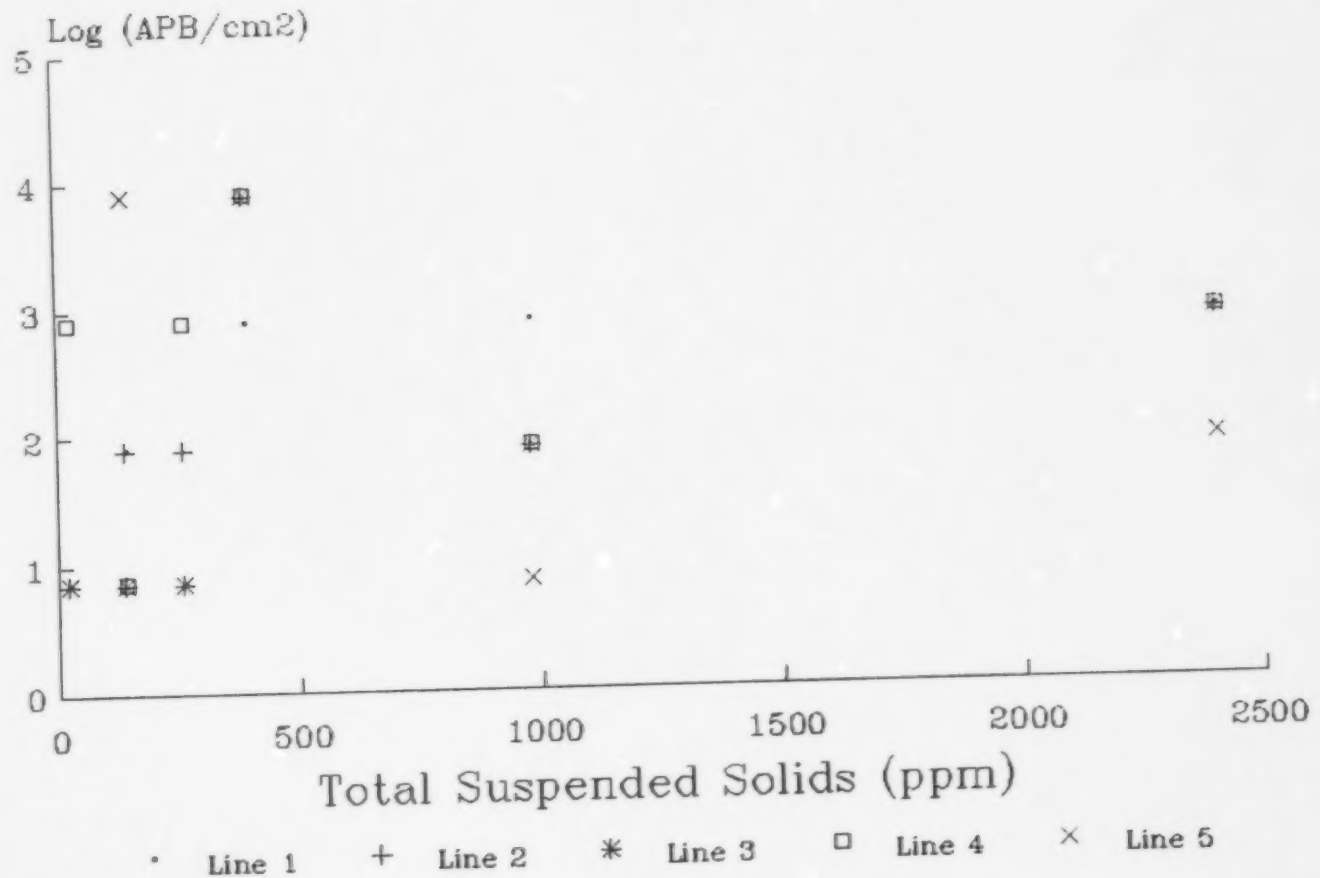

© 1991 NOVA HUSKY RESEARCH CORPORATION

FIGURE 37. Scatter plot of sulfate-reducing bacterial counts and total suspended solids in the second experiment.

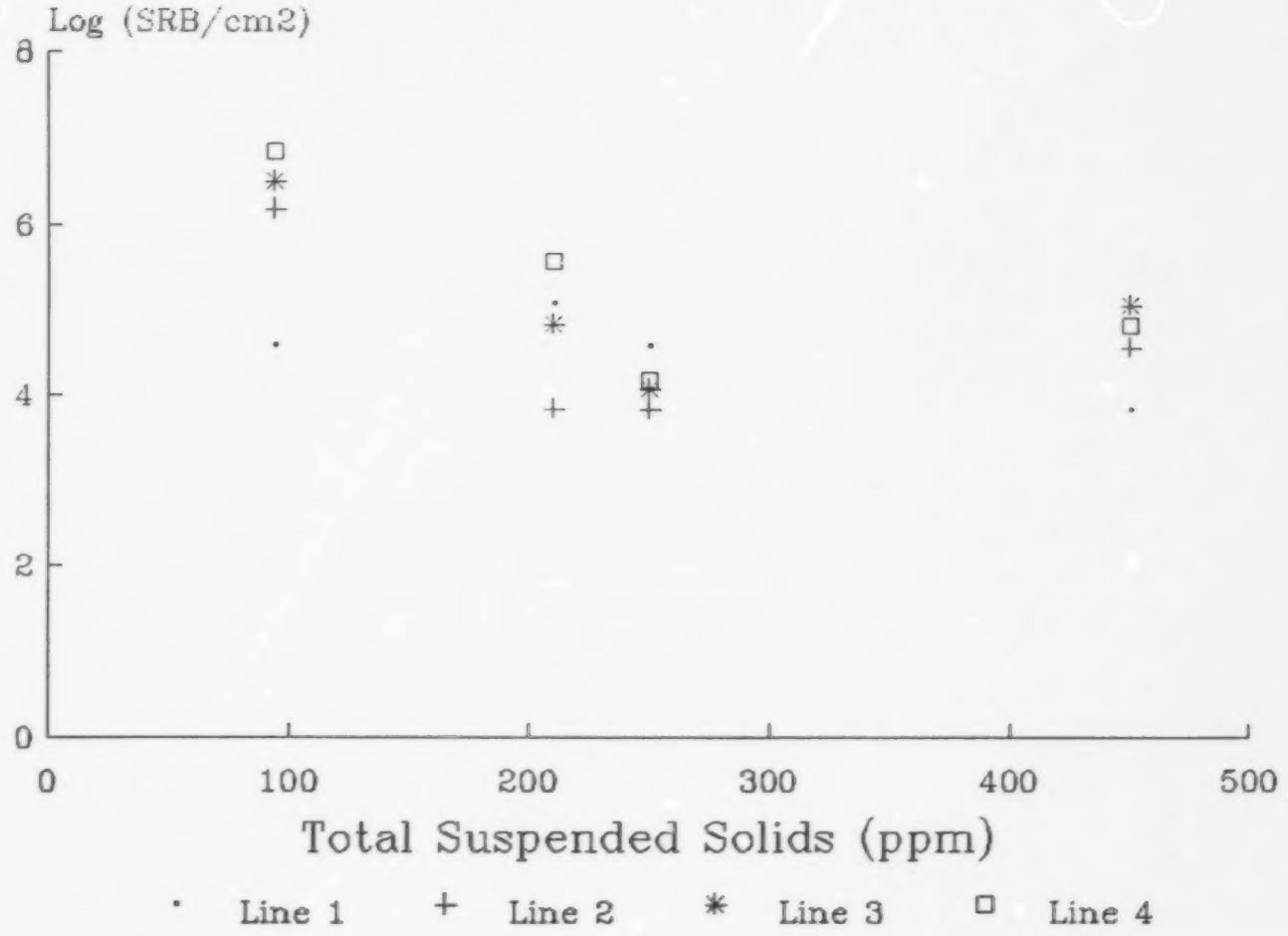

© 1991 NOVA HUSKY RESEARCH CORPORATION

FIGURE 38. Scatter plot of acid-producing bacterial counts and total suspended solids in the second experiment.

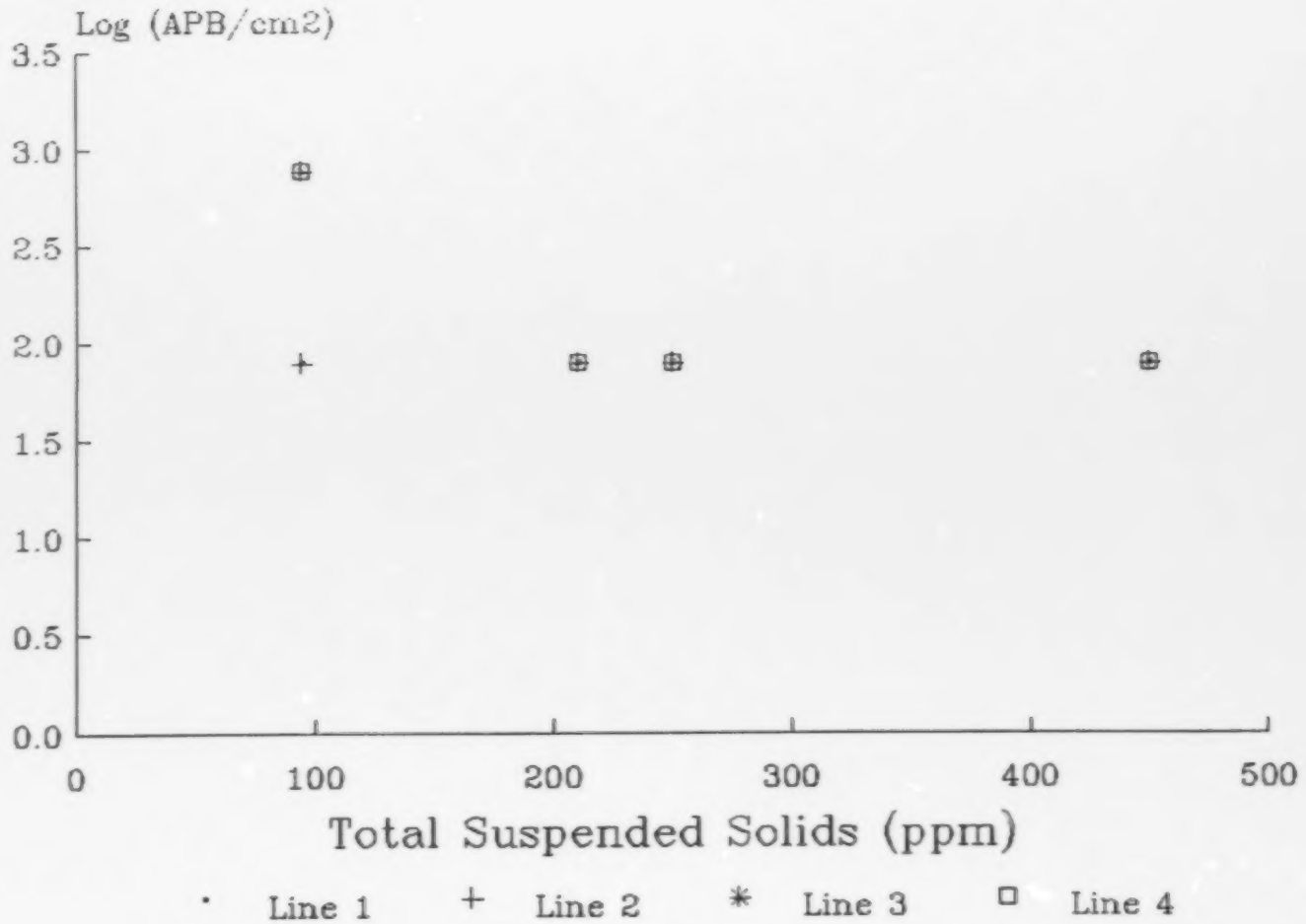

© 1991 NOVA HUSKY RESEARCH CORPORATION

FIGURE 39. Scatter plot of sulfate-reducing bacterial counts and total organic carbon in the first experiment.

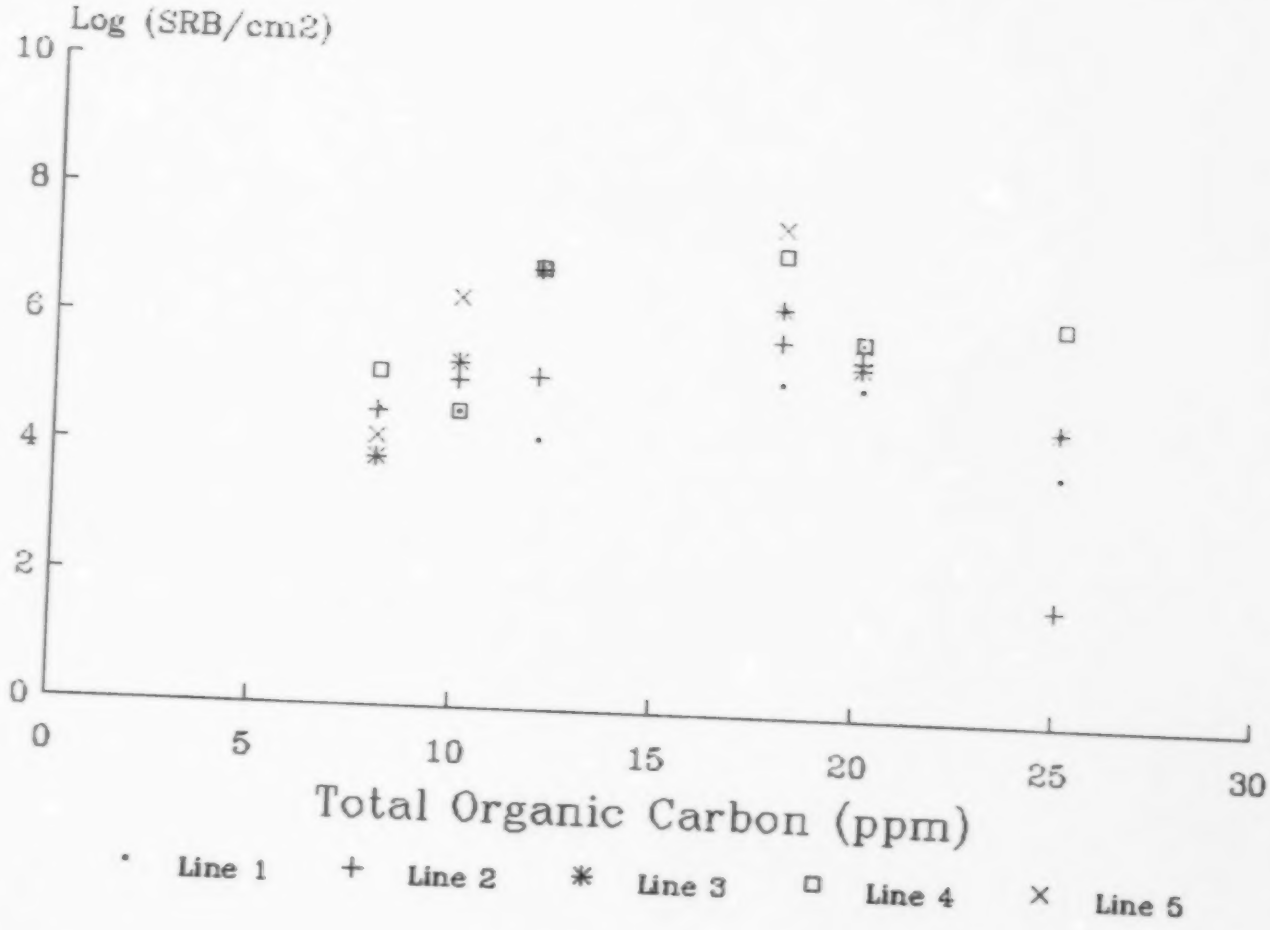

© 1991 NOVA HUSKY RESEARCH CORPORATION

FIGURE 40. Scatter plot of acid-producing bacterial counts and total organic carbon in the first experiment.

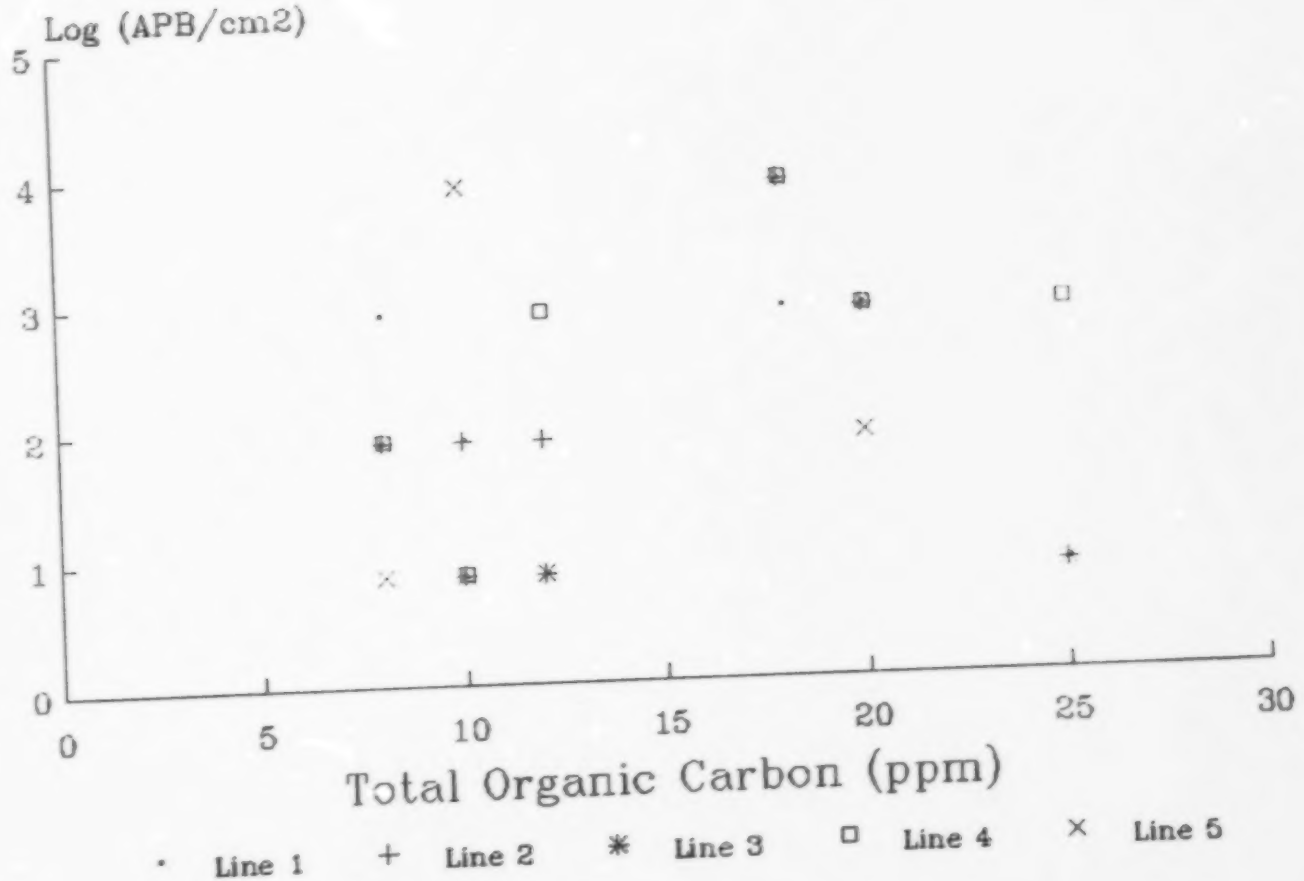

© 1991 NOVA HUSKY RESEARCH CORPORATION

FIGURE 41. Scatter plot of sulfate-reducing bacterial counts and total organic carbon in the second experiment.

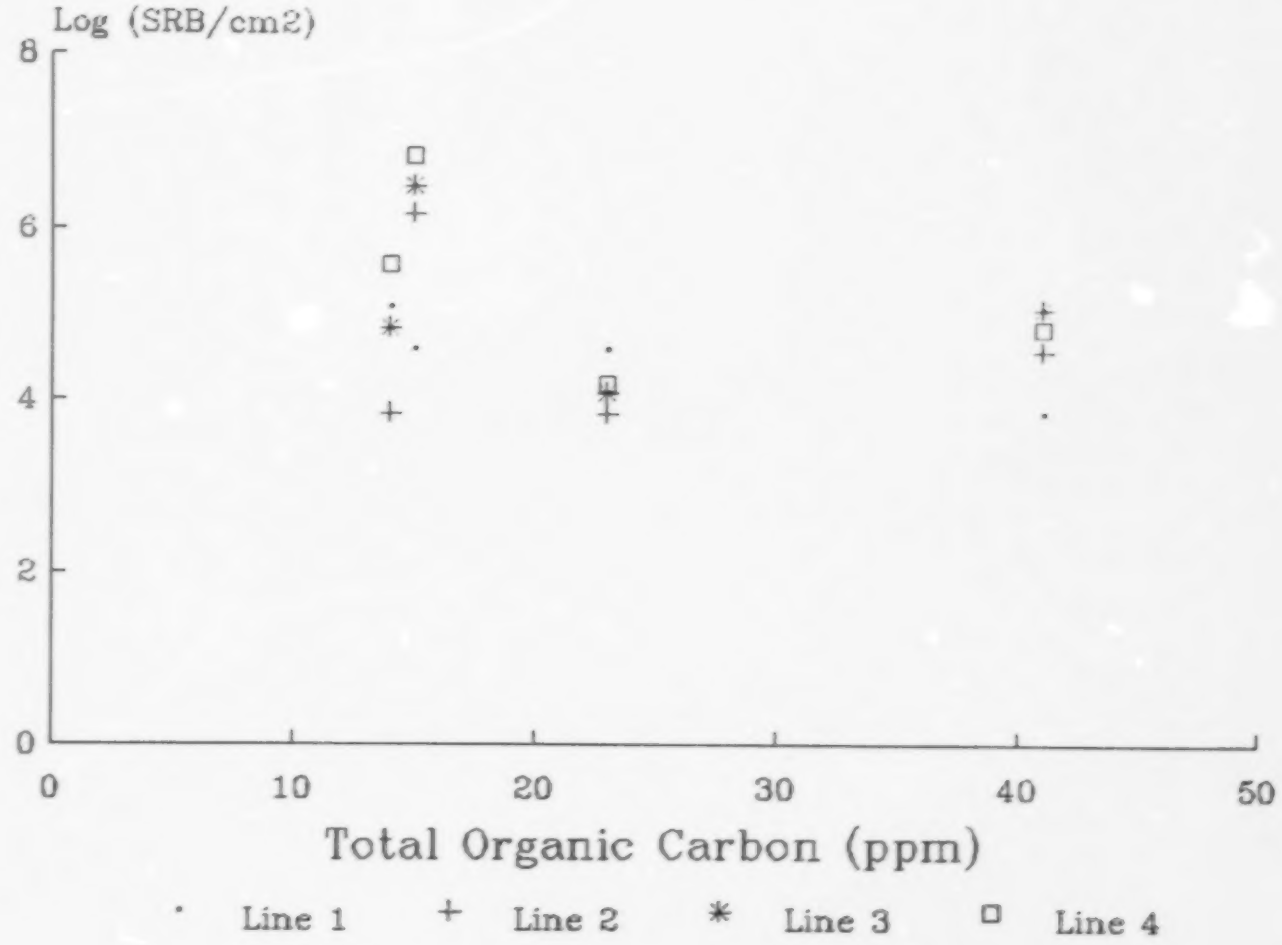

© 1991 NOVA HUSKY RESEARCH CORPORATION

FIGURE 42. Scatter plot of acid-producing bacterial counts and total organic carbon in the second experiment.

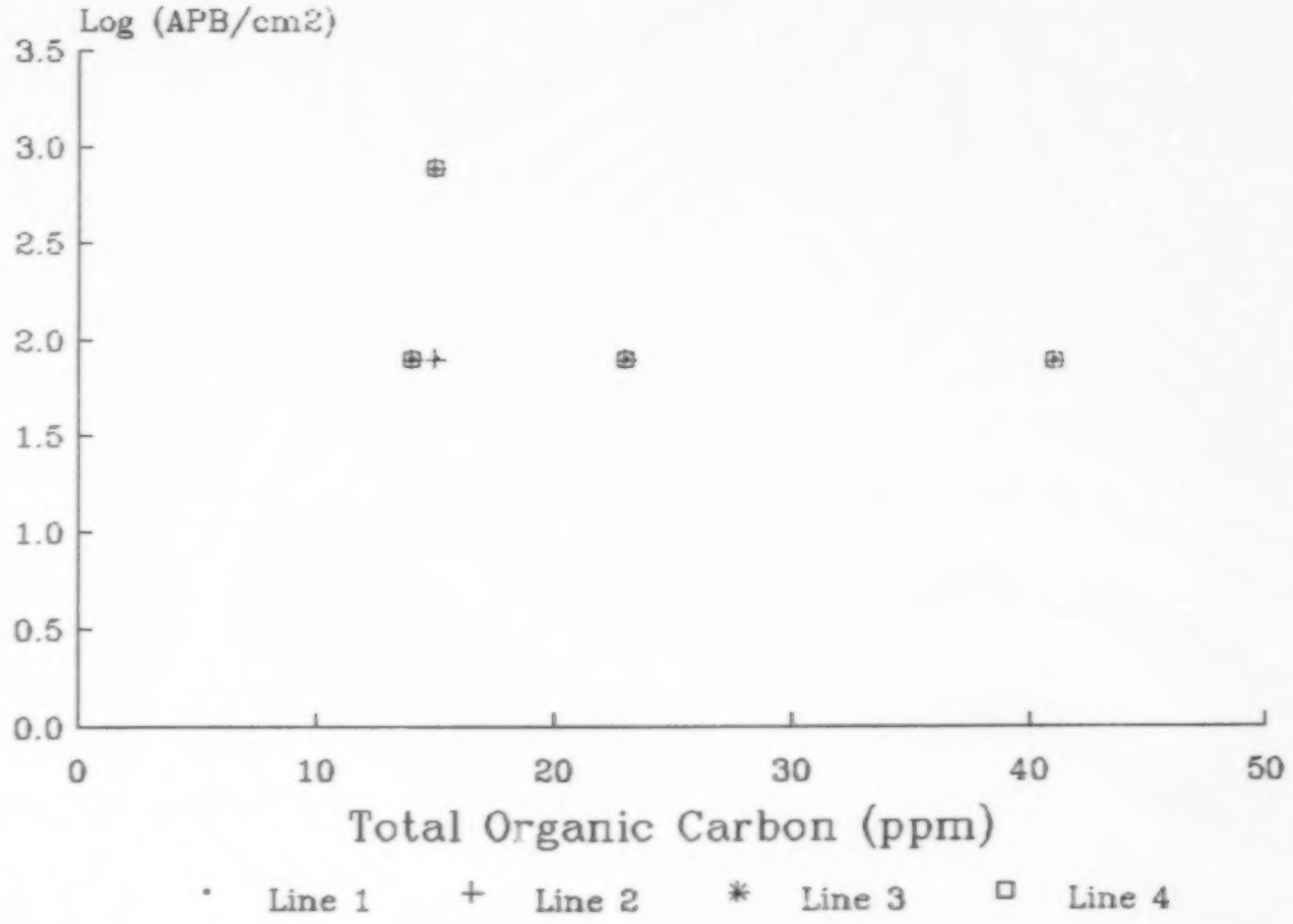

© 1991 NOVA HUSKY RESEARCH CORPORATION

FIGURE 43. Bacterial counts on bull plugs from Unit # 1 before and after exposure at the field test facility.

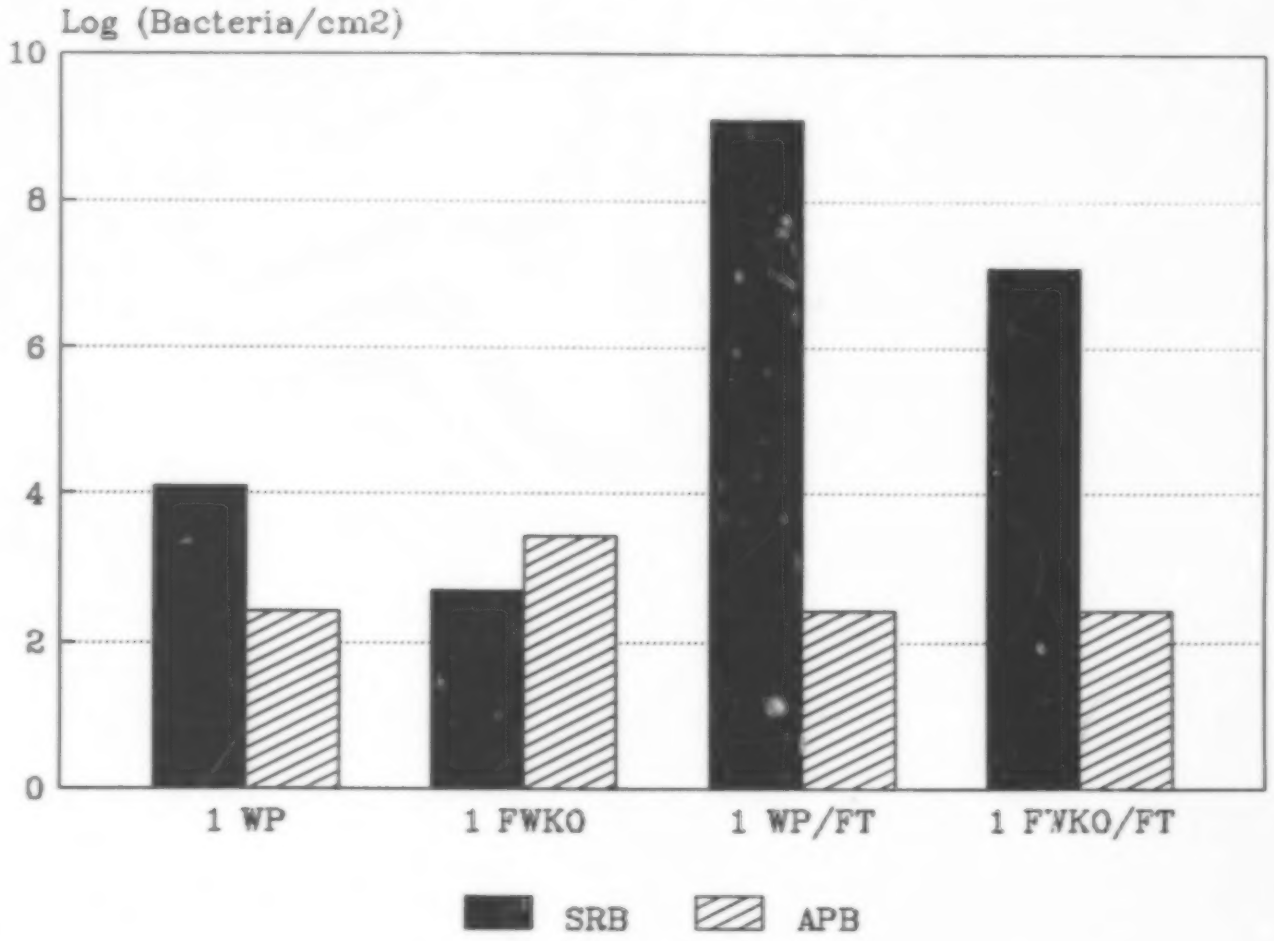

© 1991 NOVA HUSKY RESEARCH CORPORATION

FIGURE 44. Bacterial counts on bull plugs from Unit # 28 before and after exposure at the field test facility.

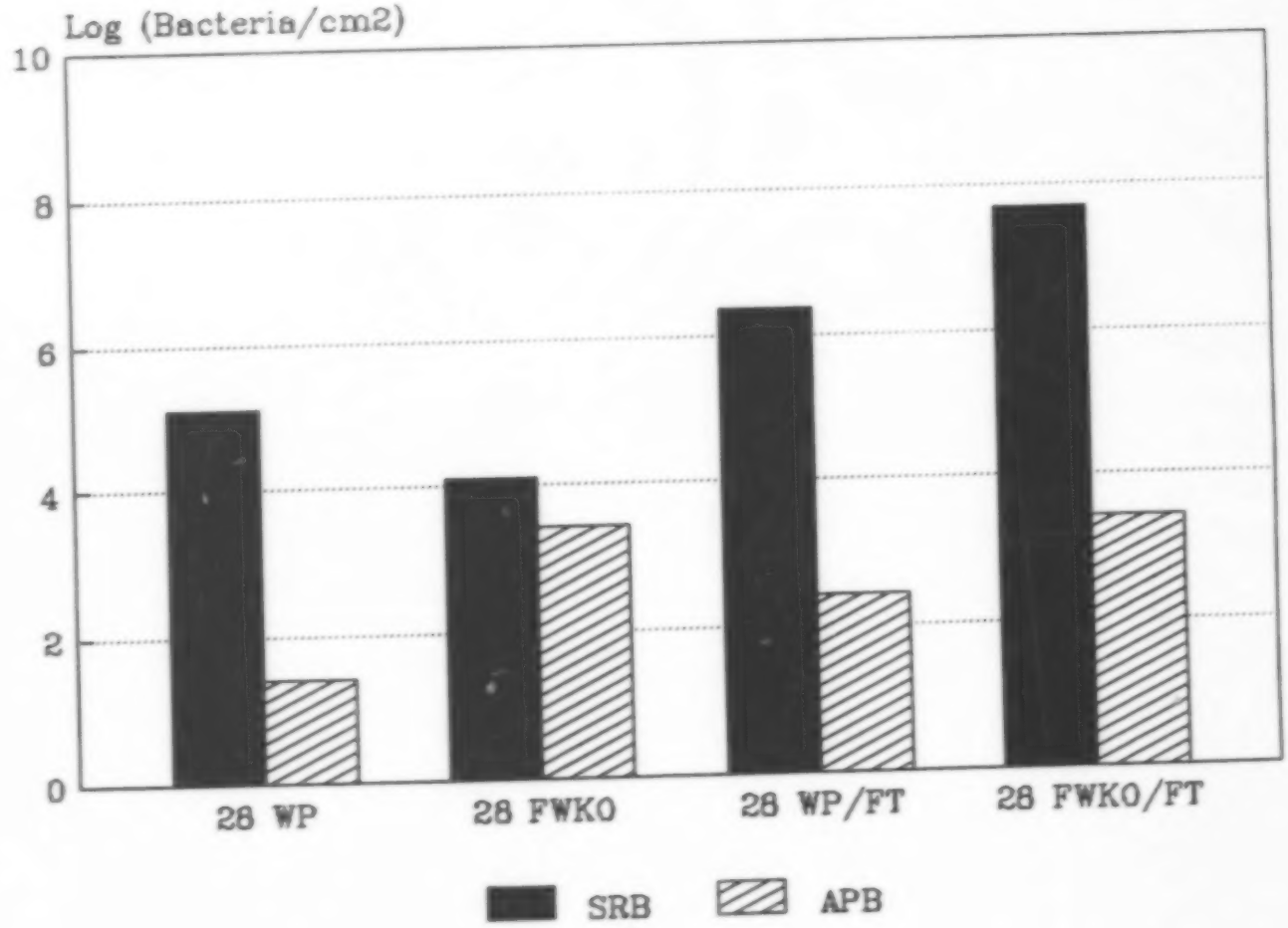

© 1991 NOVA HUSKY RESEARCH CORPORATION

FIGURE 45. Bacterial counts on bull plugs from Unit # 6 and Wildmere Washtank before and after exposure at the field test facility.

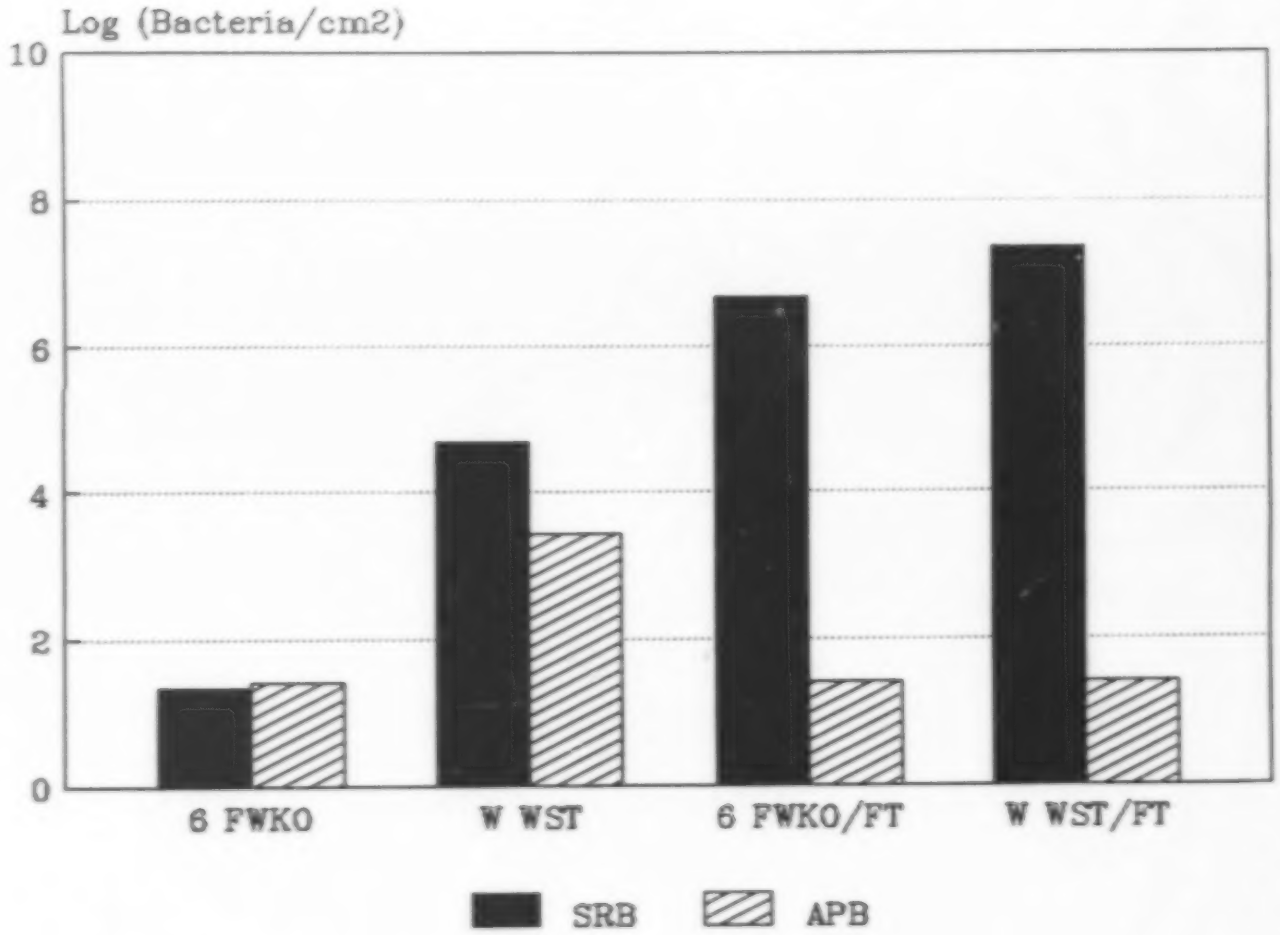

© 1991 NOVA HUSKY RESEARCH CORPORATION

FIGURE 46. Bacterial counts on bull plugs from Unit # 5 before and after exposure at the field test facility.

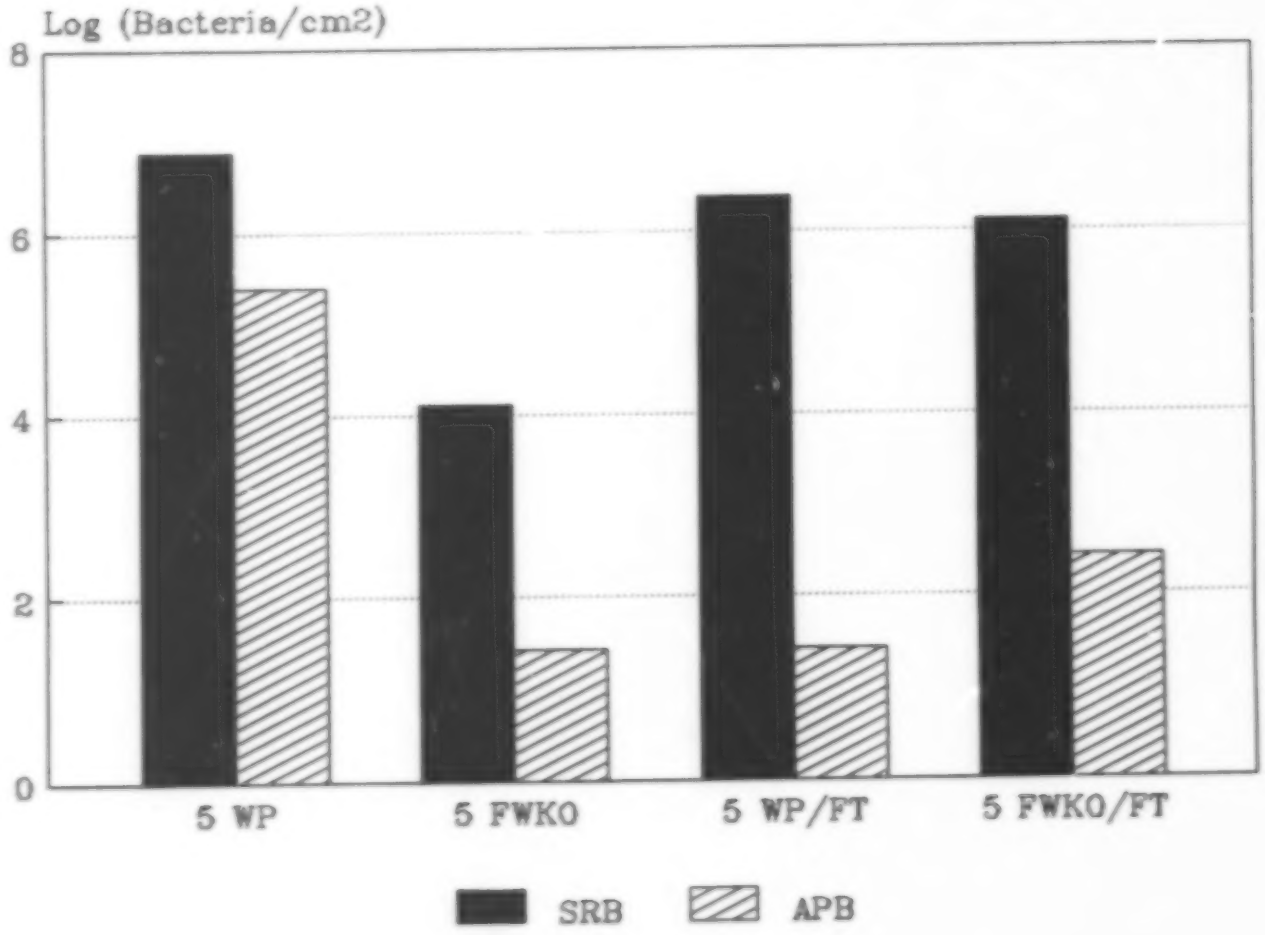

© 1991 NOVA HUSKY RESEARCH CORPORATION

FIGURE 47. Bacterial counts on bull plugs from Unit # 14 before and after exposure at the field test facility.

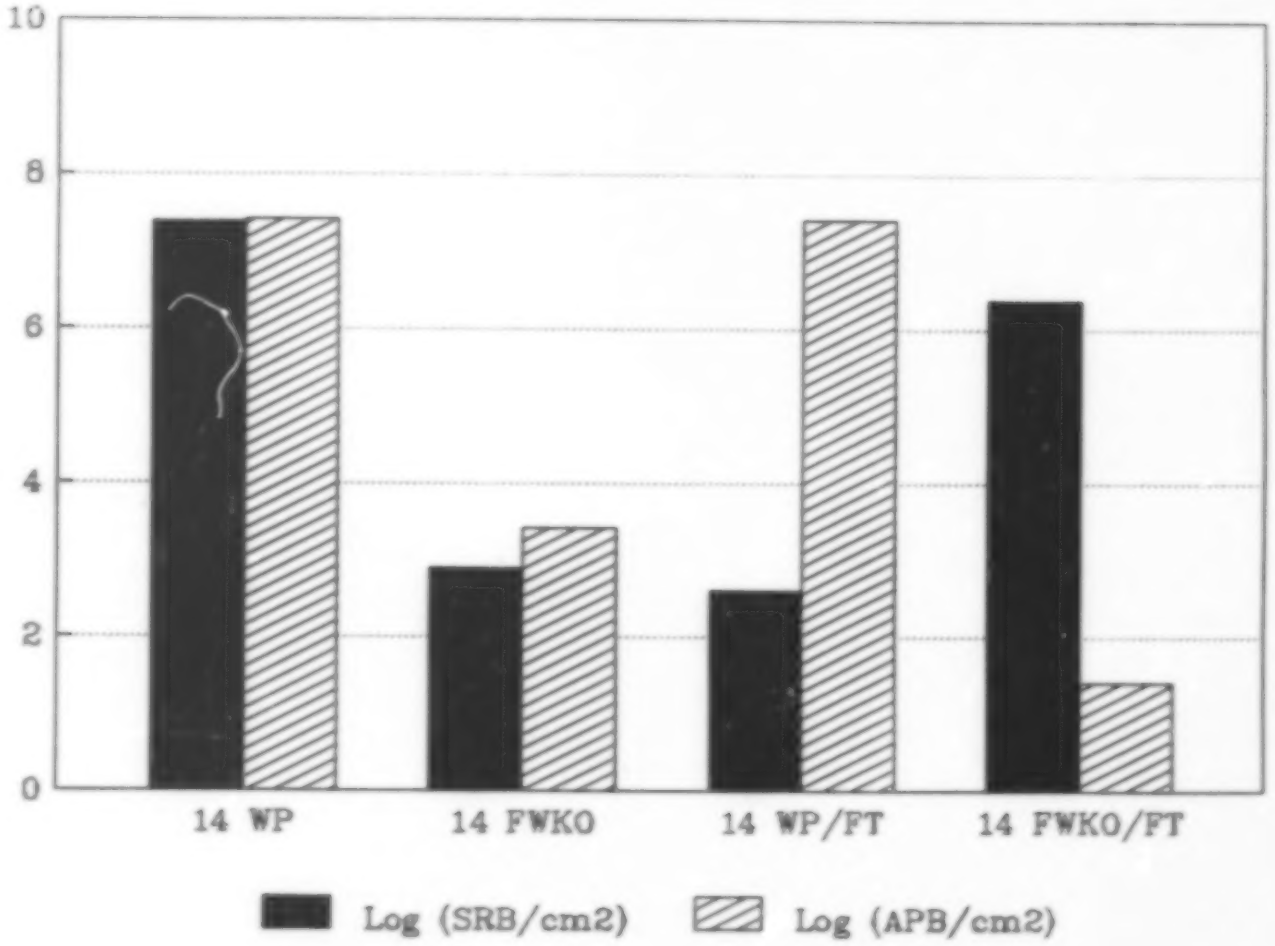

© 1991 NOVA HUSKY RESEARCH CORPORATION

FIGURE 48. Back-scattered electron image of surface on a sample coupon from the field test facility showing a mixture of corrosion deposits.

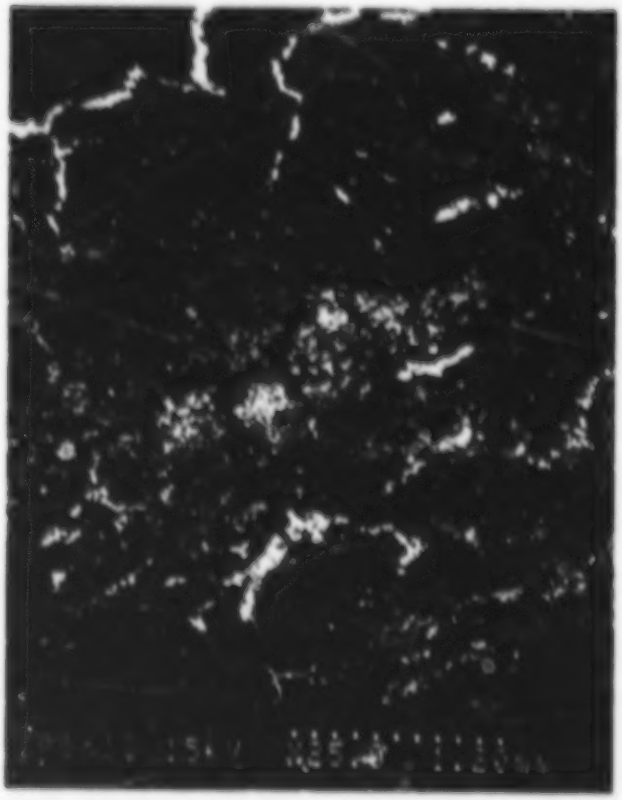

© 1991 NOVA HUSKY RESEARCH CORPORATION

FIGURE 49. Energy dispersive X-ray spectrum arising from the surface of a sample coupon from the field test facility.

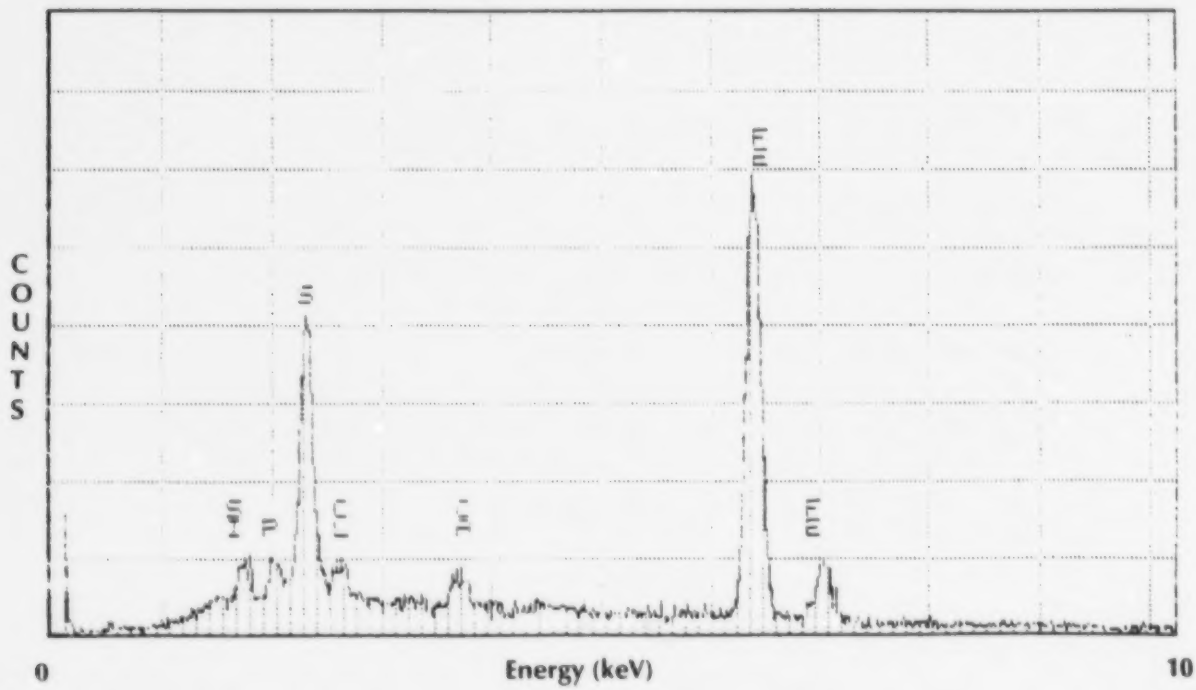

© 1990 NOVA HUSKY RESEARCH CORPORATION

FIGURE 50. Scanning electron micrography showing bacterial cells (arrows) near the surface of the iron sulfide corrosion deposit matrix.

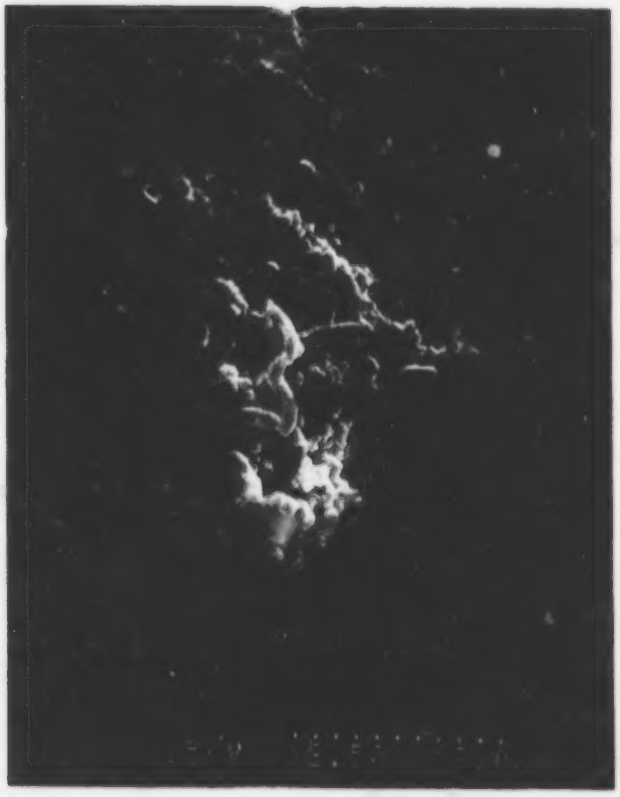

© 1991 NOVA HUSKY RESEARCH CORPORATION

FIGURE 51. Thin-section transmission electron micrograph showing bacterial cells (arrows) embedded within the iron sulfide corrosion deposit matrix.

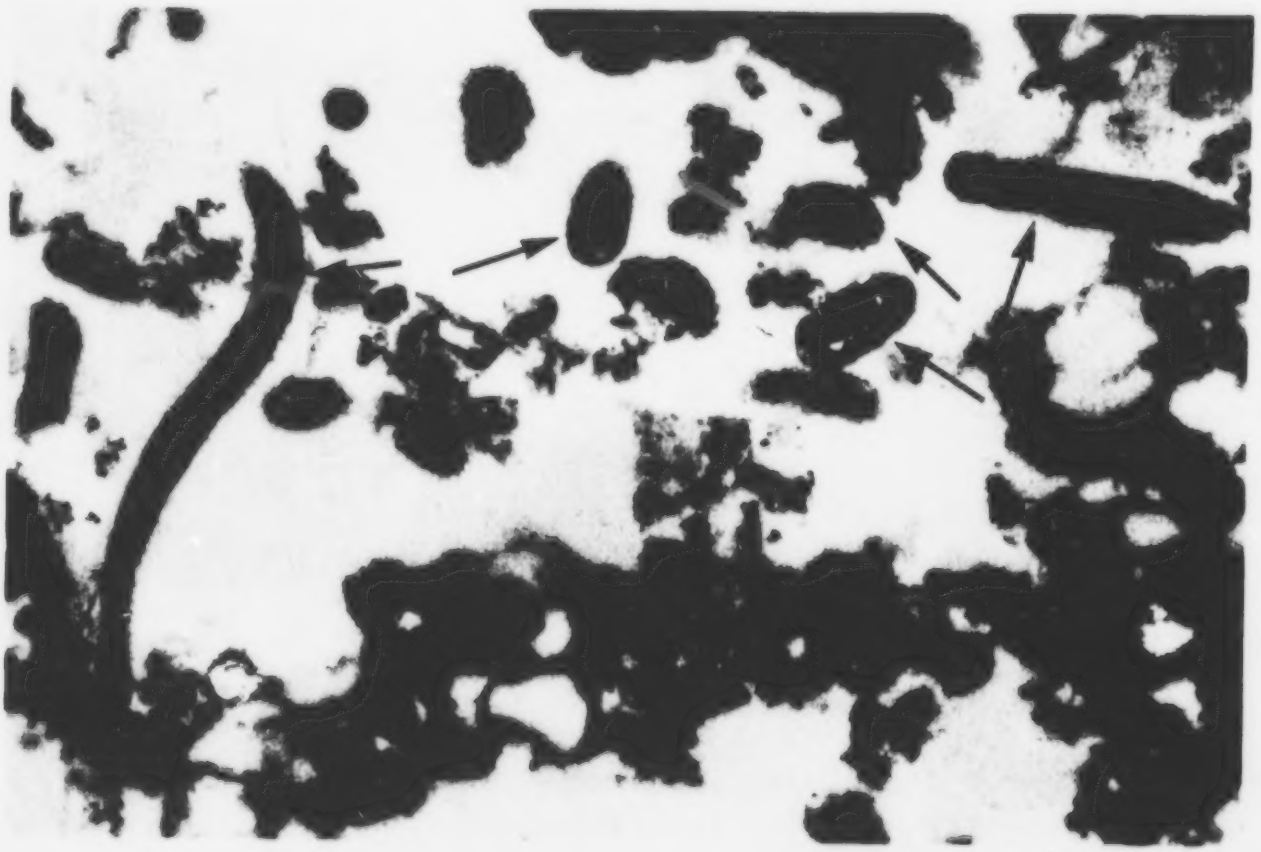

© 1991 NOVA HUSKY RESEARCH CORPORATION

FIGURE 52. Thin-section transmission electron micrograph showing a heavily mineralized cellular ghost.

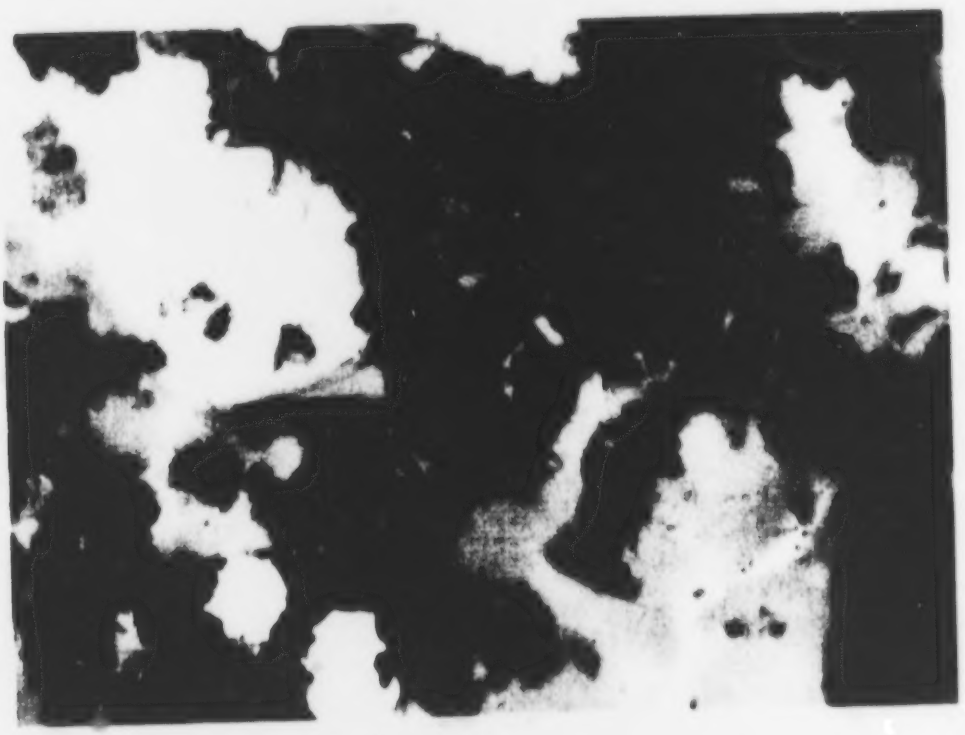

© 1991 NOVA HUSKY RESEARCH CORPORATION

FIGURE 53. Energy dispersive X-ray spectrum from amorphous iron sulfide matrix in thin-sections of corrosion deposits from field test facility sample coupons.

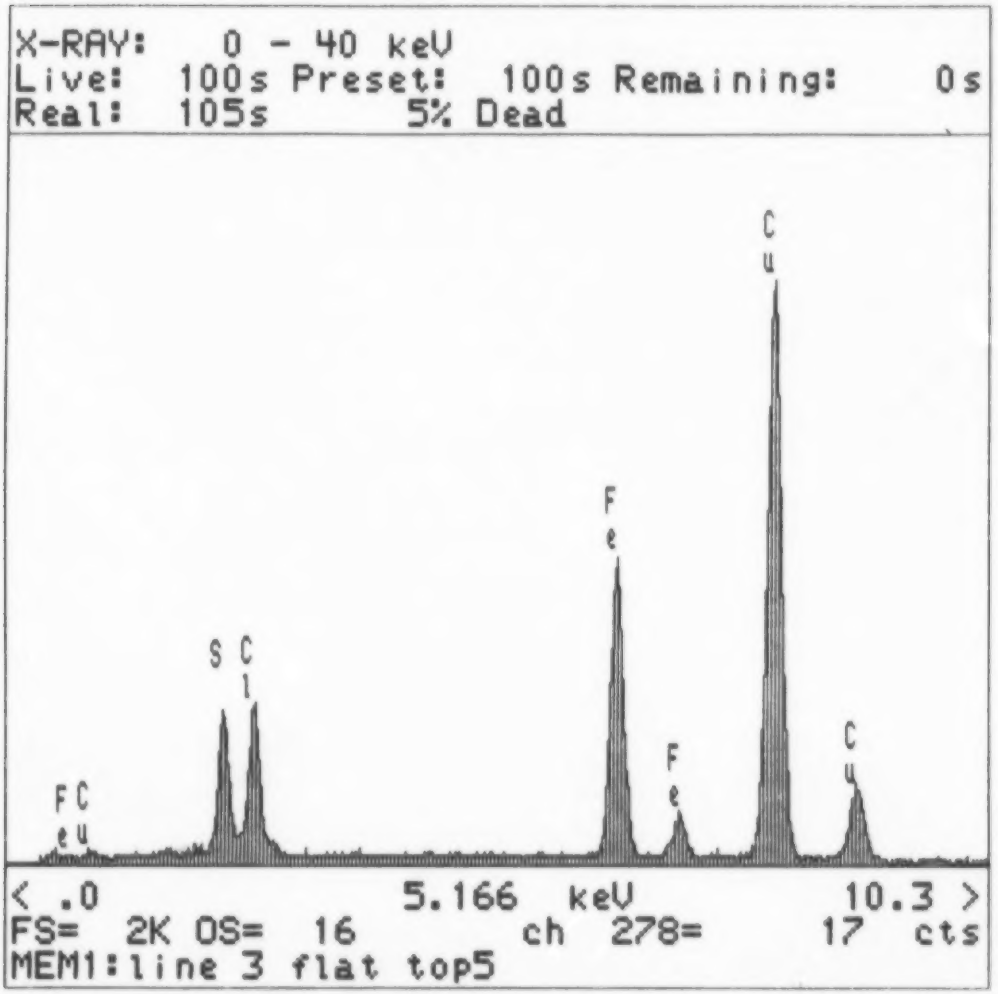

© 1991 NOVA HUSKY RESEARCH CORPORATION

FIGURE 54. Atom percent of iron, sulfur, and chlorine in the amorphous matrix and crystalloids of corrosion deposits from field test facility sample coupons.

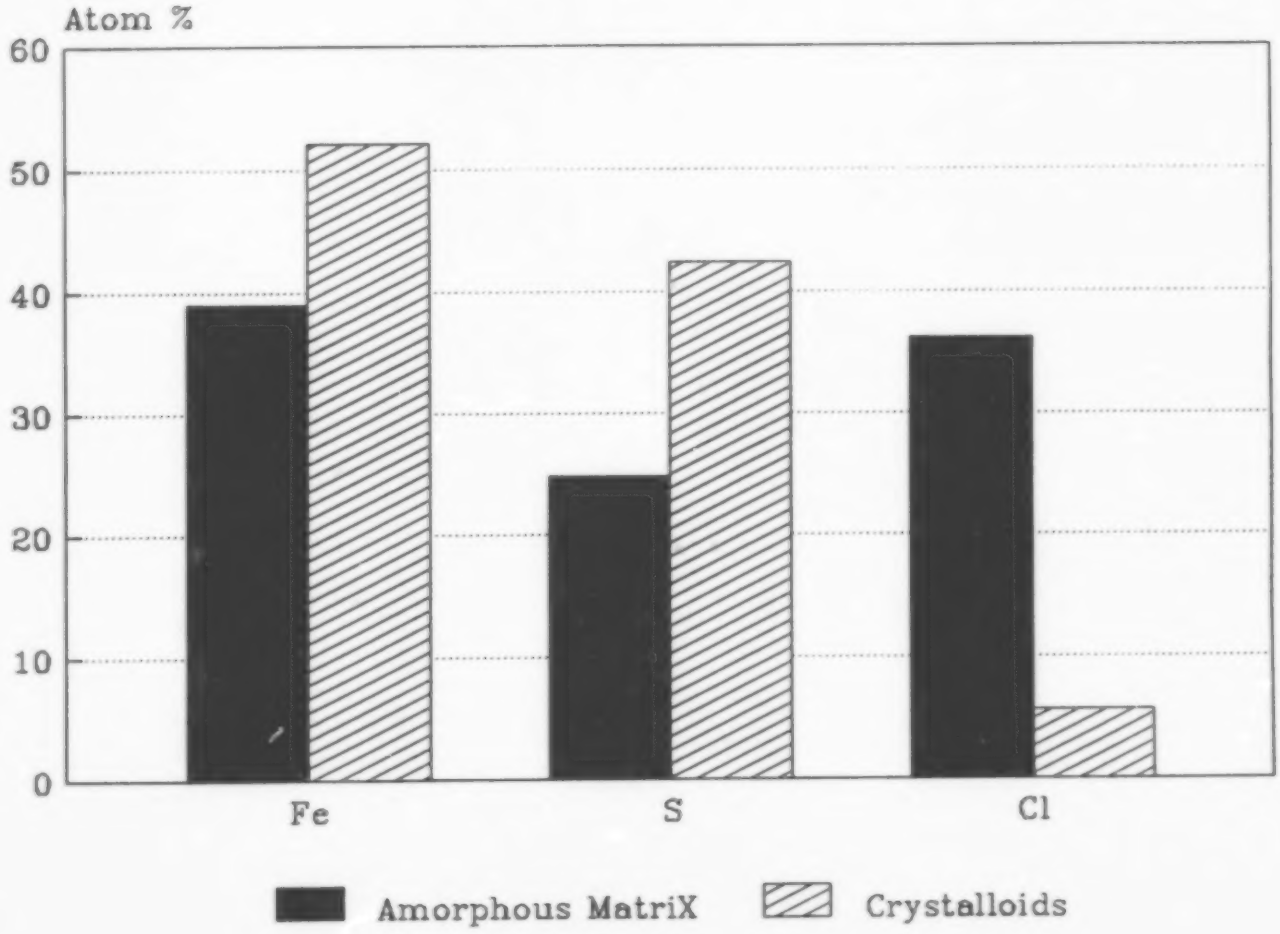

© 1991 NOVA HUSKY RESEARCH CORPORATION